
Neutron Yield in Thick Targets: Exploring Low and Intermediate Energies and Validating Model Codes

Thesis submitted to
University of Calicut in partial fulfilment
for the degree of

Doctor of Philosophy
in
Physics



by

FATHIMA SHIRIN SHANA.A.T

under the guidance of

Dr.ABDUL GAFOOR.A.K

Principal(Rtd)

Government Arts and Science College, Kondotty

Research guide

Department of Physics

Government Arts and Science College,

Calicut

May 2024

Certificate

It is certified that the work contained in this thesis entitled “Neutron Yield in Thick Targets: Exploring Low and Intermediate Energies and Validating Model Codes” is a bonafied record of research work carried out by **Fathima Shirin Shana.A.T** at Department of Physics, Government Arts and Science College Calicut, Kerala-India, under my supervision. The contents of the thesis are undergone plagiarism check using iThenticate software at C.H.M.K. Library , University of Calicut, and the similarity index found within the permissible limit. This thesis has not been submitted elsewhere for the award of any degree/diploma at this or any other University/Institution



Dr.Abdul Gafoor.A.K

Research guide

Department of Physics

Government Arts and Science

college, Calicut

Place: *Calicut*

Date: *21/10/2024*



Declaration

I hereby declare that the work presented in the thesis entitled “Neutron Yield in Thick Targets: Exploring Low and Intermediate Energies and Validating Model Codes” is based on the original work done by me under the guidance of Dr.Abdul Gafoor.A.K and has not been included in any other thesis submitted previously for the award of any degree. The contents of the thesis are undergone plagiarism check using iThenticate software at C.H.M.K. Library, University of Calicut and the similarity index found within the permissible limit. I also declare that the thesis is free from AI generated contents. .


Fathima Shirin Shana .A.T



Signature

Name of the scholar

Place: Calicut

Date: 21/10/2024


Signature of the Supervising teacher
Dr.ABDUL GAFOOR A.K.
Research Guide Name
P.G Dept.of Physics
Govt.Arts & Science College, Calicut


Signature of Co-guide

Dr. BINITHA Name
Associate Professor
Department of Physics
Govt. Arts & Science College, Calicut
673018

DEPARTMENT OF PHYSICS
GOVT. ARTS & SCIENCE COLLEGE, CALICUT -18
KERALA 673018 – INDIA



Dr. ABDUL GAFOOR A.K.
Research Guide
Research & P.G. Department of Physics
Govt. Arts & Science College, Calicut -18

[http:// www.gasckkd.ac.in](http://www.gasckkd.ac.in)
0495-232 0694
Residence-+91 9745788863
e-mail: gasusmi@gmail.com

CERTIFICATE

This is to certify that the corrections/suggestions recommended by the adjudicators have been incorporated in the thesis titled “Neutron Yield in Thick Targets: Exploring Low and Intermediate Energies and Validating Model Codes” submitted by Ms Fathima Shirin Shana.A.T and the content in the thesis and the soft copy are one and the same.

Place : Calicut

Date : 14/10/2024

Dr. Abdul Gafoor A.K.



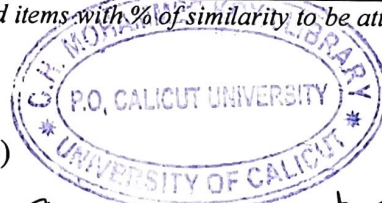


**UNIVERSITY OF CALICUT
CERTIFICATE ON PLAGIARISM CHECK**

1.	Name of the Research Scholar	FATHIMA SHIRIN SHANA A.T	
2.	Title of thesis / dissertation	Neutron Yield in Thick Targets: Exploring Low and Intermediate Energies and Validating Model Codes	
3.	Name of the Supervisor	Dr. ABDUL GAFOOR A.K.	
4.	Department/Institution	Department of Physics, Government Arts and Science College, Calicut	
5.	Similar content (%) identified	Non Core	Core
		Introduction/ Theoretical overview/Review of literature/ Materials & Methods/ Methodology	Analysis/Result/Discussion/ Summary/Conclusion/ Recommendations
		0	0
	Acceptable maximum limit (%)	10	10
6.	Software used	iThenticate	
7.	Date of verification	06/05/2024	

*Report on plagiarism check, specifying included/excluded items with % of similarity to be attached.

Checked by (with name, designation & signature)



Christine

JAMSHEER N. P.
Assistant Librarian
University of Calicut
Malappuram - 672 625

Name and signature of the Researcher

Fathima Shirin Shana A.T

Name and signature of the Supervisor.

Dr. Abdul Gafoor A.K.

DR. ABDUL GAFOOR A.K.
Research Guide

The Doctoral Committee* has verified the report on plagiarism check with the contents of the thesis, as summarized above and appropriate measures have been taken to ensure originality of the Research accomplished herein.

Name & Signature of the HoD/HoI (Chairperson of the Doctoral Committee)

Paiya.P

Paiya.P
PRINCIPAL 13/10/2024
GOVT. ARTS & SCIENCE COLLEGE
KOZHIKODE - 673018.

*In case of languages like Malayalam, Tamil etc..on which no software is available for plagiarism check, a manual check shall be made by the Doctoral Committee, for which an additional certificate has to be attached.



”Verily, With Hardship Comes Ease”

*Dedicated to My Beloved
Family and Friends*

Acknowledgements

Undertaking this PhD has been a truly life-changing experience for me and it would not have been possible to do without the support and guidance that I received from many people.

I would like to express my gratitude to my PhD Supervisor, Dr.Abdul Gafoor.A.K, and Co-Guide Dr.Binitha.M.P for their support, guidance, and valuable insights throughout the entire research work.

I am unable to begin this thesis without expressing my sincere gratitude to Dr Sugathan.P, Scientist, IUAC, NewDelhi, I am incredibly grateful to him for all the support and encouragement he given, during my doctoral period. Undoubtedly he is a gods hand to me. He is such an exceptional academic expertise, coupled with his commitment to support early career researchers truly make him a role model in the often competitive world of academia. Without his guidance and constant feedback this PhD would not have been achievable.

I extend my heartfelt appreciation to my work mentor Dr. M.M.Musthafa, Senior Professor, Department of Physics, University of Calicut for his guidance and suggestions during my research period.

The experiment work described in this thesis is carried out at IUAC, NewDelhi, and I would like to express my sincere gratitude to research scientists Golda,K.S., Saneesh and Divya for their great support in NAND facility. Also I am very much thankful to Dr.Ambar Chatterjee for his help in data acquisition.

I am also very much grateful to all my respected seniors, colleague and friends starting with my birthday partner Gokul Das,K Hajara, Shaima Akber, Swapna Balakrishnan, Anjali, Akhil ramesh, Nived, Aneena, Parvathi, Dinto, Vishnu, Anju, Ummukulsu, Vafiyya, Midhun, Farhana thesni, Bhagyasree, Rajesh KK, Abdul Kareem, Mohamed Aslam, Shafna, Nithu Ashok, Jisna rahman, Madhu.N , Ihsana, Reena.V.N, Jasna Nizam, my IUAC friends Chandra, Mayur, Ritu, and Allan all of them encouraged and helped me at every stage of my personal and academic life and longed to see this achievement come true. A special thanks to my friend Vidhya.L who brought me and guided me to the path of PhD.

I want to express my deepest gratitude to my family members. My father, Kunhimoideen master and mother Rajila Moideen, for their tireless work and unwavering commitment provided for me, while always discussing the value of education have made a significant influence on my career path. And I hope they are proud of the significant role they have played in shaping my path. Also words cannot express the cheerful support from my sweet littles, My sister Dr. Aysha Leena Liyana, brother Muhammed Shammas and sister in law Razana during my research journey. Not least many kisses to my grandparents, A.T.Saidalavi, Fathima and Rukhiyya, my uncles and aunts, Faisal Ali, Noushad Ali, Shamna, Zainul Abid, Shameema and Haseena for all their dedication and Prayers which inspired to achieve my goal.

And of course a huge hugs to my in laws: Father and Mother Abdul Khader and Safiya, sister and brothers: Noushad, Rasheeda, Shahid, Jamsheed, Rashid, Rubeena, Najeeba, Aneesha, Sofiya, Raheeb, Rashid for their constant support and prayers throughout my PhD journey.

Over all, No words to my all in all, my soulmate husband my (ikku) Dr. Shameed, Thank you for always being my rock, accompanying me through the highs and lows of this academic journey. His support and belief in me have been a source of strength and motivation.

Words Never enough for my kindred spirits, my lovely sister Rohini Anantha Padmanabhan, Achan and Amma(Mr. Venkiteswaran K and Mrs.Seethammal.K.S) how they treated me as a daughter during my Pre-PhD days, I am very much indebted for them.

Finally, As the well-known proverb tells “It takes a village to raise a child” I strongly believe that this is the time which my native place waited for, each of them directly and indirectly helped and prayed for me through out this journey and I wholeheartedly thank them all. A verymuch thankful to all my neighbours, family and natives of Jubilee road, especially, A very big awes to Mr.Musthafa kaku and Saji thatha my family friends who gifted me laptop at its most needed time in which I completed my whole PhD work.

Above all I owe to Allah Almighty for granting me the wisdom, health and strength to undertake this research task and enabling me take it to its completion.

Contents

Acknowledgements	v
List of Figures	xi
List of Tables	xv
Abbreviations	xvii
List of Publications	xviii
Preface	xx
1 Introduction	1
1.1 Background and Motivation of the study	3
1.2 Overview of the thesis structure	4
2 Literature Review	7
2.1 Nuclear reactions and its importance	7
2.2 Thick target reactions and their relevance	8
2.3 Gaps in the literature and need of this work	13
3 Basic Theory and Model Codes	15
3.1 Reaction mechanism	15
3.2 Direct Reaction	16
3.3 Compound nucleus mechanism	18
3.3.1 Weisskopf-Ewing theory	18
3.3.2 Hauser-Feshbach theory	20
3.4 Pre-equilibrium Reaction	21

3.4.1	Exciton model	22
3.4.2	Hybrid model	24
3.4.3	Multi-step Direct (M.S.D) and Multi-step Compound (M.S.C) Model	26
3.5	Optical Model	27
3.6	Nuclear level densities	28
3.6.1	Composite Gilbert-Cameron model	29
3.6.2	The Back-shifted Fermi Gas Model	30
3.6.3	The Generalized Superfluid Model	31
3.6.4	The Enhanced Generalized Superfluid Model	31
3.6.5	Microscopic level densities	32
3.7	Nuclear Reaction Codes and Tools	32
3.7.1	EMPIRE-3.2	33
3.7.2	TALYS	35
3.7.3	NeuCBOT	36
3.7.4	Directory Structure	36
3.7.5	PACE 4	38
3.7.6	SRIM	38
4	Thick target neutron yield-Low energy	41
4.1	Introduction	41
4.2	Neutron energy spectra deduced for some elements	43
4.2.1	Alpha bombarded on Silicon	43
4.2.2	Alpha bombarded on Aluminium	47
4.2.3	Alpha bombarded on Magnesium	50
4.3	Thick target neutron yield for Am-Be source.	56
4.3.1	Theoretical formalism using NeuCBOT	58
4.3.2	Theoretical formalism using EMPIRE-3.2 code	59
4.4	Conclusion	65
5	Measurement of neutron energy from Am-Be	67
5.1	Introduction	67
5.2	Facility Overview	68
5.3	Materials and Methods	68
5.3.1	Am-Be source	68
5.3.2	BC501A neutron detector	70
5.3.3	BaF ₂ Gamma detector	71
5.3.4	Measurement	72
5.3.5	Time of Flight method	73
5.4	Electronics setup and data acquisition system (DAQ)	74
5.5	TOF energy spectrum	75
5.6	Comparison of experimental results with theoretical predictions	82

5.7	Conclusion	84
6	Thick target neutron yield-Intermediate energy	85
6.1	Introduction	85
6.2	Study of intermediate energy neutron yield	87
6.2.1	¹² C on ²⁷ Al	87
6.2.2	¹² C on ^{nat} Ti	93
6.2.3	¹² C on ⁵⁶ Fe	93
6.3	Conclusion	96
7	Summary and Conclusion	97
7.1	Conclusion	98
8	Recommendation	103
	Bibliography	105

List of Figures

3.1	Nuclear reaction mechanisms	16
3.2	Nuclear reaction cross section with separation of the three reaction mechanisms depending on the emission energy	17
3.3	Schematic diagram of behaviour of particle and holes in exciton model.	23
4.1	The angle integrated neutron energy spectra for thick targets of Silicon at four different α -particle energies, determined from time of flight measurements(black line), The red line represents the result obtained from NeuCBOT. From top to bottom of the figure: 5.5MeV, 5MeV, 4.5MeV,4MeV	46
4.2	The angle integrated neutron energy spectra for thick targets of Aluminium at four different α -particle energies, determined from time of flight measurements(black line), The red line represents the result obtained from NeuCBOT. From top to bottom of the figure: 5.5MeV, 5MeV, 4.5MeV,4MeV	49
4.3	The angle integrated neutron energy spectra for thick targets of Magnesium at four different α -particle energies, determined from time of flight measurements(black line), The red line represents the result obtained from NeuCBOT.From top to bottom of the figure: 5.5MeV, 5MeV, 4.5MeV,4MeV	52
4.4	The angle integrated neutron energy spectra for thick target of Boron Nitrate at α -particle energy 5.5 MeV determined from time of flight measurements(black line), The red line represents the result obtained from NeuCBOT	53
4.5	The angle integrated neutron energy spectra for thick target of Calcium fluoride at α -particle energy 5.5 MeV determined from time of flight measurements(black line), The red line represents the result obtained from NeuCBOT	54
4.6	Neutron yield for various elements is calculated by code NeuCBOT in comparison with measurements. Neutron yield is given as the number of neutrons per 10^7 alphas.	55
4.7	Energy level diagram of ^{12}C	57
4.8	Neutron energy spectrum predicted by NeuCBOT	59
4.9	Neutron energy spectra at 90^0	60

4.10	Observed Neutron spectra,including the stragglng corresponds to energy 3.6 MeV	61
4.11	Integrated neutron energy spectrum	62
4.12	Neutron energy spectrum calculated using EMPIRE-3.2 with stragglng	63
4.13	Resultant spectra from EMPIRE-3.2(red line),Geiger spectra(dotted green line)	64
5.1	NAND facility	69
5.2	The encapsulated Am-Be source	70
5.3	5 in (diameter) x 5 in (height) BC501A liquid scintillator cell mounted on a 5 in diameter PMT	72
5.4	The schematic diagram of the experimental setup (not to scale) . . .	73
5.5	Block diagram of the electronics setup used for signal processing and data acquisition.	75
5.6	Zero-cross distribution showing distinct separation of neutrons and γ -rays interacting inside BC501A detector	76
5.7	Two dimensional histograms of zero-cross time vs. light output for untagged and gamma-tagged conditions.	78
5.8	Two dimensional histogram of zero-cross time vs. time-of-flight. . . .	79
5.9	Simulated intrinsic efficiency of 5 in. x 5 in. single cell BC501A detector as a function of neutron energy.	80
5.10	The Am-Be neutron energy spectrum from present measurement (solid line), compared with ISO 8529-2 reference spectrum[66] (red dashed line) and spectrum obtained by Scherzinger (2015) (blue dash-dotted line).	81
5.11	The neutron energy spectrum of Am-Be source measured compared with EMPIRE-3.2 calculated	82
5.12	The neutron energy spectrum of Am-Be source compared with measured TOF and calculated NeuCBOT	83
6.1	Comparison of Neutron yield data of ^{12}C on ^{27}Al at 0° reported by V. Suman et al[67],with theoretical data from EMPIRE-3.2 and PACE 4.	87
6.2	Comparison of Neutron yield data of ^{12}C on ^{27}Al at 30° reported by V. Suman et al[67],with theoretical data from EMPIRE-3.2 and PACE 4.	88
6.3	Comparison of Neutron yield data of ^{12}C on ^{27}Al at 60° reported by V. Suman et al[67] with theoretical data from EMPIRE-3.2 and PACE 4.	89
6.4	Comparison of Neutron yield data of ^{12}C on ^{27}Al at 90° reported by V. Suman et al[67],with theoretical data from EMPIRE-3.2 and PACE 4.	90
6.5	Comparison of Neutron yield data of ^{12}C on ^{27}Al reported by V. Suman et al[67],with theoretical data from EMPIRE-3.2 with pre-equilibrium(wp) and without pre-equilibrium(wop) and PACE 4. . . .	91
6.6	Comparison of neutron yield data reported by[24] with EMPIRE-3.2 and PACE 4 for ^{12}C on Ti at 144 MeV	92

6.7	Comparison of Calculated neutron yield data from HIC-1 code data reported by H.W.Bertini[68] with those obtained from model calculations EMPIRE-3.2 and PACE 4 for ^{12}C on ^{56}Fe reaction at 0^0 and 30^0	94
6.8	Comparison of Calculated neutron yield data from HIC-1 code data reported by H.W.Bertini[68] with those obtained from model calculations EMPIRE-3.2 and PACE 4 for ^{12}C on ^{56}Fe reaction at 60^0 and 90^0	95

List of Tables

2.1	Neutron yield of some (α , n) sources[10]	8
2.2	The activity, neutron emission in n/s for Am-Be	9
2.3	Thick target(α ,n) neutron yields per 10^7 α -particles reported in the literature[21], The results of Liskien and Paulsen[13][14] were obtained from calculation, the values presented by Bair and Gomez del campo[18][15] are also from calculation and by West[20] are from measurement	11
4.1	The angle integrated neutron energy spectra for thick targets of silicon at four different α -particle energies[21]	45
4.2	The integral n/α values for thick targets of silicon at four different α -particle energies obtained from literature and from the code NeuCBOT	47
4.3	The angle integrated neutron energy spectra for thick targets of Aluminium at four different α -particle energies[21]	48
4.4	The integral n/α values for thick targets of aluminium at four different α -particle energies obtained from literature and from the code NeuCBOT	50
4.5	The angle integrated neutron energy spectra for thick targets of Magnesium at four different α -particle energies[21]	51
4.6	The integral n/α values for thick targets of magnesium at four different α -particle energies obtained from literature and from the code NeuCBOT	53
4.7	Representation of ${}^9\text{Be}(\alpha, n){}^{12}\text{C}$ reaction Q-value	58

Abbreviations

PEQ	Pre-equilibrium
MSD	Multistep Direct
MSC	Multistep compound
EGSM	Enhanced Generalized Superfluid Model
NAND	National Array of Neutron Detectors
TOF	Time of Flight
ADC	Analog to Digital Converter
CFD	Constant fraction Discriminator
PSD	Pulse Shape Discrimination
DAQ	Data Acquisition

List of Publications

Publications

1. Energy measurement of ^{241}Am - ^9Be neutrons by tagged neutron time-of-flight, **F.S. Shana**, K.S. Golda , N. Saneesh , D. Arora and P. Sugathan. *Applied Radiation and Isotopes*,193(2023) 110655,
2. Secondary neutron production from ^{56}Fe bombarded by ^{12}C ,**A.T. Fathima Shirin Shana**, M.M. Musthafa, A.K. Abdul Gafoor, M.P. Binitha *Oncology and Radiotherapy*,16 (8)(2022)5-8,

Publications Co-authored

1. Entrance channel dependence of quasi fission in reactions leading to ^{206}Po compound nucleus. Hajara, K, M.M. Musthafa, **Fathima Shirin Shana** et al.,*Nuclear Physics A*. 1042. (2023).122789.
2. Evaporation residue cross section measurements for the $\text{Si } 30 + \text{Yb } 176$ reaction. Hajara, K, M.M. Musthafa, **F.S.Shana** et al.,*Physical Review C*. 105. (2022)

Conference Proceedings

1. Gamma gated neutron spectrum from Am-Be source, **A.T.Fathima Shirin Shana**, M.M.Musthafa, A.K.Abdul Gafoor, C .V. Midhun, Divya Arora, N. Saneesh, K.S Golda, P. Sugathan and S.Ganesan,*Proceedings of the DAE Symp. on Nucl. Phys. 64* (2019)

2. Measurement of neutron energy spectrum from ^{241}Am -Be source using CR-39 track detector, **A.T.Fathima Shirin Shana**, M.M.Musthafa, C.V.Midhun, Gokul Das.H, Arun.P.V, *Proceedings of the DAE Symp. on Nucl. Phys.* 66(2022)
3. Probing Pre-equilibrium Neutron Emission in heavy ion reactions at large projectile energies, **A.T.Fathima Shirin Shana**, M.M.Musthafa, C.V.Midhun, *Proceedings of the DAE Symp. on Nucl. Phys.* 67(2024)
4. A study of alpha-induced pre-equilibrium neutron emission in natural Titanium, Gokul Haridas, C V, Midhun, Musthafa, **F.S.Shana** et al., *Advanced Reactor Physics Conference*(2022)
5. Lifetime measurement of $19/2$ isomer in ^{175}Re , Ritu Rani, Anu Rathi, N. Bansal, **F. S. Shana** et al., *Proceedings of the DAE Symp. on Nucl. Phys.* 66(2022)

List of Conference/Workshop attended

1. DST-PURSE supported Satellite Symposia on Physical Sciences, held at Bharathiar University, Coimbatore, Tamil Nadu during September 13-15, 2022.
2. DAE-BRNS Workshop on “Nuclear Reaction data and its compilation for EXFOR database” to be held at Department of Physics, Bharathiar University, Coimbatore, Tamilnadu, India during November 14-18, 2023.
3. DAE Symposium on Nuclear Physics held at Indian Institute of Technology Indore, Madhya Pradesh during December 09-13, 2023.
4. Workshop on Geant4 for Applied Nuclear Physics held at University of Calicut, Kerala during February 19-21, 2024.

Neutron Yield in Thick Targets: Exploring Low and Intermediate Energies and Validating Model Codes

Fathima Shirin Shana.A.T
Research Scholar

Dr. Abdul Gafoor A.K.
Supervisor

ABSTRACT

This research work focused to the detailed evaluation of neutron yield from thick target materials, that covers a broad range of nuclear reactions and simulations. One of the major aspects of this study involved the detailed evaluation of neutron yield at low and intermediate projectile energies, for this, two distinct case studies was carried out both involved neutron emission in thick targets and the validation of nuclear reaction model codes. This was achieved through the utilization of two prominent nuclear reaction model codes, EMPIRE-3.2 and NeuCBOT. These codes served as powerful tools for predicting neutron production across a range of scenarios. In the first case study, the focus is on low-energy neutron emission from thick targets. For this the measurement data of alpha bombardment on various light target materials were collected and their neutron yields were calculated using the NeuCBOT code. The neutron spectra generated by EMPIRE-3.2 and NeuCBOT were subjected to detailed investigation. In order to validate these predictions and ensure their accuracy, an experimental validation of model code was performed with Am-Be (Americium-Beryllium) system, which was selected as a relevant case study. The Am-Be system provided unique insights into the neutron spectra generation under specific conditions, offering a valuable benchmark for the performance of the model codes. In the second case study, our investigations extended into the field of the intermediate energy range, here the code EMPIRE-3.2 was used. This code calculated both ion-induced reactions and pre-equilibrium emission. This study results to understand the effect of Pre-equilibrium contribution in intermediate energy range.

Keywords: Neutron yield, Model code, Neutron spectra, Americium-Beryllium, Pre-equilibrium

Fathima Shirin Shana.A.T



Dr.ABDUL GAFOOR A.K.
Research Guide
P.G Dept. of Physics
Govt. Arts & Science College, Calicut

ന്യൂട്രോൺ യീൽഡ് ഇൻ തിക്ക് ടാർഗെറ്റ്സ്: എക്സ്പോറിംഗ് ലോ ആന്റ് ഇന്റർമീഡിയറ്റ് എനർജിസ് ആന്റ് വാലിഡേറ്റിംഗ് മോഡൽ കോഡ്സ്


ഫാത്തിമ ഷിറിൻ ഷാന.എ.ടി
വിദ്യാർത്ഥിനി


ഡോ. അബ്ദുൾ ഗഫൂർ എ.കെ.
സൂപ്പർവൈസർ

സംഗ്രഹം

വിശാലമായ ന്യൂക്ലിയർ പ്രതികരണങ്ങളും സിമുലേഷനുകളും ഉൾക്കൊള്ളുന്ന കട്ടിയുള്ള ടാർഗെറ്റ് മെറ്റീരിയലുകളിൽ നിന്നുള്ള ന്യൂട്രോൺ യീൽഡ് ന്റെ വിശദമായ വിലയിരുത്തലിലാണ് ഈ ഗവേഷണ പ്രവർത്തനം ശ്രദ്ധ കേന്ദ്രീകരിച്ചത്. ഈ പഠനത്തിന്റെ പ്രധാന വശങ്ങളിലൊന്ന് കുറഞ്ഞതും ഇടത്തരവുമായ പ്രൊജക്റ്റിൽ ഊർജ്ജങ്ങളിൽ ന്യൂട്രോൺ യീൽഡ് വിശദമായി വിലയിരുത്തുന്നതിൽ ഉൾപ്പെടുന്നു, ഇതിനായി, കട്ടിയുള്ള ലക്ഷ്യങ്ങളിലെ ന്യൂട്രോൺ ഉദ്യമനം, ന്യൂക്ലിയർ റിയാക്ഷൻ മോഡൽ കോഡുകളുടെ മൂല്യനിർണ്ണയം എന്നിവ ഉൾപ്പെടുന്ന രണ്ട് വ്യത്യസ്ത കേസ് പഠനങ്ങൾ നടത്തി. രണ്ട് പ്രമുഖ ന്യൂക്ലിയർ റിയാക്ഷൻ മോഡൽ കോഡുകളായ എമ്പയർ-3.2, ന്യൂസിബോട്ട് എന്നിവയുടെ ഉപയോഗത്തിലൂടെയാണ് ഇത് നേടിയത്. വിവിധ സാഹചര്യങ്ങളിലുടനീളം ന്യൂട്രോൺ ഉൽപ്പാദനം പ്രവചിക്കുന്നതിനുള്ള ശക്തമായ ഉപകരണങ്ങളായി ഈ കോഡുകൾ പ്രവർത്തിച്ചു. ആദ്യത്തെ കേസ് പഠനത്തിൽ, കട്ടിയുള്ള ലക്ഷ്യങ്ങളിൽ നിന്നുള്ള കുറഞ്ഞ ഊർജ്ജ ന്യൂട്രോൺ ഉദ്യമനത്തിലാണ് ശ്രദ്ധ കേന്ദ്രീകരിക്കുന്നത്. ഇതിനായി വിവിധ ലൈറ്റ് ടാർഗെറ്റ് മെറ്റീരിയലുകളിൽ ആൽഫ ബോംബാർഡ്മെന്റിന്റെ അളവ് ഡാറ്റ ശേഖരിക്കുകയും അവയുടെ ന്യൂട്രോൺ യീൽഡ് ന്യൂസിബോട്ട് കോഡ് ഉപയോഗിച്ച് കണക്കാക്കുകയും ചെയ്തു. എമ്പയർ-3.2, ന്യൂസിബോട്ട് എന്നിവ ഉൽപാദിപ്പിക്കുന്ന ന്യൂട്രോൺ സ്പെക്ട്രം വിശദമായ അന്വേഷണത്തിന് വിധേയമാക്കി. ഈ പ്രവചനങ്ങൾ സാധൂകരിക്കുന്നതിനും അവയുടെ കൃത്യത ഉറപ്പാക്കുന്നതിനും, അനുയോജ്യമായ കേസ് പഠനമായി തിരഞ്ഞെടുത്ത ആം-ബി (അമേരിസ്യം-ബെറിലിയം) സിസ്റ്റം ഉപയോഗിച്ച് മോഡൽ കോഡിന്റെ പരീക്ഷണാത്മക മൂല്യനിർണ്ണയം നടത്തി. പ്രത്യേക സാഹചര്യങ്ങളിൽ ന്യൂട്രോൺ സ്പെക്ട്രം തലമുറയെക്കുറിച്ച് സവിശേഷമായ ഉൾക്കാഴ്ചകൾ നൽകുന്ന ആം-ബി സംവിധാനം മോഡൽ കോഡുകളുടെ പ്രകടനത്തിന് വിലപ്പെട്ട മാനദണ്ഡം വാഗ്ദാനം ചെയ്യുന്നു. രണ്ടാമത്തെ കേസ് പഠനത്തിൽ, അന്വേഷണങ്ങൾ ഇന്റർമീഡിയറ്റ് എനർജി റേഞ്ചിന്റെ മേഖലയിലേക്ക് വ്യാപിച്ചു, ഇവിടെ എമ്പയർ-3.2 കോഡ് ഉപയോഗിച്ചു. ഈ കോഡ് അയോൺ-ഇൻഡ്യൂസ്ഡ് പ്രതികരണങ്ങളും പ്രി-ഇക്വിലിബ്രിയം എമിഷനും കണക്കാക്കുന്നു. ഇന്റർമീഡിയറ്റ് എനർജി റേഞ്ചിൽ പ്രി-ഇക്വിലിബ്രിയം സംഭാവനയുടെ പ്രഭാവം മനസിലാക്കാൻ ഈ പഠനം കാരണമാകുന്നു.

കീവേഡുകൾ: ന്യൂട്രോൺ വിളവ്, മോഡൽ കോഡ്, ന്യൂട്രോൺ സ്പെക്ട്രം, അമേരിസ്യം-ബെറിലിയം, പ്രി-ഇക്വിലിബ്രിയം

Fathima Shirin Shana.A.T



Dr.ABDUL GAFŪOR A.K.
Research Guide
P.G Dept.of Physics
Govt.Arts & Science College,Calicut

Preface

The nucleus and its characteristics were a mysterious thing to humankind for a long time. Many inventions have resulted from the constant attempt of mankind to explain the complete structure of the nucleus. The foundations of "Nuclear Physics" was set by Dalton's theory of the atomic structure of matter, J.J. Thomson's discovery of the electron, Henry Becquerel's discovery of radioactivity, Rutherford's discovery of the atomic nucleus and the nuclear constituent particles and Chadwick's discovery of the neutron. The study of the nucleus is considered to be started with the discovery of radioactivity by Henry Becquerel in 1896. A nuclear reaction is a tool to study the characteristics of the nucleus and the nature of the force between the nucleons. A nuclear reaction occurs when a projectile nucleus is bombarded with a target nucleus, leading to the emission of particles and/or radiation leaving behind the residual nucleus. The residual nucleus will generally be at an excited energy level. One has the information of the system before the reaction and the system after the reaction but does not have the information of what exactly happening inside a nucleus during the reaction process. This information is drawn from the reaction outcomes. Thus to explain the reaction mechanism, Niels Bohr proposes a satisfactory model for the nuclear reaction. According to this model, the incident particle fuses with the target forming a compound nucleus system by sharing its energy and angular momentum with all the nucleons in the target. The compound nucleus then decays by emitting particles and/or gamma rays. This decay is independent of the mode of formation. This is known as Bohr's compound nuclear mechanism or independent hypothesis. Analysing nuclear reaction in relatively larger energy, it is observed that the compound nuclear reaction theory is valid at relatively lower excitation energies. On the other hand, at very high excitation energies, the direct reaction mechanism will prevail. However, the emission of a particle from the nucleus before attaining

the equilibrium state can be observed in many nuclear reactions induced by fast projectiles and the process is referred to as the Pre-equilibrium Emission. At moderate excitation energies, Pre-equilibrium (PEQ) emission process has been identified as the prominent reaction mechanism. In PEQ mechanism, the projectile may share its energy among a small number of nucleons which may further, interact with other nucleons and during this cascade of nucleon-nucleon interaction through which the projectile energy is progressively shared among the target nucleons and there is a reasonable chance that the particles are emitted long before the attainment of statistical equilibrium.

In order to test the validity of nuclear reaction models and predict the behaviour of unknown system, it is essential to have a large number of data on nuclear reactions covering a large number of nuclei in the periodic table over a wide range of excitation energy. Nuclear reaction data is also important in the fields like Nuclear engineering and Energy production, Medical and Industrial Applications, Astrophysics and Cosmology, Materials Science and Radiation Shielding, etc.

In Nuclear Engineering, data informs reactor design by influencing parameters such as power levels, neutron flux distributions and fuel cycle management. Accurate predictions of neutron yield aid in optimizing reactor efficiency and safety measures. Further data is vital for predicting fuel depletion and burn-up in nuclear reactors. These calculations guide fuel management strategies and ensure efficient reactor operation.

Data is critical for Medical isotope production for radiography, cancer treatment and other medical applications. The data are also employed in non-destructive testing of materials. Neutron yield data aids in designing efficient neutron sources for material analysis, defect detection and quality control.

Further data plays an important role in Stellar Evolution and Nucleosynthesis, Accurate neutron yield data is essential for modeling stellar evolution and understanding nucleosynthesis process.

From the above findings it is well understood the facts that a wide range of studies have been done with nucleon and heavy ion induced reaction regimes. The studies at low and intermediate energies holds immense significance in the areas of both theoretical nuclear physics and practical applications. Hence this thesis aims to solve the complexities of thick target reaction in the low to intermediate energy range.

In the present work a theoretical estimate of neutron yield from thick targets for low and intermediate energy projectile system for different energies has been carried out. The nuclear model codes were used as a tool to compare the results. These nuclear models were used to predict the neutron emission results at various selected incident energies. The models are based on an agreement with the nuclear data available in experimental data library EXFOR. The theoretical code EMPIRE-3.2, NeuCBOT(TALYS+SRIM) and PACE 4 is used in the present work for the code validation.

The present work focuses on two distinct case studies, both involving neutron emission in thick targets and the validation of nuclear reaction model codes. In the first case study, the focus is on low-energy neutron emission from thick targets. This involves a comprehensive comparison of neutron yield predictions obtained from two nuclear reaction model codes, EMPIRE-3.2 and NeuCBOT, with experimental results. The experimental data is derived from α bombardment of several light elements, including boron, carbon, oxygen, fluorine, magnesium, aluminium and silicon at four distinct monoenergetic α -particle energies (4.0, 4.5, 5.0 and 5.5MeV). Furthermore, to generate neutron energy spectra theoretically, a special case of Am-Be source is explored, The neutron yield from Am-Be is evaluated as it is a case of (α,n) reaction. The spectra generated by NeuCBOT, calculates the neutron

yield using TALYS, The mass stopping power are read from a library generated by SRIM. In EMPIRE-3.2 total neutron yield was achieved by integrating the neutron spectra over the range 0-9.37MeV. We computed the straggling and energy loss for alpha particle in Am-Be using SRIM code. It shows the peak corresponding to ground(0MeV), first(4.4MeV) and second-excited states(7.65MeV)respectively. To test the code validation the resultant spectrum from EMPIRE-3.2 code is compared with spectrum generated by Geiger. The code predicted a good spectrum with peaks of n_0 colony around 8MeV and 9MeV. Prominent peaks around 1.9MeV, 2.2MeV and 4.8MeV contribute n_1 colony and the spikes formed from thermal to 1.5MeV results the n_2 colony respectively. This work will be helpful in calibration facilities, in laboratories, shielding and the radiation protection protocols etc.

Furthermore, Inorder to validate these predictions and ensure their accuracy, an experimental validation of model code was also performed using Am-Be source. α -particles from ^{241}Am fuses with ^9Be at an incident α energy of 5.48MeV is measured using TOF method. experiment was performed using one of the BC501A neutron detector from NAND facility, IUAC, New Delhi. The neutron yield obtained from present TOF measurement shows the neutron yield distribution from 0.3 to $\sim 6.5\text{MeV}$. The experimental data have been compared with the standard neutron reference spectrum as well as earlier measured data. In the overlapping energy region of 0.3 - 6.5MeV, our data agrees well with the ISO 8529-2 reference neutron radiation spectrum. As compared to earlier measurements, we have extended the neutron yield measurements down to 0.3MeV and applied neutron detection efficiency correction to the data. With respect to earlier measured data, we observed significant improvement within the energy interval from 0.3 to 3MeV. The technique provides a simple means for characterization of the neutron sources used in calibrating and optimizing the performance of BC501A based neutron ToF facility. The measured data is also compared with EMPIRE-3.2 and NeuCBOT

code, agreement between measured data and EMPIRE-3.2 evaluated spectrum is found to be good between 2.5MeV to 6MeV, the two prominent peaks at 2.8MeV and 4.6MeV are estimated. The comparison with NeuCBOT with TOF spectra is also made. It is found a discrepancy around 2MeV to 5MeV, the way in which Am-Be source are made seems to have an influence on the neutron emission rate in these energy ranges, as the NeuCBOT code works with material composition .

So far we studied on compound reactions within the area of low-energy scenarios. However, as we move into higher energy regimes, we observed a different phase of nuclear reactions, where mechanisms like pre-equilibrium emissions dominates. Here we use the nuclear reaction model code EMPIRE-3.2 as it can account pre-equilibrium contribution. Inorder to study the pre-equilibrium emission, the neutron emission in intermediate energy range has been estimated for different target-projectile systems ^{12}C on ^{56}Fe , ^{27}Al , ^{nat}Ti . The chosen targets are important because these are prominent accelerator structural materials. This study results to understand the effect of PEQ contribution in intermediate energy range. Here we have used the code EMPIRE-3.2 and PACE 4 for estimating neutron yields. We investigated the effect of pre-equilibrium, various level densities and optical potentials in this study. The comparison of the estimated neutron yield from both the reaction model codes EMPIRE-3.2 and PACE 4 with available experimental data has been made. In ^{12}C on ^{27}Al and ^{12}C on ^{nat}Ti , available experimental data were compared with EMPIRE-3.2 and PACE 4 code, the data is found to be in good agreement with theoretical results made using level density model-3 of code EMPIRE-3.2. It has been also observed that the PEQ parameters of the code EMPIRE-3.2 satisfactorily reproduces the result, whereas, the code PACE 4 calculations falls of faster than the EMPIRE-3.2 code because PACE 4 do not have the PEQ model included. For the system ^{12}C on ^{56}Fe available calculated data is compared with the codes with same optimized parameters

of above systems. This comparison allows us to evaluate the reliability of our calculations by expecting experimental data to fall within the same region as our computational results.

Above findings concluded that in low energy neutron emission studies NeuCBOT code gives a better results as it can calculate energy loss in case of thick targets, while in intermediate data neutron emission EMPIRE-3.2 code gives better prediction and simulation as it can calculate for high energy ion projectiles. Also it is understood that at intermediate energy range approx 7 A MeV, the PEQ neutron emission is preferred and PEQ emission increases with increase in energy range. These model calculation would be useful to improve theoretical codes which are based on different models, potentials and phenomenological parameters. These model calculation of neutron emission studies for different structural materials are important for evaluation of nuclear data which are having application in accelerator environment and nuclear energy programmes.

Chapter 1

Introduction

The nucleus and its characteristics were a mysterious thing to humankind for a long time. Many inventions have resulted from the constant attempt of mankind to explain the complete structure of the nucleus. The foundations of "Nuclear Physics" was set by Dalton's theory of the atomic structure of matter, J.J. Thomson's discovery of the electron, Henry Becquerel's discovery of radioactivity, Rutherford's discovery of the atomic nucleus and the nuclear constituent particles and Chadwick's discovery of the neutron. The study of the nucleus is considered to be started with the discovery of radioactivity by Henry Becquerel in 1896[1]. A nuclear reaction is a tool to study the characteristics of the nucleus and the nature of the force between the nucleons. A nuclear reaction takes place when a projectile nucleus hits a target nucleus, leading to the emission of particles or radiation leaving behind the residual nucleus. The residual nucleus will generally be at an excited energy level. One has the information of the system before the reaction and the system after the reaction but does not have the information of what exactly happening inside a nucleus during the reaction process. This information is drawn from the reaction outcomes. Niels Bohr[2] proposed a model, which satisfactorily explains

the reaction mechanism. According to this model, the incident particle fuses with the target forming a compound nucleus system by sharing its energy and angular momentum with all the nucleons in the target. The compound nucleus then decays by emitting particles and/or gamma rays. This decay is independent of the mode of formation. This is known as Bohr's compound nuclear mechanism or independent hypothesis[2]. By analyzing nuclear reactions, it is observed that the compound nuclear reaction theory found to be valid at relatively lower excitation energies only and at higher excitation energies it is found to be not valid. On the other hand, at very high excitation energies, the direct reaction mechanism will prevail[3]. However, the emission of a particle from the nucleus before attaining the equilibrium state can be observed in many nuclear reactions induced by fast projectiles and the process is referred to as the Pre-equilibrium Emission[4]. At moderate excitation energies, Pre-equilibrium (PEQ) emission process has been identified as the prominent reaction mechanism. In PEQ mechanism, the projectile distributes its energy among a limited number of nucleons which then interact with other nucleons and during this nucleon-nucleon distribution the projectile energy is gradually distributed among the target nucleons and there is a reasonable chance that the particles are emitted long before the attainment of statistical equilibrium.

In order to test the validity of nuclear reaction models and predict the behaviour of unknown system, it is essential to have a large number of data on nuclear reactions covering a large number of nuclei in the periodic table over a wide range of excitation energy. Nuclear reaction data is also important in the fields like Nuclear engineering and Energy production, Medical and Industrial Applications, Astrophysics and Cosmology, Materials Science and Radiation Shielding, etc.

In Nuclear Engineering, data informs reactor design by influencing parameters such as power levels, neutron flux distributions and fuel cycle management. Accurate predictions of neutron yield aid in optimizing reactor efficiency and safety measures. Further data is vital for predicting fuel depletion and burn-up in nuclear reactors. These calculations guide fuel management strategies and ensure efficient reactor operation.

Data is critical for Medical isotope production for radiography, cancer treatment and other medical applications. The data are also employed in non-destructive testing of materials. Neutron yield data aids in designing efficient neutron sources for material analysis, defect detection and quality control.

From the above findings it is well understood that a wide range of studies have been done with nucleon and heavy ion induced reaction regimes. The studies at low and intermediate energies holds immense significance in the areas of both theoretical nuclear physics and practical applications. Hence this thesis aims to solve the complexities of thick target reaction in the low to intermediate energy range, employing model codes for validation, thus bridging the gap between theory and experiment.

1.1 Background and Motivation of the study

Nuclear reactions at low and intermediate energies exhibit compound nucleus formation, direct reactions and particle emissions[5, 6, 7, 8]. Nuclear reaction data in thick targets subjected to such interactions provide an understanding on dynamics of these processes. The primary objective of this research are two case studies of neutron emission in low and intermediate energy in thick target scenarios and to develop a comprehensive validation framework for the

nuclear reaction model codes. The central theme of this thesis revolves around three key pillars:

1.Theoretical framework of neutron yield:

An extensive discussion of the theoretical framework governing nuclear reactions in the low to intermediate energy regime with essential concepts and to develop mathematical foundations.

2.Experimental data collection:

A systematic study of (α , n) reactions in thick targets, particularly focusing on the case of Am-Be as the target nucleus and an incident alpha energy of 5.48 MeV. Experimental data will provide a benchmark for model code validation.

3.Model Code Comparison and Validation:

A critical examination of established nuclear reaction model codes, including NeuCBOT, EMPIRE and others, with a detailed comparison of their predictions against the experimental data.

1.2 Overview of the thesis structure

The chapters of this thesis are organized as:

Chapter 2: Literature Review:

This chapter gives a thorough review of existing literature covering thick target neutron yield, nuclear reaction models and validation methodologies.

Chapter 3: Nuclear models and Codes:

This chapter covers an extensive discussion of the theoretical framework governing nuclear reactions in the low to intermediate energy regime, along with an overview of nuclear reaction model codes EMPIRE-3.2, PACE 4,

TALYS and NeuCBOT. This chapter equips with essential concepts and mathematical foundations.

Chapter 4: Thick target neutron yield-Low energy:

This chapter critically evaluates the codes performance. A comprehensive comparison made of the experimental data with predictions from nuclear reaction model codes.

Chapter 5: Measurement of neutron energy from Am-Be:

In this chapter a detailed explanation of the Time Of Flight experimental setup and measurement techniques employed to collect the neutron yield data necessary for validation.

Chapter 6:Thick target neutron yield-Intermediate energy:

In this chapter, a theoretical examination of neutron yield in thick target materials in the intermediate energy range is conducted. The primary focus has been on estimating the contribution of pre-equilibrium (PEQ) emissions of neutron yields.

Chapter 7: Summary and Future works:

This chapter summarizes the research findings, accomplishments and new possibilities for research in the areas of thick target neutron yield measurements and nuclear reaction model codes.

Chapter 2

Literature Review

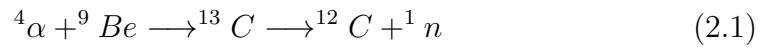
2.1 Nuclear reactions and its importance

A nuclear reaction is found to occur when two nuclei interact with each other. This interactions might be elastic or inelastic. Experimentally it is achieved by bombarding projectiles like proton, neutron, α -particle, γ -ray, photon or a heavy nucleus on a target nucleus[9]. In order to overcome the Coulomb repulsive force between the two nuclei, the projectile should have enough kinetic energy to approach the target nucleus. If the incident energy is below Coulomb barrier, a nuclear reaction will not take place. The interaction occurs within an inter nuclear distance of 10^{-14} m. The energy and angular momentum exchange may take place between the nuclei during the interaction stage and a compound nucleus is formed. This nucleus de-excite by the emission of one or more nucleons leaving behind the residual nucleus or emit radiation.

2.2 Thick target reactions and their relevance

The primary objective of this research is to evaluate the (α, n) reactions in thick target scenarios to study the low energy range and to study the neutron emissions in intermediate energy range to understand the pre-equilibrium emission and develop a comprehensive validation framework for the nuclear reaction model codes.

A comprehensive literature survey on the ${}^9\text{Be}(\alpha, n)$ reaction was made. Normally Be is chosen to get maximum neutron yield. Here the neutron is produced through the reaction;



Other light elements like Li, B and F can be used otherthan Be, while Be yields the greatest neutron output per α -particle Table. 2.1 [10] shows the Neutron yield of some (α, n) sources

TABLE 2.1: Neutron yield of some (α, n) sources[10]

α -emitter	Target	Reaction	Q-Value	Neutron yield per α
${}^{241}\text{Am}$	B	${}^{10}\text{B}(\alpha, n)$	+1.07 MeV	1.3×10^{-5}
${}^{241}\text{Am}$	F	${}^{19}\text{F}(\alpha, n)$	-1.93 MeV	4.1×10^{-6}
${}^{241}\text{Am}$	Be	${}^9\text{Be}(\alpha, n)$	+5.71 MeV	7.0×10^{-5}
${}^{238}\text{Pu}$	C	${}^{13}\text{C}(\alpha, n)$	+2.2 MeV	1.1×10^{-5}
${}^{210}\text{Po}$	Li	${}^7\text{Li}(\alpha, n)$	-2.79 MeV	1.0×10^{-6}

TABLE 2.2: The activity, neutron emission in n/s for Am-Be

Activity	Emission neutron n/s
1mCi	2.2×10^3
10mCi	2.2×10^4
100mCi	2.2×10^5
1Ci	2.2×10^6
10Ci	2.2×10^7

Am-Be source is the most popular amongst various (α, n) sources due to its low γ -dose rate and long half life(458 y). Also it is widely employed as a calibration source for neutron instrumentation. The activity, emission neutron n/s and dimension is given in Table. 2.2

Neutron energy spectrum of an Am-Be source using gamma gated NTOF technique was measured in 1998, in that study the neutron groups populated the 2+ states and higher states were identified[11]. Furthermore the neutron energy spectra observed using time of flight technique agrees qualitatively with calculated energy spectra by Geiger and Van Der Zwan in 1975[12].

When α particles of energy E_α bombarded on thick targets, the resulting neutron yields $Y(E_\alpha)$ is evaluated from available (α, n) cross sections $\sigma(E_\alpha)$ with linear stopping powers $dE_\alpha/dx(E_\alpha)$, of the α particles in the target material by the equation:

$$Y(E_\alpha) = \rho \cdot \int_{E_\alpha}^0 \sigma(E_\alpha) \frac{1}{dE_\alpha/dx(E_\alpha)} \cdot dE_\alpha \quad (2.2)$$

where ρ is the atomic density.

Liskien and Paulsen [13][14] presented findings derived from computations involving elements such as Lithium, Beryllium, Boron, Carbon, Nitrogen, Oxygen, Fluorine, Neon, Magnesium, Aluminium and Silicon. They also examined Uranium compounds, including UC, UO₂ and UF₆, across alpha-particle energy levels spanning from the threshold to 7 MeV. The outcomes indicated an average uncertainty of approximately 30%, inferred from variations in linear stopping powers and cross-sectional data.

Thick target (α,n) yields were experimentally measured using 4π flat response moderator detectors, where the target is placed at the center of the moderator and the Van de Graaff accelerators produced the α -particles. Bair and Gomez del Campo [15] measured thick targets of ⁶Li, ⁷Li, Li, Be, ¹⁰B, ¹¹B, B, ZnF₂, PbF₂, Mg, Al, Si and ²⁸SiO₂ for α -particle energies in the range from 3 to 9 MeV with a typical uncertainty of 5%. They measured with eight SF₃ counters were embedded close to the surface of a 1.5 m diameter spherical graphite moderator[16]. They also reported calculated yields for the compounds UO₂ and UC. Macklin and Gibbons[17]and Bair [18] measured thick target neutron yields for carbon. The yields were measured with the same detector as used by Bair and Gomez del Campo.

West and Sherwood [19][20] measured α on thick targets of Be, BeO, BN, C, Mg, Al, Si, Fe, Zr, UC, UO₂ and stainless steel for α -particle energies 3.6 to 10 MeV with a typical uncertainty of 1.5%. They performed experiment with a cylindrical polythene moderator (diameter 1.0 m, length 1.0 m) with nine ³He counters at a particular known distances from the axis. A systematical uncertainty in the yield data occurs due to lack of information about neutron energy spectra. This is pointed out by Bair and Gomez del Campo[15].

Data for thick target (α,n) yields obtained from the above mentioned calculations and experiments, which are comparable with results presented in this thesis, are shown in Table. 2.3

TABLE 2.3: Thick target(α,n) neutron yields per 10^7 α -particles reported in the literature[21], The results of Liskien and Paulsen[13][14] were obtained from calculation, the values presented by Bair and Gomez del campo[18][15] are also from calculation and by West[20] are from measurement

$E_\alpha(MeV)$	B	C	O	F	Mg	Al	Si	BN	UO ₂	References
4.0	100	0.37	0.13	7.9	1.0	0.19	0.10	–	0.040	
4.5	170	0.42	0.24	19.0	2.7	0.87	0.31	–	0.072	[13]
5.0	240	0.53	0.36	39.0	5.8	2.9	–	–	0.11	[14]
5.5	–	1.1	0.51	–	–	7.4	–	–	0.15	
4.0	62	0.42	–	8.8	0.77	0.169	–	–	0.050	
4.5	106	0.48	–	21.6	2.63	0.802	0.16	–	0.107	[18]
5.0	156	0.63	–	43.9	6.44	2.64	0.52	–	0.164	[15]
5.5	206	1.08	–	77.5	12.6	6.97	1.14	–	0.236	
4.0	–	0.43	–	–	0.83	0.166	0.040	28.8	0.049	
4.5	–	0.50	–	–	2.93	0.812	0.156	42.3	0.103	[20]
5.0	–	0.65	–	–	7.04	2.81	0.565	62.6	0.157	
5.5	–	1.12	–	–	13.7	7.56	1.24	90	0.221	

More over the neutron yield from thick target heavy ion interaction is also considered. The data is important for neutron dosimetry, shielding design of accelerators and medical applications. Modern carbon ion therapy uses high energy ^{12}C beam for medical therapy and the design and operation of

such accelerator facility require accurate knowledge on neutron shielding due to background neutrons produced by beam hitting on surfaces. The present work discusses about the neutron yield from thick targets of ^{56}Fe , ^{27}Al and ^{nat}Ti when bombarded by ^{12}C . Since these targets are widely used in building accelerators and cavities.

However, it is understood that at high beam energy, the pre-equilibrium neutron emission is preferred and pre-equilibrium neutron emission was observed even at 7.2 A MeV for the reaction ^{16}O on ^{181}Ta thick target by Nandy et.al[22]. Energy distributions of emitted neutrons were measured at 0° , 30° and 60° with respect to the beam direction using the proton recoil scintillation technique. The results from equilibrium and Pre-equilibrium (PEQ) nuclear reaction models compared provided the emission of PEQ neutrons at this projectile energy. This model also shows that PEQ emissions occurs only before any scattering between target and projectile nucleons start.

C.Sunil et.al[23] measured energy distributions of emitted neutrons for 110 MeV ^{19}F ions bombarding thick ^{27}Al target. He made the measurements at 0° , 30° , 60° , 90° and 120° employing time-of-flight technique using scintillation detector. The data compared with calculated results from equilibrium nuclear reaction model codes like PACE 2 and EMPIRE-3.2 using various level density options. In another work, the angle-integrated energy distribution of neutron dose was calculated for ^{12}C incident on Ag and Ti targets at 12 A MeV[24]. It was observed that for both the reactions the calculated dose under predicted the measured values below 22 MeV neutron energy. At higher energies, the agreement is good for Ti target, but for Ag target experimental data are slightly over predicted by the calculations. J.Acharya et.al[25] measured emission spectra at beam energies of 130, 140, 145, and 150 MeV for

^{19}F -induced reactions on ^{181}Ta , ^{89}Y and ^{51}V . Measurements were performed with liquid scintillator detectors kept at eight angles ranges from 25-143 degrees using time-of-flight and pulse-shape discrimination. He made comparison with ALICE 2014 and PACE 4 calculations to study the role of breakup and pre-equilibrium effects. Predictions with ALICE 2014 without adjusting the parameters gives a good agreement with the measured data. Comparison with PACE 4 brings out the contributions arising from pre-equilibrium effects. Neutron multiplicity distribution at high energy heavy ion collision have been measured by Holub[26] and Hilsher et.al[27]. The neutron detector array at IUAC have also been extensively used for neutron multiplicity from fission induced by heavy ions[28][29][30]

A comparison between different codes to calculate neutron yields and spectra and experimental data has been given in several papers[31][32][33][34].

2.3 Gaps in the literature and need of this work

There are many works reported in literature on thick target (α, n) energies [22][23][24][25]. The available data are still inadequate to provide additional inputs to test the accuracy and validity of the reaction models used in most popular reaction codes. More over the neutron yield from thick target ion induced data in intermediate energy range are very few to generate a systematic and consistent description of the dynamics of pre-equilibrium reactions and its dependence on projectile energy. There are very less comparison with model codes that brings out the contributions arising from pre-equilibrium effects.

In the light of these findings from national and international researchers, we studied the thick target (α, n) yield and pre-equilibrium contribution in neutron emission in ion induced reactions at intermediate beam energies and analysed data based on nuclear reaction models.

Chapter 3

Basic Theory and Model Codes

A set of well-designed nuclear reaction models is necessary to theoretically explain experimental results. Various researchers have used them as a foundation. The international nuclear community has used them as a foundation and developed many nuclear codes that can predict nuclear data using computer programming. However, it is also essential to validate the codes by comparing the experimental data with the data predicted by the codes. The nuclear modular codes NeuCBOT, TALYS, EMPIRE-3.2, PACE 4, codes have been used in the present study. The following sections provide a brief discussion of the various reaction models.

3.1 Reaction mechanism

On the basis of the energy range of the incident particles, there are three common nuclear reaction mechanisms: (1) Compound nuclear reaction mechanism, (2) Direct reaction mechanism and (3) Pre-equilibrium reaction mechanisms. This are shown in Fig. 3.1. Fig. 3.2 shows how these reaction processes work as reaction products in relation to projectile energy.

A brief description of the compound nuclear reaction theory and some of the compound nuclear mechanism and pre-equilibrium mechanisms which were actually used in the statistical theoretical model codes are explained in the following sections.

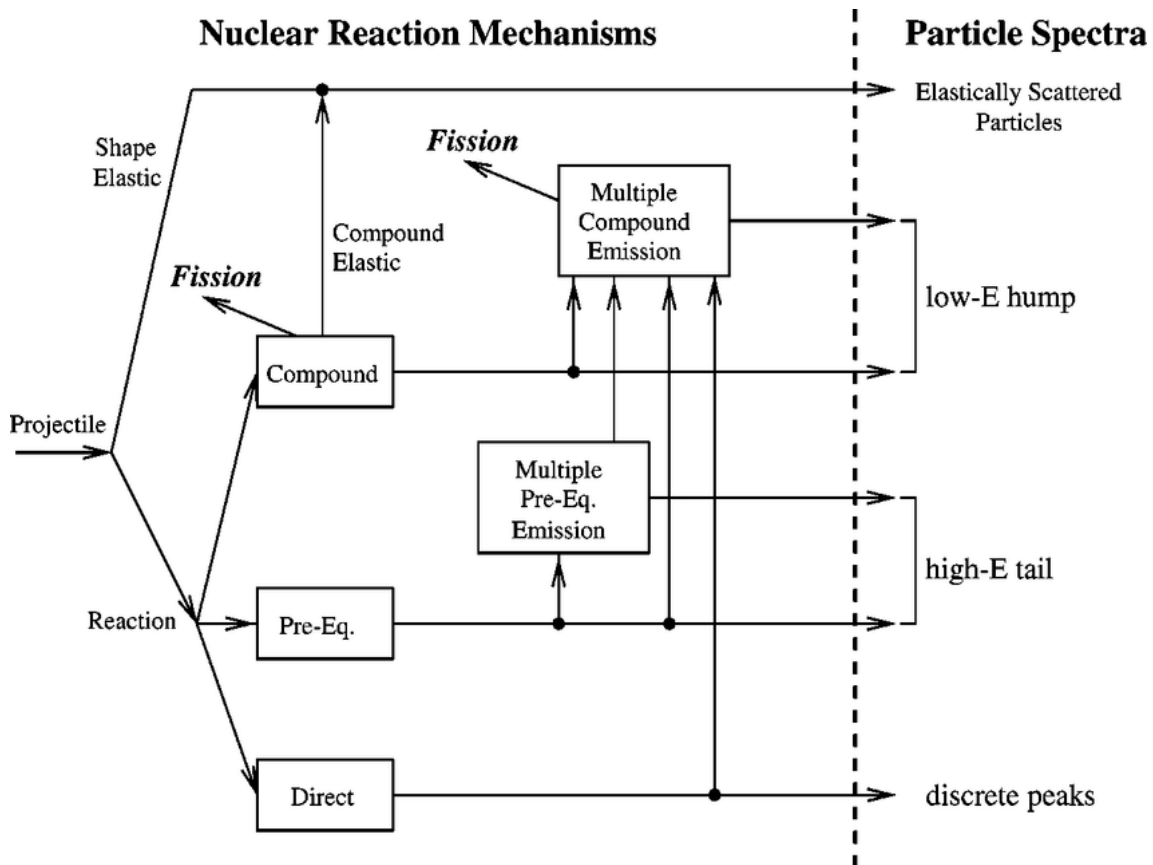
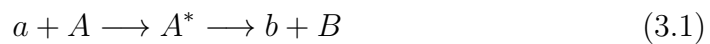


FIGURE 3.1: Nuclear reaction mechanisms



3.2 Direct Reaction

The direct reaction occurs the lowest time, 10^{-22} s, which is nearly the same as a particle passing through a nucleus. An incident particle takes one or more nucleon from the target nucleus or it may lose its constituent particles in the

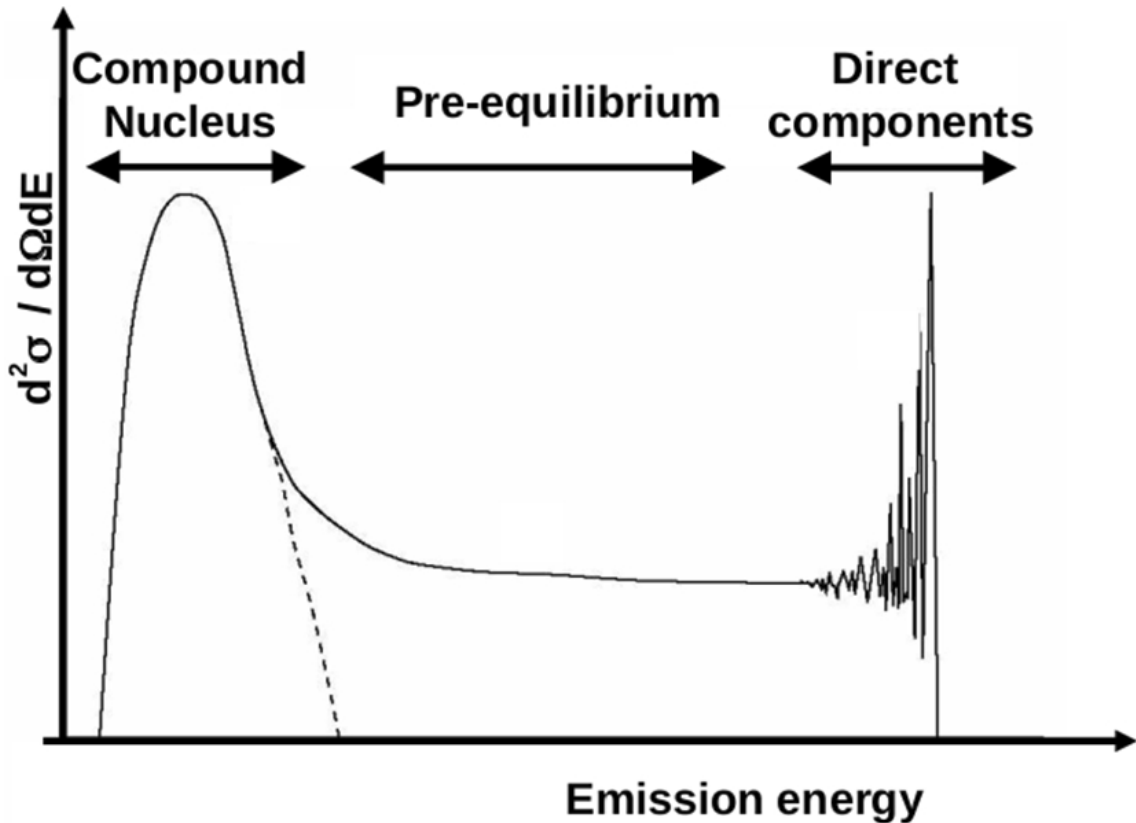


FIGURE 3.2: Nuclear reaction cross section with separation of the three reaction mechanisms depending on the emission energy

target. The former reaction is known as pick up, whereas the latter is known as stripping. In inelastic scattering, a particle just interacts, gets or loses energy and then ejects a particle. The reaction is likely to occur if the particle's energy (>10 MeV). The associated angular distributions in the direct reaction mechanism exhibit a significant peak in the forward direction. One useful method for understanding the direct reaction process is the couple channelled approach or Distorted Wave Born Approximation (DWBA). Here are some examples of direct reactions:

Stripping reaction: $A(d, n)B$, $A(d, p)C$, etc.

Pick up reaction: $X(n, d)Y$ or $X(n, t)Z$, etc.

Inelastic scattering: $A(n, n')A$.

3.3 Compound nucleus mechanism

Bohr (1936)[1] provided an explanation of this reaction mechanism. A low energy particle or nucleon that hits and penetrates a target nucleus shares all of its kinetic energy among all of the target nucleons. As a result, the nucleus, which was previously in the ground state, is currently excited due to an excess of energy. The mean lifetime of this equilibrium state is extremely short, approximately 10^{-16} s. After that, it decomposes, releasing a residue and an ejectile. Suppose a nucleon "a" hits a target "A," and before it produces the products "b" and "B," the compound nucleus "A*" has formed. The Weisskopf-Ewing and Hauser-Feshbach models both incorporate the compound nucleus mechanism[35, 36]. The reaction mechanism can be categorized into 2 steps; The first stage involves the formation of the compound nucleus and the second stage involves its decay. The compound nucleus, which is in the excited state, is formed by the energy lost by the projectile in the target nucleus. The second stage involves the release of more energy by the ejection of particles or electromagnetic radiation.

3.3.1 Weisskopf-Ewing theory

Breit-Wigner theory describes how compound nuclear states are excited at low energy by resonance through individual states. [37] for the process's absorption cross section $\alpha \rightarrow \beta$ at the resonance energy E_r , having corresponding total width, partial width of formation and decay Γ , Γ_α , Γ_β respectively. The statistical factor g , accounts the spin of particles forming the resonance and

the total angular momentum J .

$$\sigma_{\alpha\beta}(E) = \frac{\Pi}{k^2} \frac{g\Gamma_\beta\Gamma_\alpha}{(E - E_r)^2 + \frac{\Gamma^2}{4}} \quad (3.2)$$

$$g = \frac{(2J + 1)}{(2S_\alpha + 1)(2S_\beta + 1)} \quad (3.3)$$

One can write:

$$\sigma_{\alpha\beta} \sim \sigma_{CN}(C) \frac{\Gamma_\beta}{\Gamma} \quad (3.4)$$

$$\Gamma = \sum_{\alpha} \Gamma_{\alpha} \quad (3.5)$$

$$\Gamma_{\alpha} \propto g_{\alpha} k_{\alpha}^2 \sigma_{CN} \quad (3.6)$$

So finally the cross-section can be written as:

$$\sigma_{\alpha\beta} = \sigma_{CN}(C) \frac{g_{\beta} k_{\beta}^2 \sigma_{CN}(\beta)}{\sum_{\alpha} g_{\alpha} k_{\alpha}^2 \sigma_{CN}(\alpha)} \quad (3.7)$$

If the ejectile's energy falls between E_{β} to $E_{\beta} + dE_{\beta}$ keeping the residual system in the energy range of U_{β} to $U_{\beta} + dU_{\beta}$, then $U_{\beta} = E_{CN} - B_{\beta} - E_{\beta}$. Since, $k^2 = 2\mu E$,

$$\sigma_{\alpha\beta}(E_{\beta})dE_{\beta} = \sigma_{CN}(C) \frac{(2I_{\beta} + 1)\mu_{\beta}E_{\beta}\sigma_{CN}(\beta)\omega(U_{\beta})dU_{\beta}}{\sum_c \int (2I_{\alpha} + 1)\mu_{\alpha}E_{\alpha}\sigma_{CN}(\alpha)\omega(U_{\alpha})dU_{\alpha}} \quad (3.8)$$

Where, μ_{β} is the ejectile's reduced mass. This is the angle integrated cross-section in Weisskopf-Ewing form.

3.3.2 Hauser-Feshbach theory

Reaction cross sections with large number of complex nuclear states are described by Hauser-Feshbach theory. The cross section is expressed as the product of two factors, the cross section σ_a for the compound nucleus formation and the probability P_b for the decay into channel b:

$$\sigma_{ab} = \sigma_a P_b \quad (3.9)$$

At a given orbital angular momentum l , the compound nucleus formation cross section is given by

$$\sigma_a = \pi \lambda_a^2 (2l + 1) T_a \quad (3.10)$$

Where λ_a is the reduced wavelength in the incident channel, T_a is the transmission coefficient

$$T_a = 1 - |S_{aa}|^2 \quad (3.11)$$

Where S_{aa} is the average S-matrix. Decay probability can be expressed in terms of transmission coefficient as

$$P_b = \frac{T_b}{\sum_c T_c} \quad (3.12)$$

Thus obtained,

$$\sigma_{ab} = \pi \lambda_a^2 (2l + 1) \frac{T_a T_b}{\sum_c T_c} \quad (3.13)$$

Where T_a and T_b are the transmission coefficient of incident and exit channel and T_c is the collective transmission coefficient for all exit channels. Considering the interacting particle with spin, the spin of the projectile and the spin of the target combined to form the spin of channel 's', which in turn

combine with orbital angular momentum l to form the total nucleus angular momentum J . In the case of the outgoing channel, the probability of getting particular 's' is given by,

$$P_s = \frac{(2s + 1)}{(2i + 1)(2I + 1)} \quad (3.14)$$

Similarly, the probability of s combining with l to give J is

$$P_J = \frac{(2J + 1)}{(2s + 1)(2l + 1)} \quad (3.15)$$

Weighting the partial waves by $(2l+1)$ the crosssection becomes

$$\sigma_{ab} = \pi \lambda_a^2 \sum_{J\pi} \frac{(2J + 1)}{(2s + 1)(2l + 1)} \frac{T_a T_b}{\sum_c T_c} \quad (3.16)$$

Where π is the parity of compound state, The transmission coefficient depends on angular momenta l, s and J .

3.4 Pre-equilibrium Reaction

In the process of compound nucleus, a nucleus enters a transient equilibrium stage before decaying, whereas there is no equilibrium in the direct response mechanism. The pre-equilibrium process is the stage of the process where the nucleus decays into reaction products before achieving complete statistical equilibrium. The experimental observations that unable to properly explained by the compound nucleus or direct reaction mechanism discovered in the 1950s. These data were in the moderate energy range. It implies that a third mechanism, the pre-equilibrium, could exist somewhere in between these two. This

process is significant between 10 MeV to 200 MeV. According to the mechanism, the nucleus enters a series of excited states and generates a complex energy structure, but before it reaches a statistically stable stage with a specific angular momentum, it decays. Two semi-classical models from Griffin (1966) and Kalbach (1973), called the exciton model and the hybrid model, respectively, can be used to describe this mechanism[38, 39]. The quantum mechanical explanations are given by Feshbach, Kerman and Koonin by developing the Multi-step direct reaction (MSD) and Multi-step compound (MSC) reaction mechanism.

3.4.1 Exciton model

This model expects that the projectile by interacting with the target, gives rise to a simple arrangement distinguished by a few number of excitons ($n=p+h$), which are excited particles and holes. The basic exciton model[38] is shown in Fig. 3.3. For a nucleus with excitation energy E_c , the partial level density at exciton number n can be expressed as follows:

$$\rho_n(E) = \frac{g^n E^{n-1}}{p!h!(p+h-1)!} \quad (3.17)$$

where, g is the single particle level density and p and h are the number of excited particles and holes respectively. It is seen that for small value of n , the level density function increases quickly and hence the rate of transition $\Delta n = 2$ is larger than the $\Delta n = -2$. As n increases the particle level density moderately levels off. At $n = \bar{n}$, the exciton number becomes constant and there are as many $\Delta n = 2$ transitions as $\Delta n = -2$ until equilibrium is finally established. Then the energy differential pre-equilibrium cross-section $\sigma_{PEQ}(E)$, is the sum

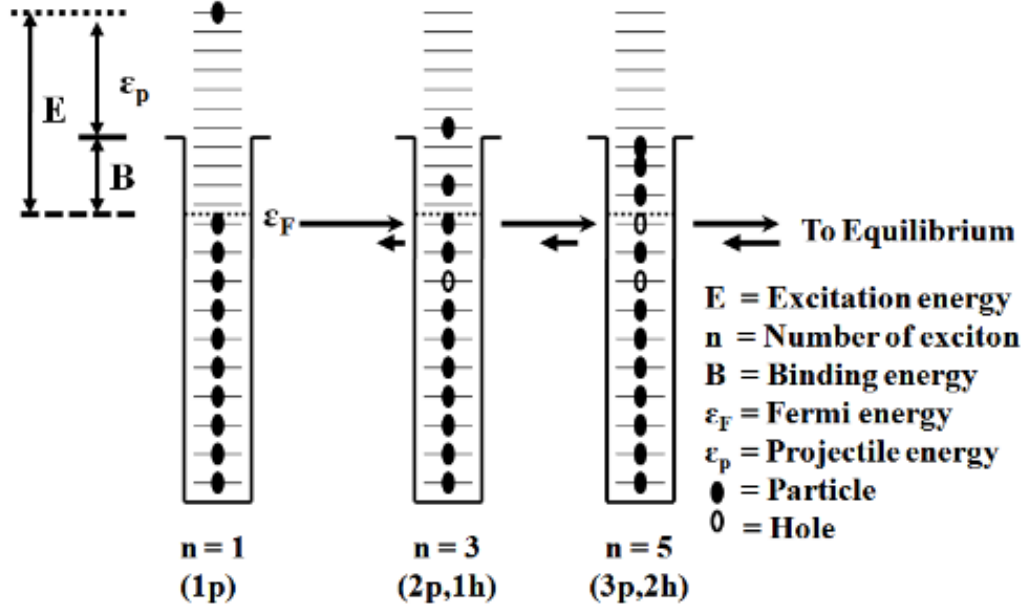


FIGURE 3.3: Schematic diagram of behaviour of particle and holes in exciton model.

of the cross-sections from each exciton state:

$$\sigma_{PEQ}(E) = \sigma_{abs} \sum_{\substack{\bar{n} \\ n=n_0 \\ \Delta n=2}} D_n, P_n(E) \quad (3.18)$$

where, σ_{abs} is the projectiles absorption cross-section by the target. D_n refers the probability of reaching the n exciton state (the depletion factor). $P_n(E)$ refers the ejectiles emission probability with energy E from the n exciton state. If the projectile is a nucleon the summation begins from the initial exciton number n_0 which is 3. In the case of cluster projectiles n_0 is commonly assumed to be equivalent to the number of nucleons in the projectile plus 2 (1 excited particle + 1 hole)

The depletion factor D_n is given by [109],

$$D_n = \prod_{\substack{n'=n_0 \\ \Delta n=2}}^n \left[1 - \int dE P_{n'}(E) \right] \quad (3.19)$$

The emission probability, $P_n(E)$, is defined as the ratio of the emission rate with energy E from exciton state n to the rates of all transitions (collision + emission) from n at all energies. If $\lambda_n^c(E)$ is the emission rate from n exciton state to definite channel c with energy E and the emission from $n = +2, -2$ and 0 transitions are λ_+^n , λ_-^n and λ_0^n respectively. Then the emission probability can be defined as:

$$P_n(E) = \frac{\lambda_c^n(E)}{\lambda_+^n + \lambda_-^n + \lambda_0^n + \int dE \lambda_c^n(E)} \quad (3.20)$$

Hence, to obtain $P_n(E)$ the emission rates are summed over all E in the denominator. The general expression for the emission rate is:

$$\lambda_c^n(E) = \frac{\rho_{n'}(U)}{\rho_n(E_c)} \frac{(2s+1)m\epsilon\sigma_{inv}(\epsilon)}{\pi^2\hbar^3} \quad (3.21)$$

where, n' is the exciton number following the ejectiles emission with ν nucleons: $n' = n - \nu$, U is the excitation energy of residue given by $U = E_c - B - \epsilon$ with B the ejectile separation energy, s and m are the intrinsic spin and the reduced mass of the ejectile and $\sigma_{inv}(\epsilon)$ is the inverse cross-section, i.e., the cross-section of the time-reversed process of ejectiles absorption by the residual nucleus.

3.4.2 Hybrid model

The hybrid model calculates PEQ energy-differential cross-section $\sigma_{PEQ}(a; x, \epsilon)$ of a nucleon x (x : proton or neutron) as sum of energy-differential cross-sections from each exciton state n :

$$\sigma_{PEQ}(a : x, \epsilon) = \sigma_{abs}(a) \sum_{\substack{n=n_0 \\ \Delta n=2}}^{\bar{n}} D_n P_n^x(\epsilon) = \sum_{\substack{n=n_0 \\ \Delta n=2}}^{\bar{n}} D_n \sigma_n(a : x, \epsilon) \quad (3.22)$$

$P_n^x(\epsilon)$ is the probability of emission of x-type ejectile from n-exciton state with energy ϵ . $P_n^x(\epsilon)$ can be written as,

$$P_n^x(\epsilon) = \left[f_n^x \cdot P_n(x, \epsilon) \right] P_c^n(x, \epsilon) \quad (3.23)$$

Where f_n^x denotes the number of x type of exciton in the n exciton state, P_n^x is the probability of x having energy ϵ in the n-exciton state. This can now write as:

$$\sigma_n(a : x, \epsilon) = \sigma_{abs}(a) \left[\frac{f_n^x \rho_n(U, E)}{\rho_n(E_c)} \right] P_c^n(x, \epsilon) \quad (3.24)$$

The ratio $\rho_n(U, E)/\rho_n(E_c)$ gives the probability of the number of excitons in a particular state. The emission probability $P_c^n(x, \epsilon)$ is,

$$P_c^n(x, \epsilon) = \frac{\lambda_c^n(x, \epsilon)}{\lambda_c^n(x, \epsilon) + \lambda_t^n(\epsilon)} \quad (3.25)$$

Substituting this in above equation the hybrid model expression becomes

$$\sigma_{PEQ}(a : x, \epsilon) = \sigma_{abs}(a) \sum_{\substack{\bar{n} \\ n=n_0 \\ \Delta n=2}}^{\bar{n}} D_n \left[\frac{f_n^x \rho_n(U, E)}{\rho_n(E_c)} \right] \frac{\lambda_c^n(x, \epsilon)}{\lambda_c^n(x, \epsilon) + \lambda_t^n(\epsilon)} \quad (3.26)$$

The emission rate can be expressed as,

$$\lambda_c^n(x, \epsilon) = \frac{2m\epsilon\sigma_{inv}(\epsilon)}{g\pi^2\hbar^3} \quad (3.27)$$

Also,

$$\lambda_t^n(x, \epsilon) = \left[1.4x10^{21}(\epsilon + S_x) - 6x10^{18}(\epsilon + S_x)^2 \right] k^{-1}sec^{-1} \quad (3.28)$$

3.4.3 Multi-step Direct (M.S.D) and Multi-step Compound (M.S.C) Model

Feshbach, Kerman and Koonin (FKK) proposed the break-up of the pre-equilibrium emission spectra into Multi-step direct (MSD) and Multi-step compound (MSC) components in their quantum mechanical theory of pre-equilibrium reactions. The Multi-step Direct (M.S.D) model based on the theory that at every excitation there should be a minimum of one particle in the continuum and so there is a finite probability of particle emission per stage. Obviously, the M.S.D model works only in the first few interactions only when the particle just enters the nucleus. The particle momentum is in the direction of the projectile and hence it is peaked in the forward direction.

After a few number of two-body interactions it shares complete energy and momentum, the energy per particle is small, while the excited number of particles will be higher. Also, at this stage there is no particle in the continuum, but the statistical fluctuation in energy will provide a particle in the continuum. Hence the direction of emission will be either isotropic or symmetric about 90. This corresponds to the Multi-step Compound (M.S.C) nucleus formation, where there is an equilibrium in energy sharing has taken place but the energy per particle in each state is less. In this way this theory of pre-equilibrium explained the energy sharing process through two non interacting chains called P-chain (At least one particle is in the continuum) and Q-chain (All the particles are in the bound state). The MSD and MSC components can be evaluated separately since the P-chain and the Q-chain do not interfere with one another. Their sum is the overall pre-equilibrium cross-section:

$$\sigma_{PEQ}(\epsilon) = \sigma_{MSD}(\epsilon) + \sigma_{MSC}(\epsilon) \quad (3.29)$$

In the FKK theory, $\sigma_{MSD}(\epsilon)$ and $\sigma_{MSC}(\epsilon)$ are calculated quantum mechanically. $\sigma_{MSD}(\epsilon)$ is evaluated by partitioning the partial level densities into bound and unbound states of densities. The exciton model calculates $\sigma_{PEQ}(\epsilon)$ and after evaluating $\sigma_{MSD}(\epsilon)$ the $\sigma_{MSC}(\epsilon)$ component is obtained by subtracting $\sigma_{MSD}(\epsilon)$ from $\sigma_{PEQ}(\epsilon)$.

In calculating $\sigma_{PEQ}(\epsilon)$ D_n is defined as the probability of reaching the n-exciton state without any prior particle emission. However, different combinations of excited particles and holes may result in the same n. Therefore $S_u(p, h)$ is employed instead of D_n which is the probability of reaching a (p,h) configuration with at least one excited particle in the unbound state. D_n is given by, $D_n = S_u(p, h) + S_b(p, h)$ where $S_b(p, h)$ represent the probability of all the particle in the bound state, which doesn't lead to emissions.

Now the equation for σ_{PEQ} can be written as:

$$\sigma_{PEQ} = \sigma_{abs} \sum_{p=p_0}^{\bar{p}} S_u(p, h) T_u(p, h) \lambda_c^u(p, h, \epsilon) \quad (3.30)$$

The quantities $S_u(p, h)$, $T_u(p, h)$ have been calculated quantum mechanically by Kalbach[40].

3.5 Optical Model

A significant amount of "projectile-target" reaction data has been successfully interpreted by the nuclear optical model in terms of the complex interaction potential. During a nuclear reaction, the two nuclei interact, and all of the other nucleons in the system combine to produce a single nucleon. If a system has N nucleons, then subsequently N Schrödinger's equations are needed to describe the system. In order to solve the equations, It is necessary to have

the suitable form of potential. This potential is considered complex in the optical model, which is having real part and an imaginary part. It is considered that the incident particle's interaction with the nucleus constitutes an optical phenomenon. Any obstacles in the path of an electromagnetic wave cause it to be diffracted or refracted when it moves from one medium to another. The nucleus also diffracts the incident particle wave in the similar way. As a result, the total potential $V(r)$ has a real portion that represents the diffraction phenomena and an imaginary part that represents the refraction part. The potential is represented by the following equation, with real part $U(r)$ and imaginary part $W(r)$

$$V(r) = U(r) + jW(r) \quad (3.31)$$

The model was proposed by Bethe(1937)[41], which was explored by Feshbach (1954)[36] in order to apply to neutron-induced nuclear processes. Optical model is effective and reliable in explanation for most of the experimental data. This model has been modified as per the requirements from time to time.

3.6 Nuclear level densities

According to quantum mechanics, energy is quantized, resulting in energy states. Nuclear level density refers to the energy states per unit energy interval. This parameter plays significant role in the nuclear reaction mechanism. Bethe has done significant work in the field of nuclear level density in 1936. The space between energy levels becomes smaller as density increases. If it is infinite, the state should be a continuum. This parameter has played a significant role in the development of nuclear modular codes. Various level density models are provided in the EMPIRE-3.2 code[42]. The validity of these model code

has been evaluated and described in Chapters 5 of the present study. Each model for level density is described briefly here. Five models are featured in the most recent version of EMPIRE-3.2. Bethe provided the basic formula for level density which is given below.

$$\Delta E^{ex} = \frac{1}{\rho(E^{ex})} \quad (3.32)$$

Where, ΔE^{ex} represents the energy interval and $\rho(E^{ex})$ denotes the level density.

According to this, a nucleus can be considered as a gas of nucleons, with each nucleon occupying a distinct energy level based on the nucleus' temperature. Thus, the nuclear level density can be written as

$$\rho(E^{ex}) = ce^{2\sqrt{aE^{ex}}} \quad (3.33)$$

Where c indicates proportionality constant, a is the level density parameter and E^{ex} represents the excitation energy of the compound nucleus. In order to make the calculated data match with the experimental data, the parameter a is adjusted. This model is also regarded as a constant temperature model as well. This basic idea is used to modify the other level density models.

3.6.1 Composite Gilbert-Cameron model

In 1965 Gilbert Cameron[43] modified the constant temperature level density formula as,

$$\rho_T(E) = \frac{1}{T} \exp\left[\frac{E - \Delta - E_0}{T}\right] \quad (3.34)$$

Where T denotes temperature, E denotes excitation energy, δ is the pairing energy and E_0 is an adjustable energy shift and the Fermi gas formula is used when the excitation energy E exceeds the matching point energy U_x .

$$\rho_f(U) = \frac{\exp(2\sqrt{aU})}{12\sqrt{2}\sigma^2(U)a^{\frac{1}{4}}U^{\frac{5}{4}}} \quad (3.35)$$

Where, σ^2 is spin cut of parameter, the level density parameter a is given by

$$\tilde{a}(U) = a \left(1 + \delta W \frac{1 - \exp(-\gamma U)}{U} \right) \quad (3.36)$$

Where, \tilde{a} is the asymptotic level density parameter, W is the shell correction energy and δW is the damping parameter. The parameter for asymptotic level density is given by

$$\tilde{a} = \alpha A + \beta A^{\frac{2}{3}} \quad (3.37)$$

Where A is the mass number, α and β are the global parameters.

3.6.2 The Back-shifted Fermi Gas Model

In this theoretical model, the pairing energy is regarded as an adjustable parameter[44]. Up to 0 MeV, the fermi gas expression is applied. The overall density is:

$$\rho_F^{tot}(E_x) = \frac{1}{\sqrt{2\pi}\sigma} \frac{\sqrt{\pi} \exp(2\sqrt{aU})}{12 a^{\frac{1}{4}}U^{\frac{5}{4}}} \quad (3.38)$$

And the level density is,

$$\rho_F(E_x, J, \pi) = \frac{1}{2} \frac{2J+1}{2\sqrt{2\pi}\sigma^3} \exp \left[\frac{(J + \frac{1}{2})^2}{2\sigma^2} \right] \frac{\sqrt{\pi} \exp(2\sqrt{aU})}{12 a^{\frac{1}{4}}U^{\frac{5}{4}}} \quad (3.39)$$

3.6.3 The Generalized Superfluid Model

The generalised superfluid model (GSM) is based on the superconducting nature theory of Bardeen-Cooper-Schrieffer. The phenomenological model exhibits a low-energy superfluid phase transition[45, 46], where the pairing energy term has a significant effect on the level density. There are two distinct energy regions in the GSM model: low and high. An additional shift of the excitation energy δ_{shift} is given in the GSM to enhance the level density parameter[46].

$$U = E_X + N\Delta_0 + \delta_{shift} \quad (3.40)$$

Where $\Delta_0 = \frac{12}{\sqrt{A}}$ and $n = 0, 1$ and 2 for even-even, odd-even and odd-odd nuclei, respectively.

$$a(U, Z, A) = \left\{ \tilde{a}(A) \left(1 + \delta E_0 \frac{f(U^*)}{U^*1} \right), U > U_{cr} \right. \quad (3.41)$$

Where U_{cr} denotes the condensation energy subtracted from the effective excitation energy.

3.6.4 The Enhanced Generalized Superfluid Model

The Enhanced Generalized Superfluid Model (EGSM) make use of the superfluid model below the excitation energy. It has the enhancement of spin distribution contribution in Fermi gas model which is different from the GSM[47]. The non-adiabatic form of nuclear rotation is used to improve the level density for evaluation. As a result, it takes the geometry of the nucleus in a dynamical condition. This deformation is included into level density formulations via moments of inertia and the level density parameter, which increases as the surface

of the nucleus increases. The role of the nuclear surface component and linear dependence on asymptotic have vanished in the parameterization of EGSM, which covers collective enhancement. EGSM global systematics does not take discrete levels into consideration.

3.6.5 Microscopic level densities

Several microscopic methods are available to evaluate the level densities. In the microscopic super fluid model, the GSM approach was employed to compute the level density and other parameters of the excited nucleus. It considers realistic single particle level schemes [48]. In the collective model, the codes use this method to generate the level density for the reaction data prediction. In the development of the codes, two basic microscopic level density models are employed. S. Goriely estimated the level densities for the RIPL data library using Hartree-Fock calculations [48] for excitation energies up to 150 MeV and spin values up to $I = 30$. Hilaire and Goriely suggested this novel energy, spin and parity dependent nuclear level densities based on the microscopic combinatorial model[49]. This model is having intrinsic state density and collective enhancement. The calculations make use of nuclear structure properties determined within the deformed Skyrme-Hartree-Fock-Bogolyubov framework[50]. Recent versions of the codes also include temperature-dependent Hartree-Fock-Bogolyubov calculations utilising the Gogny force.

3.7 Nuclear Reaction Codes and Tools

Statistical nuclear reaction models are developed in order to validate the data and evaluate the predictive power of the nuclear theories. Computer codes

are developed in accordance with particular models. To evaluate nuclear reaction data and nuclear data analysis, the nuclear reaction computer code with specific nuclear reaction models are employed. In the present work, statistical nuclear reaction computer codes EMPIRE-3.2[42] and TALYS-1.8[51] and NeuCBOT[52] are employed for theoretical analysis.

3.7.1 EMPIRE-3.2

The nuclear model code EMPIRE takes account compound, direct and pre-equilibrium nuclear reactions. EMPIRE-3.2 reads as much data from the RIPL input directory and the local input parameter library as feasible. Only the input parameters that the code does not know, such as incident energy, projectile, target and the number of emitted particles, must be given by the user for the following ejectiles: neutrons, protons, deuterons, tritons and light ions.

EMPIRE input consists of two parts. Mandatory Input and Optional input

Mandatory input contains basic data necessary to specify the case and the structure is given below:

```

14.8                               ;INCIDENT ENERGY (IN LAB)
56      26                         ;TARGET A , Z
  1      0                         ;PROJECTILE A, Z
  3                                           ;NUMBER OF NEUTRONS TO BE EMITTED
  1                                           ;NUMBER OF PROTONS TO BE EMITTED
  1                                           ;NUMBER OF ALPHAS TO BE EMITTED
  1                                           ;NUMBER OF DEUTERONS TO BE EMITTED
  1                                           ;NUMBER OF TRITONS TO BE EMITTED
  1                                           ;NUMBER OF HELIONS (3He=h) TO BE EMITTED
  0      0.      0.                 ;NUMBER OF L.I. TO BE EMITTED, AND ITS A AND Z

```

The first line indicates the incident energy in the laboratory system (in MeV). The second and third represents the mass and atomic numbers of a target and a projectile. The next seven lines define the number of emissions

to be followed for each ejectile. The code automatically sums over all possible decay sequences to reach the given residual nucleus. The mandatory input is followed by optional input, which allows modifications to the default model parameters.

Optional input comprises of an arbitrary number of records, entered in any order and closed with the GO record, which specifies the end of the input. EMPIRE-3.2 [42] is a modular system of nuclear reaction codes that may be used to calculate over a wide range of energies and incident particles. It consists of several nuclear models. A projectile can be a neutron, proton, any ion (including heavy-ions) or a photon. The energy range extends from the unresolved resonance region for neutron-induced reactions (keV) and goes up to several hundred MeV for heavy-ion induced reactions. The code calculates the major nuclear reaction mechanisms, including direct, pre-equilibrium and compound nucleus ones. Direct reactions are described by a generalized optical model (ECIS03) or by the simplified coupled-channels approach (CCFUS). The pre-equilibrium mechanism can be employed by a deformation dependent Multi-step direct (ORION + TRISTAN) model. Finally, the compound nucleus decay is described by the full featured Hauser-Feshbach model with γ -cascade and width-fluctuations. A comprehensive library of input parameters covers nuclear masses, optical model parameters, ground state deformations, discrete levels and decay schemes, level densities, fission barriers, moments of inertia and γ -ray strength functions[53].

In this work the theoretical estimation was done by EMPIRE-3.2 code. System of codes for modelling the reaction and an extensive parameter library. Which is mainly helpful here to retrieve the data points which obtained as the output file.

3.7.2 TALYS

TALYS is a software that evaluates nuclear reactions within the energy range of 1 keV to 200 MeV of several particles neutrons, gamma rays, protons, deuterons, tritons, helions and alpha particles. The program gives detailed and exact information on reaction cross sections based on several reaction mechanisms, including direct reactions, pre-equilibrium emission and compound nucleus processes. The code calculates the cross sections for all the reaction channels for a given incident energy. The key elements of a TALYS input file are projectile, element, mass and energy. The input can be run with default parameters or with multiple options and parameters provided in the TALYS manual[51]. The code involves different nuclear models for each mechanism such as statistical theory of Hauser-Feshbach for the compound nuclear, exciton model using PCROSS code for pre-equilibrium contribution and the ECIS06 code for calculating the transmission coefficient and direct reaction contributions using suitable optical model potential. In the output, one can get all possible reaction channel nuclear data such as reaction cross-sections, angular distribution, the cross section from different excitation levels, etc. There are a total of six level density models (ldmodel 1–6) defined in the TALYS code:[51]

ldmodel-1 is described as Constant temperature and Fermi gas model (CTFM)

ldmodel-2 is Back-Shifted Fermi gas model (BSFG)

ldmodel-3 is Generalized Superfluid model (GSM)

ldmodel-4 as Microscopic level densities (Skyrme force) from Gori-ely's tables.

ldmodel-5 as Microscopic level densities (Skyrme force) from Hilaire's combinatorial tables.

ldmodel-6 as Microscopic level densities (temperature dependent HFB, Gogny

force) from Hilaire's combinatorial tables.

3.7.3 NeuCBOT

NeuCBOT is a nuclear reaction tool used to evaluate the (α, n) yield of materials to a given set of α particle energies or α -emitting nuclei, it compiles output from code TALYS [51] with nuclear decay information from the ENSDF database[54] and stopping power calculations from code SRIM [55].

NeuCBOT allows the user to provide a material composition in order to calculate (α, n) yields for any arbitrary material. This can be done by specifying the elemental composition of the material and the mass fraction of each element[52]. A list of α particle energies and branching ratios is obtained for each isotope from the ENSDF database. NeuCBOT evaluates the neutron yield and energy spectrum for each α particle as it slows down in a material and interacts with each isotope present[52].

The basis of the calculations with this tool is the nuclear reaction database produced by TALYS and SRIM code which is explained below:

3.7.4 Directory Structure

Here the databases are stored in the `./Data` directory. inside this directory there are sub directories, which are given below[52]:

- `./Data/StoppingPowers/` : Here we get the stopping powers generated by SRIM for each element
- `./Data/Decays/` : This directory contains the ENSDF files with alpha decay data for given isotopes

- `./Data/abundances.dat` : This contains the natural abundances of every isotope[56]
- `./Data/Isotopes/` : This directory is having the TALYS-generated (alpha,n) reaction data library.

There is a directory called `NSpectra/` within an isotope's directory, which contains outgoing neutron energy spectra for alpha particles of a given energy undergoing the (alpha,n) reaction on this isotope. The `TalysOut/` directory is having the output from TALYS, from each generated alpha particle at a given energy on the isotope. Files in this directory is having cross sections for the different alpha-induced nuclear reactions, including the (alpha,n) reaction, as well as cross sections for producing various excited nuclei and gammas at various energies[52]. In order to run NeuCBOT, provided a material description (`-m material_file_name`) and an alpha energy list (`-l alpha_list_name`) also supply a list of contaminants in the decay chain of interest (`-c contaminants_list_name`). The other list of arguments used by NeuCBOT is given below, followed by parameters required by that option (written in square brackets) and the description of what that option does is written in parenthesis[52].

- `-l [alpha list file name]` (file with a list of alpha energies to be used)
- `-c [decay chain file name]` (file with a list of alpha-emitting contaminants)
- `-m [material composition file name]` (file with a description of the material composition)
- `-s [alpha step size in MeV]` (the step size to be used when integrating over the alpha energy, minimum of 0.01)

- -t [no arguments] (tells NeuCBOT to run TALYS for reactions not in libraries)
- -d [no arguments] (if an element is missing from the (alpha,n) database, automatically run the download_element.sh script to download the element's database)
- -o [output file name] (name of text file to store output to)

The NeuCBOT files have been taken in a right way during the calculations in order to obtain a better result.

3.7.5 PACE 4

PACE 4, works with Hauser-Feshbach formalism which follows the angular momentum coupling at each stage of de-excitation of an excited nucleus[57]. For light ions, optical model calculations are used whereas, for heavy projectiles bass model is used for fusion cross section and initial spin distribution[58]. The Gilbert-Cameron level density is used in the calculation, with level density parameter, $a=A/10$, where A is mass number of compound nucleus.

3.7.6 SRIM

SRIM is a set of programs which calculate the stopping and range of ions (10 eV - 2 GeV /amu) into matter. In this code the user can choose ion type, energy and direction to evaluate target damage. In this work SRIM 2008 code has been used to calculate SRIM stopping power, range and energy straggling[55].

These model codes have been used in the present study to calculate neutron yield. So to estimate the emission spectrum from a system the code need to

run with different nuclear models. A brief description of this estimation is discussed in the following section.

Chapter 4

Thick target neutron yield-Low energy

4.1 Introduction

In this chapter, the nuclear model codes introduced in Chapter 3 are applied to predict neutron spectra resulting from thick target interactions. In the context of nuclear reaction applications, thick target neutron energy spectra resulting from the bombardment of various light elements by α - particles are of great significance. The computations of these spectra are conducted for elements such as Boron, Fluorine, Magnesium, Aluminium and Silicon at four different monoenergetic α -particle energies 4.0, 4.5, 5.0 and 5.5 MeV, employing the NeuCBOT code. Here the primary objective is to study alpha-induced neutron yield in thick targets. The integral of the angle-integrated spectrum is compared with the angle integrated neutron energy spectra (and their integrals; n/α -values), from time-of-flight measurement by G.J.H. Jacobs et.al.

[21]. Furthermore, to generate neutron energy spectra theoretically, a special case of Am-Be source is explored

The yield $Y_i(E_\alpha, E_n)$ of neutrons at energy E_n produced by an α particle of energy E_α travelling a distance dx is given by

$$Y(E_\alpha, E_n) = \eta_i \sigma_i(E_\alpha, E_n) dx \quad (4.1)$$

where $\sigma_i(E_\alpha, E_n)$ is the cross section for this particular interaction. The mass stopping power is given by,

$$S(E) = \frac{-1}{\rho} \frac{dE}{dx} \quad (4.2)$$

Where ρ is the total density of the material, integrating over E_α as the α particle slows down gives

$$Y_i^\alpha = \frac{\eta_i}{\rho} \int_0^{E_\alpha} \frac{\sigma_i(E_\alpha^{|}, E_n)}{S(E_\alpha^{|})} dE_\alpha^{|} \quad (4.3)$$

$$= \frac{N_A C_i}{A_i} \int_0^{E_\alpha} \frac{\sigma_i(E_\alpha^{|}, E_n)}{S(E_\alpha^{|})} dE_\alpha^{|} \quad (4.4)$$

where N_A is Avogadro's number, $Y_i^\alpha(E_n)$ indicates the thick-target yield of neutrons of energy E_n from a given α particle, C_i is the mass fraction of isotope in the material and A_i is the target isotope's mass number, The net yield of a material is then calculated by adding the yields of each target isotope.

$$Y^\alpha(E_n) = \sum_i Y_i^\alpha(E_n) \quad (4.5)$$

If P_α to be the probability of an α particle appearing in a decay of the decay chain. The total neutron yield of energy E_n is then defined as

$$Y(E_n) = \sum_\alpha P_\alpha Y^\alpha(E_n) \quad (4.6)$$

The total number of neutrons obtained at any energy is the integral of $Y(E_n)$ over the entire neutron energy spectrum [52].

4.2 Neutron energy spectra deduced for some elements

NeuCBOT is used to calculate (α, n) yields, here (α, n) yields for several materials using NeuCBOT is calculated and compared with the calculations performed using measured yields.

4.2.1 Alpha bombarded on Silicon

The experimental work reported by G.J.H. Jacobs [21] contains three stable isotopes of Natural Silicon; ^{28}Si , ^{29}Si and ^{30}Si . The ground state of the residual nucleus has Q-values of -8.1 MeV, -1.5 MeV, and -3.5 MeV for the (α, n) reactions. $^{29}\text{Si}(\alpha, n)^{32}\text{S}$ and $^{30}\text{Si}(\alpha, n)^{33}\text{S}$ are the only energetically allowed (α, n) reactions. It may be possible for both residual nuclei to remain in the first

excited states and the ground states. The maximum possible neutron energy produced by 5.5 MeV α -particles is 3.7 MeV and 1.7 MeV, respectively. In this work only the neutrons from the $^{29}\text{Si}(\alpha, n)$ reaction contribute above 1.7, 1.2, 0.7 and 0.2 MeV neutron energy for the range of alpha energies 5.5, 5.0, 4.5 and 4.0 MeV. Below these energies both reactions, $^{29}\text{Si}(\alpha, n)$ and $^{30}\text{Si}(\alpha, n)$ equally contribute. This is due to its isotope abundances and cross sections have the same order of magnitude. The four angle-integrated spectra are presented numerically in Table. 4.1

Calculations of angle-integrated cross sections using the model code NeuCBOT were made for Silicon. These cross sections, together with linear stopping powers were used to construct angle-integrated spectrum. This is compared with the experimentally obtained result. Systematically, the calculated spectra are too low. However, they agree on their shapes in a reasonable way. The calculated four angle-integrated spectra along with the spectra obtained from time-of-flight measurements are presented graphically in Fig. 4.1.

The integral n/α - values are shown in Table. 4.2. All n/α - values from the literature are included for comparison and are consistent with the current NeuCBOT results.

TABLE 4.1: The angle integrated neutron energy spectra for thick targets of silicon at four different α -particle energies[21]

$E_n(MeV)$	5.5 MeV $\phi(E_n)$	5 MeV $\phi(E_n)$	4.5 MeV $\phi(E_n)$	4 MeV $\phi(E_n)$
0.1	42.4	35.3	9.52	1.92
0.2	43	34.1	9.58	1.9
0.3	42.3	32.1	9.95	2.02
0.4	45.3	35.4	8.93	1.95
0.5	59.4	48.9	6	1.09
0.6	74.8	58.3	5.56	0.51
0.7	79.5	51.5	2.05	0.51
0.8	81.3	39.9	1.03	0.62
0.9	78.8	27.9	1.07	0.54
1	71.9	17.7	1.34	0.55
1.1	63	8.84	1.51	0.11
1.2	44.5	2.96	1.98	0.86
1.3	32.4	1.5	2.42	0.98
1.4	24.5	1.81	2.95	1.52
1.5	18.5	2.99	4.21	2.67
1.6	13.1	4.52	5.82	3.94
1.7	9.5	5.99	6.87	3.84
1.8	8.4	7.6	7.23	3.27
1.9	9.5	9.66	8.05	3.34
2	10.4	11.2	8.34	3.69
2.1	12.4	12.3	7.57	2.78
2.2	14.7	14.9	6.63	1.2
2.3	17	18.2	5.8	0.24
2.4	18.3	18	4.87	0.01
2.5	18.8	15.5	4.27	
2.6	20.6	12.8	3.12	
2.7	22.6	10.5	1.44	
2.8	23.8	9.19	0.3	
2.9	23.3	9.15	0.02	
3	21.5	9.73		
3.1	19.1	1.76		
3.2	14.7	3.61		
3.3	11.7	0.86		
3.4	10.4			
3.5	9.3			
3.6	7.8			
3.7	5.5			
3.8	2.3			

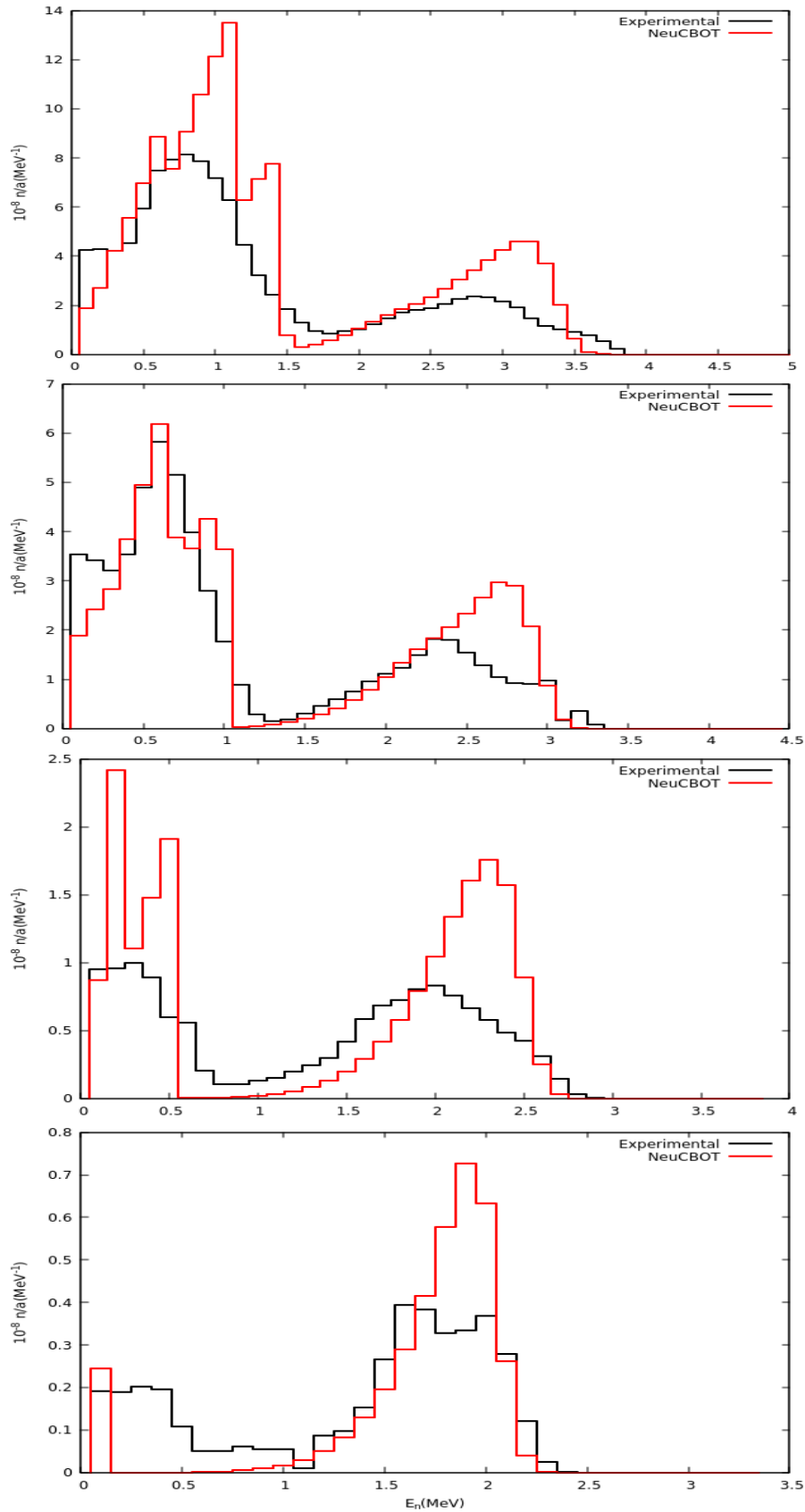


FIGURE 4.1: The angle integrated neutron energy spectra for thick targets of Silicon at four different α -particle energies, determined from time of flight measurements (black line), The red line represents the result obtained from NeuCBOT.

From top to bottom of the figure: 5.5 MeV, 5 MeV, 4.5 MeV, 4 MeV

TABLE 4.2: The integral n/α values for thick targets of silicon at four different α -particle energies obtained from literature and from the code NeuCBOT

$E_\alpha(\text{MeV})$	5.5	5.0	4.5	4	References
	–	–	3.7	1	[Lis 77[13]]
In unit of	11.4	5.2	1.6	–	[Bai 79[15]]
$10^{-8} n/\alpha$	12.4	5.65	1.56	0.40	[Wes 82[20]]
	11.3	5.81	1.38	0.41	[Jacob et al[21]]
	15	6.2	1.88	0.37	[NeuCBOT]

4.2.2 Alpha bombarded on Aluminium

According to the work reported by G.J.H. Jacobs [21] the maximum possible neutron energy produced by 5.5 MeV α -particles is 2.6 MeV. The four angle-integrated experimental spectra along with the calculated spectra obtained from NeuCBOT are presented graphically in Fig. 4.2

The calculated spectra are again symmetrically high as compared with experimental but the shape is well reproduced. the angle-integrated spectra presented in Table. 4.3.

The integral n/α - values are presented in Table. 4.4. For comparison, all n/α - values obtained from the literature are given and are matches clearly with the recent NeuCBOT results.

TABLE 4.3: The angle integrated neutron energy spectra for thick targets of Aluminium at four different α -particle energies[21]

$E_n(MeV)$	5.5 MeV $\phi(E_n)$	5 MeV $\phi(E_n)$	4.5 MeV $\phi(E_n)$	4 MeV $\phi(E_n)$
0.1	34.8	12	2.53	1.7
0.2	34.2	13.3	3.21	0.8
0.3	31.7	12.1	4	0.79
0.4	26.9	6.8	5.55	1.01
0.5	32.4	8.9	7.27	2.1
0.6	34.5	13.1	7.63	3.09
0.7	34.1	16	7.35	3.4
0.8	32.6	17.3	6.18	2.15
0.9	31.8	11.8	8.84	1.96
1	31.6	11.5	9.95	1.19
1.1	35.7	18.2	9.1	0.46
1.2	34.2	17.5	6.4	0.07
1.3	33.6	15.6	3.94	
1.4	35.8	16.6	2.26	
1.5	37.1	16.3	1.27	
1.6	38.2	14.8	0.29	
1.7	37.1	11.3		
1.8	31.4	7.5		
1.9	27.3	4.5		
2	25.9	2.1		
2.1	24.3	0.3		
2.2	22			
2.3	18.5			
2.4	13.4			
2.5	6			
2.6	1.5			

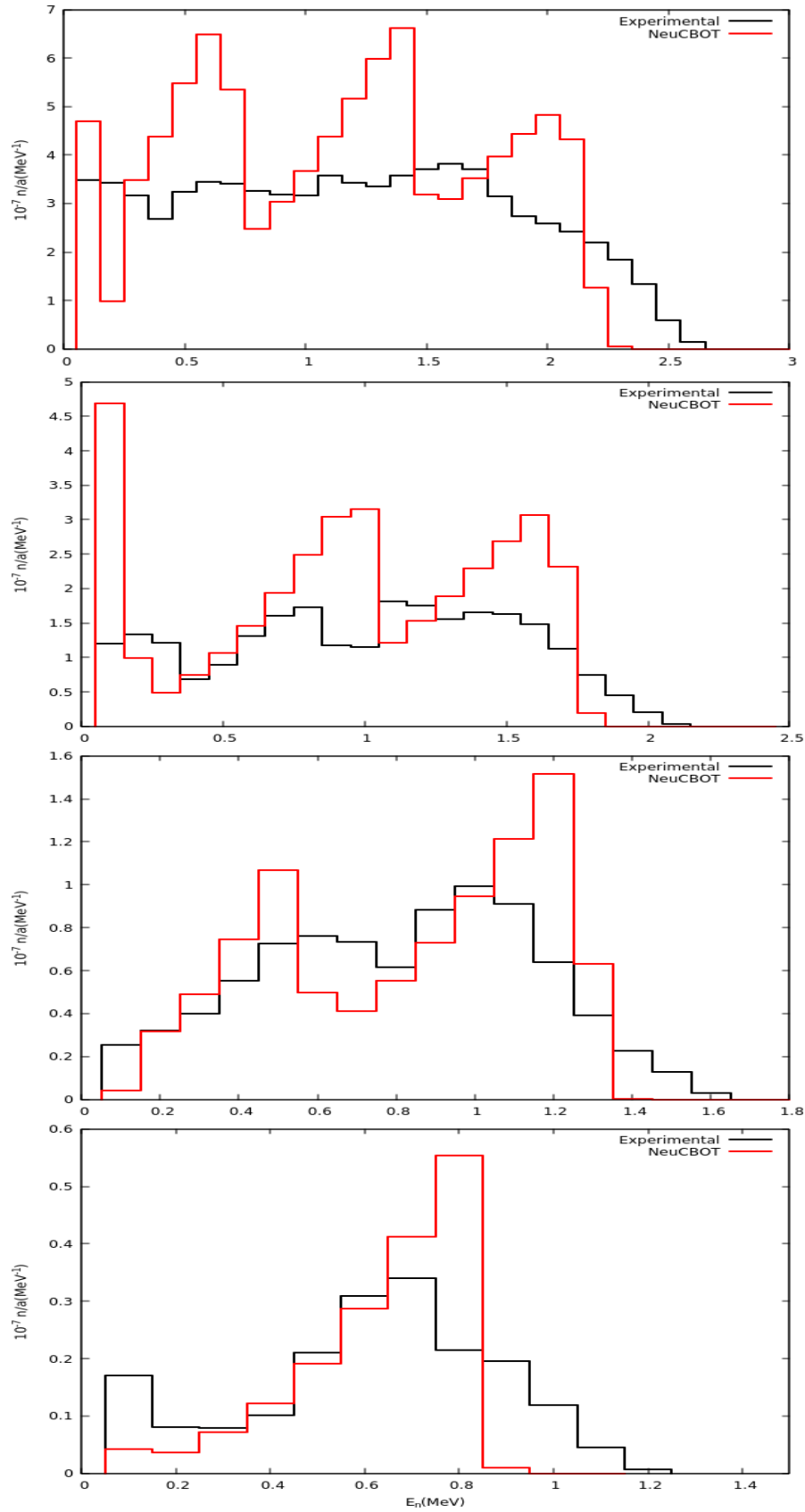


FIGURE 4.2: The angle integrated neutron energy spectra for thick targets of Aluminium at four different α -particle energies, determined from time of flight measurements (black line), The red line represents the result obtained from NeuCBOT.

From top to bottom of the figure: 5.5 MeV, 5 MeV, 4.5 MeV, 4 MeV

TABLE 4.4: The integral n/α values for thick targets of aluminium at four different α -particle energies obtained from literature and from the code NeuCBOT

$E_\alpha(MeV)$	5.5	5.0	4.5	4	References
	7.4	2.9	0.87	0.19	[Lis 77[13]]
In unit of	6.97	2.64	0.802	0.169	[Bai 79[15]]
$10^{-7} n/\alpha$	7.55	2.81	0.812	0.166	[Wes 82[20]]
	7.47	2.60	0.87	0.19	[Jacob et al[21]]
	9.08	3.52	0.916	0.172	[NeuCBOT]

4.2.3 Alpha bombarded on Magnesium

From the work of G.J.H. Jacobs[21] the four angle-integrated spectra are presented graphically in Fig. 4.3. Only neutrons from the $^{25}\text{Mg}(\alpha,n)$ reaction contribute above 5.4, 4.9, 4.4 and 3.9 MeV neutron energy for the α energies 5.5, 5.0, 4.5 and 4.0 MeV spectrum respectively. The integral n/α values are given in Table. 4.5. The figure clearly shows a relatively good match with NeuCBOT estimates, the yields are found to be significantly higher than the corresponding experimental observations.

The integral n/α - values are presented in Table. 4.6. For comparison, all n/α - values obtained from literature are given and are well matches with the present NeuCBOT results.

TABLE 4.5: The angle integrated neutron energy spectra for thick targets of Magnesium at four different α -particle energies[21]

E_n (MeV)	5.5 MeV $\phi(E_n)$	5 MeV $\phi(E_n)$	4.5 MeV $\phi(E_n)$	4 MeV $\phi(E_n)$
0.1	18.4	7.4	2.04	0.5
0.2	16.4	6.3	1.99	0.5
0.3	16.5	6.1	2.05	0.52
0.4	17.3	6.6	1.99	0.55
0.5	17.1	7.6	2.08	0.57
0.6	17.6	8.5	2.96	0.8
0.7	18.7	9.5	3.83	0.98
0.8	18.4	9.8	4.06	1.45
0.9	18	10.1	4.35	1.81
1	18.1	10.5	4.69	1.91
1.1	18.7	10.8	5.33	2
1.2	19.6	12	6.2	2.22
1.3	19.9	13.7	7.01	2.06
1.4	21.9	15.9	8.05	1.89
1.5	25.1	19.1	9.25	1.61
1.6	29.2	21.8	9.4	1.66
1.7	29.6	21.1	8.89	1.56
1.8	31.9	21.7	7.95	1.47
1.9	37	22.7	7.11	1.34
2	38	21.9	6.85	1.37
2.1	40.5	21.6	7.12	1.34
2.2	39.9	20.2	6.54	1.21
2.3	37.5	17.6	5.32	1.09
2.4	36.4	16.2	5	1.01
2.5	35.7	16	4.82	0.85
2.6	34.6	15.3	4.7	0.82
2.7	34.4	14.5	4.71	1.08
2.8	34.5	13.4	4.59	1.38
2.9	34.1	12.8	4.21	1.47
3	30	11.6	3.61	1.44
3.1	25.8	10.2	3.27	1.43
3.2	20.4	8.8	3.33	1.48
3.3	16.6	7.9	3.75	1.6
3.4	16.6	8.9	4.51	1.73
3.5	17.5	9.7	4.86	1.91
3.6	17.9	9.4	4.96	2.05
3.7	18	9.3	4.9	1.94
3.8	18	9.7	5.18	1.86
3.9	18	10.4	5.46	1.79
4	18.1	11.2	5.61	1.69
4.1	18	11.6	5.63	1.69
4.2	18.6	12.2	5.68	1.51
4.3	18.9	12.3	5.17	1.4
4.4	18.2	11.6	4.22	1.29
4.5	17.4	10.2	3.62	1.16
4.6	16.8	9.2	3.27	1.06
4.7	17.1	8.8	3	0.88
4.8	17.2	8.3	2.67	0.62
4.9	16.8	7.3	2.35	0.5
5	15.8	6.1	2.7	0.48
5.1	15.4	5.3	1.77	0.51
5.2	14.9	4.8	1.51	0.56
5.3	13.9	4.3	1.32	0.61
5.4	12	3.9	1.25	0.6
5.5	10.4	3.5	1.25	0.6
5.6	9.1	2.9	1.26	0.56
5.7	8.1	2.4	1.27	0.52
5.8	7.3	2	1.27	0.48
5.9	6.3	1.7	1.25	0.43
6	5.6	1.7	1.18	0.38
6.1	5.1	1.7	1.04	0.33
6.2	4.5	1.7	0.95	0.3
6.3	3.9	1.7	0.85	0.27
6.4	3.6	1.6	0.73	0.2
6.5	3.4	1.4	0.64	0.16
6.6	3.4	1.3	0.55	0.11
6.7	3.1	1.2	0.45	
6.8	3	1	0.39	
6.9	2.7	1	0.32	
7	2.5	0.9	0.23	
7.1	2.4	0.8	0.14	
7.2	2.1	0.7		
7.3	2.1	0.6		
7.4	2	0.5		
7.5	2	0.4		
7.6	2	0.2		
7.7	2			
7.8	2.1			
7.9	1.8			
8	1.6			
8.1	0.4			

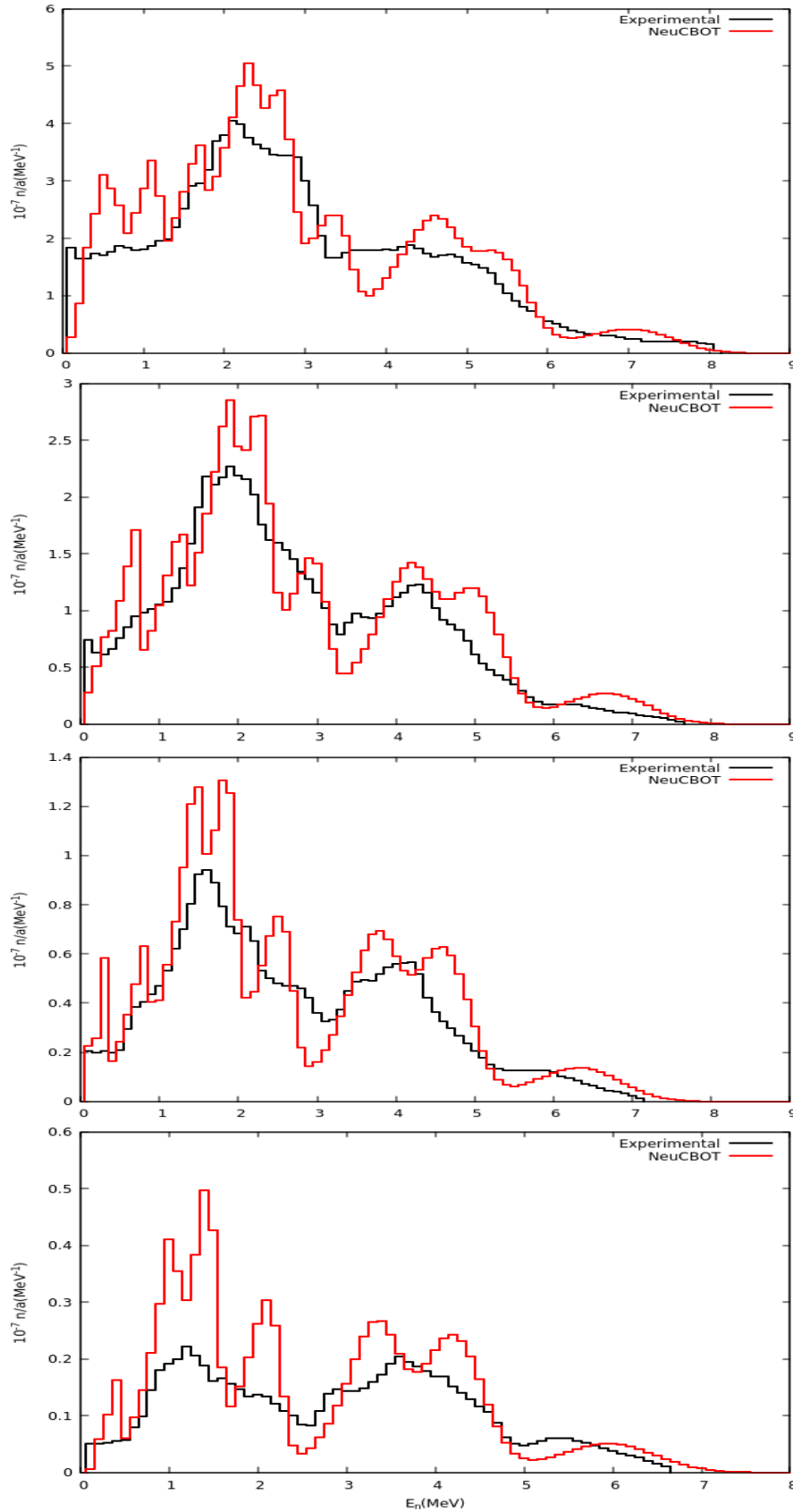
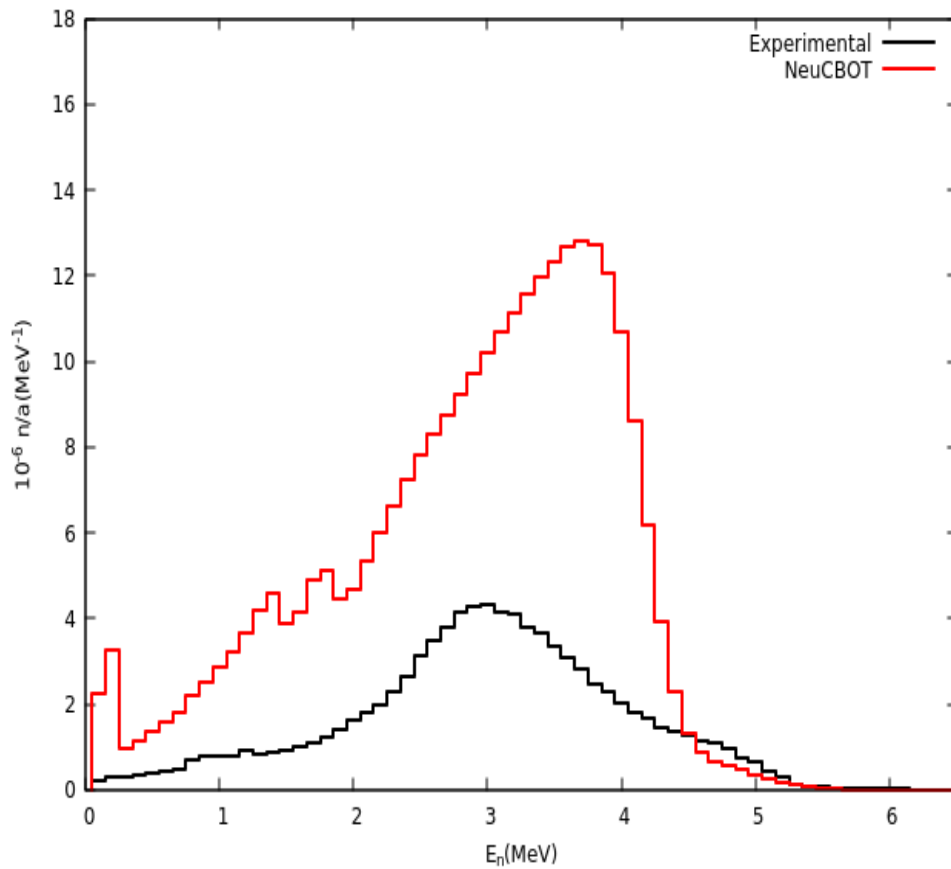


FIGURE 4.3: The angle integrated neutron energy spectra for thick targets of Magnesium at four different α -particle energies, determined from time of flight measurements (black line), The red line represents the result obtained from NeuCBOT. From top to bottom of the figure: 5.5 MeV, 5 MeV, 4.5 MeV, 4 MeV

TABLE 4.6: The integral n/α values for thick targets of magnesium at four different α -particle energies obtained from literature and from the code NeuCBOT

$E_\alpha(\text{MeV})$	5.5	5.0	4.5	4	References
	–	5.8	2.7	1.0	[Lis 77[13]]
In unit of	12.6	6.4	2.63	0.77	[Bai 79[15]]
$10^{-7} n/\alpha$	13.7	7.04	2.93	0.83	[Wes 82[20]]
	13.3	6.65	2.60	0.73	[Jacobs[21]]
	14.7	7.39	3.09	0.991	[NeuCBOT]

FIGURE 4.4: The angle integrated neutron energy spectra for thick target of Boron Nitrate at α -particle energy 5.5 MeV determined from time of flight measurements (black line), The red line represents the result obtained from NeuCBOT

In order to check the code validation, The spectra for Boron and Fluorine were calculated out of the compounds Boron Nitride and Calcium Fluoride respectively. The corresponding spectra is compared with the experimental spectra obtained from G.J.H. Jacobs [21]. Natural Boron contains only 19.8% ^{10}B compared with ^{11}B 80.2% . This explains the predominant contribution of neutrons produces by the later reaction in the neutron energy spectra. The spectra together with calculated spectra for Boron Nitrate are shown in Fig. 4.4 and the spectra for Calcium Fluoride is shown in Fig. 4.5

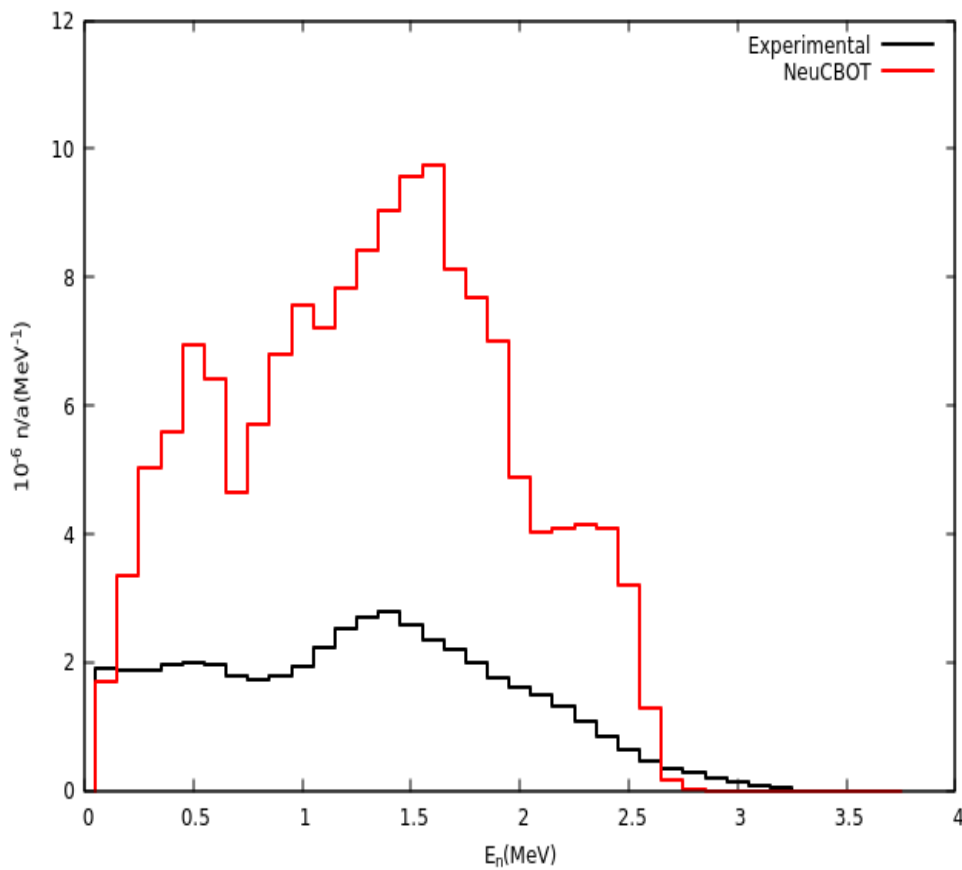


FIGURE 4.5: The angle integrated neutron energy spectra for thick target of Calcium fluoride at α -particle energy 5.5 MeV determined from time of flight measurements(black line), The red line represents the result obtained from NeuCBOT

The two spectra are in good agreement for producing the shape, however in both cases NeuCBOT yield shows systematically higher yield.

NeuCBOT in comparison with experimental data are presented in Fig. 4.6, which shows the neutron yield for various elements calculated by code. The neutron yield is given as the number of neutrons per 10^7 alphas, which is compared with the works of [19][15]. A fair agreement between NeuCBOT and experimental data is seen for most elements.

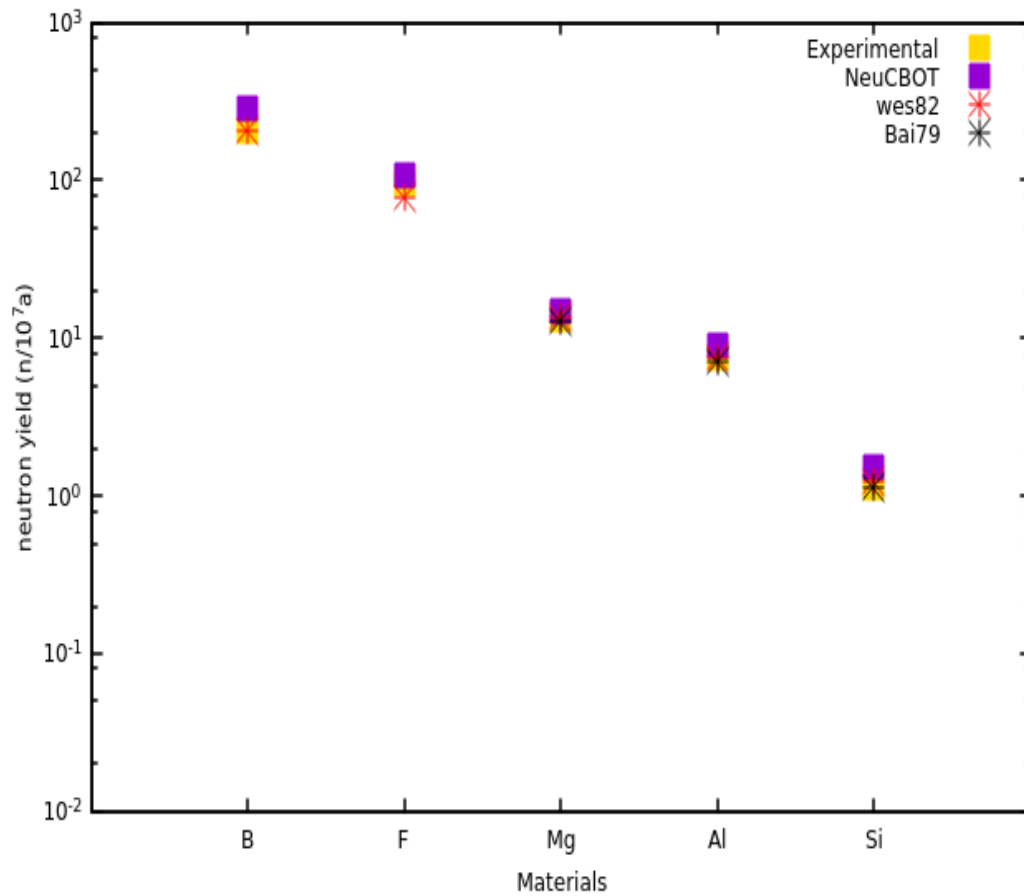


FIGURE 4.6: Neutron yield for various elements is calculated by code NeuCBOT in comparison with measurements. Neutron yield is given as the number of neutrons per 10^7 alphas.

In general the angle-integrated n/α values, which calculated from the NeuCBOT nearly reproduces the shape of spectra which obtained experimentally, However in all the cases the values from the NeuCBOT are consistent with experimentally determined results published by wes et al.[20]. It is found that the calculated values are generally larger than the experimentally determined values in all the cases.

The neutron spectra are also calculated theoretically at various combination of energies using EMPIRE-3.2 nuclear reaction code as EMPIRE-3.2 code is a comprehensive code that can handle a broad range of nuclear reactions, including neutron-induced reactions, proton-induced reactions, ion-induced reactions and more. The subsequent section provides a comprehensive explanation of these calculation.

4.3 Thick target neutron yield for Am-Be source.

To generate the neutron energy spectrum using the NeuCBOT and EMPIRE-3.2 code, specifically focusing on low-energy alpha particles the Am-Be system is selected as a special case study. Am-Be source is the most popular amongst various (α,n) sources due to its low γ -dose rate and long half life(458 y). Also it is widely employed as a calibration source for neutron instrumentation. The 5.48MeV α particle from the ^{241}Am source undergo fusion with ^9Be to form the compound nucleus of ^{13}C at an excitation energy of around 14.4 MeV. Depending on the thickness of Be the excitation energy of ^{13}C may vary from 10.6 MeV to 14.4 MeV. Neutron from such resonance populate various states of ^{12}C depending on the structure of states. The expected neutron spectrum from Am-Be is simulated using NeuCBOT (Neutron Calculator Based On TALYS)[52]. Alpha straggling and tunneling affected to spectrum is also taken

in to consideration. Due to the source composition matrix effects in alpha energy loss and multiple scattering of neutrons inside the source, the emitted neutrons are having a continuous energy. To understand the exact nature of neutron spectrum, the individual neutron colonies corresponding to residual energy states of ^{12}C has to be correlated through the level scheme of ^{12}C . An approximate idea of neutron energies obtained from energy levels of ^{12}C of the reaction $^9\text{Be}(\alpha, n)^{12}\text{C}$ is given in Fig. 4.7.

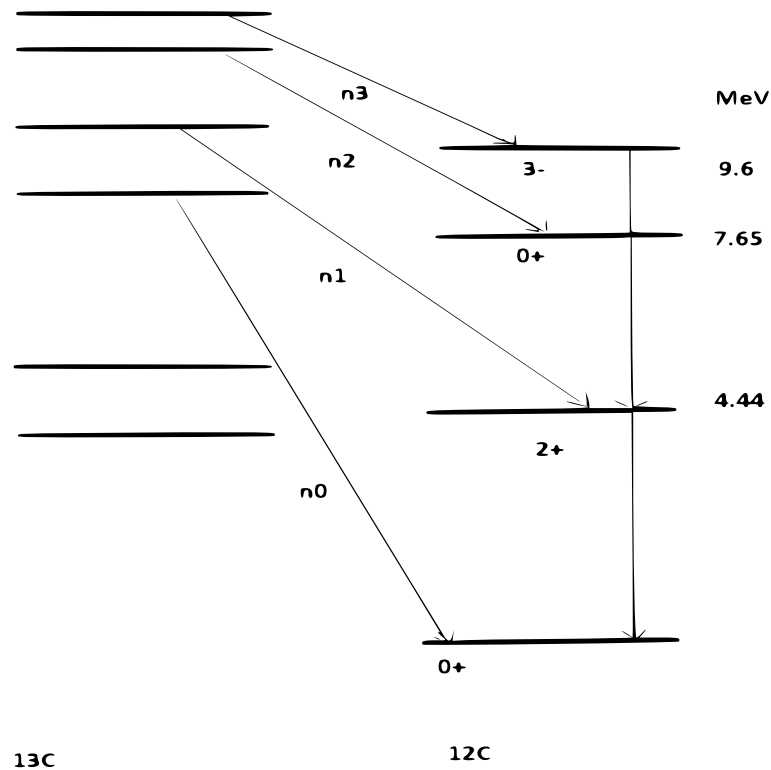


FIGURE 4.7: Energy level diagram of ^{12}C

The following Table. 4.7 presents the reaction Q-values.

TABLE 4.7: Representation of ${}^9\text{Be}(\alpha, n){}^{12}\text{C}$ reaction Q-value

State	Q-Value
Ground state	5.70 MeV
4.4 MeV	1.27 MeV
7.65 MeV	-1.95 MeV

4.3.1 Theoretical formalism using NeuCBOT

NeuCBOT is having a material composition to calculate (α, n) yields for Am-Be material. Here the material is described as AmO₂Be 80%Be 20% AmO₂ by mass. There are two ways to specify the list of α particle energies and relative intensities. Either the user can directly give these values, or NeuCBOT provide a list of α -emitting isotopes and their relative probabilities.

As NeuCBOT runs, it outputs the alpha energy every 10 keV (with the -d option) and it automatically acquires (alpha,n) data. Otherwise, if TALYS is already installed, use the -t option. The output gives the overall neutron production, which is computed by integrating all of the (alpha,n) cross sections along the alphas' trajectories as they slow down, the derivation used for this is well discussed in chapter 2. The number of neutrons produced per decay of the entire decay chain or list of alpha energies being simulated is given in

units. Therefore, the integral over the entire cross sections provides the total yields output of NeuCBOT. The neutron energy spectrum of Am-Be given by NeuCBOT is shown in Fig. 4.8

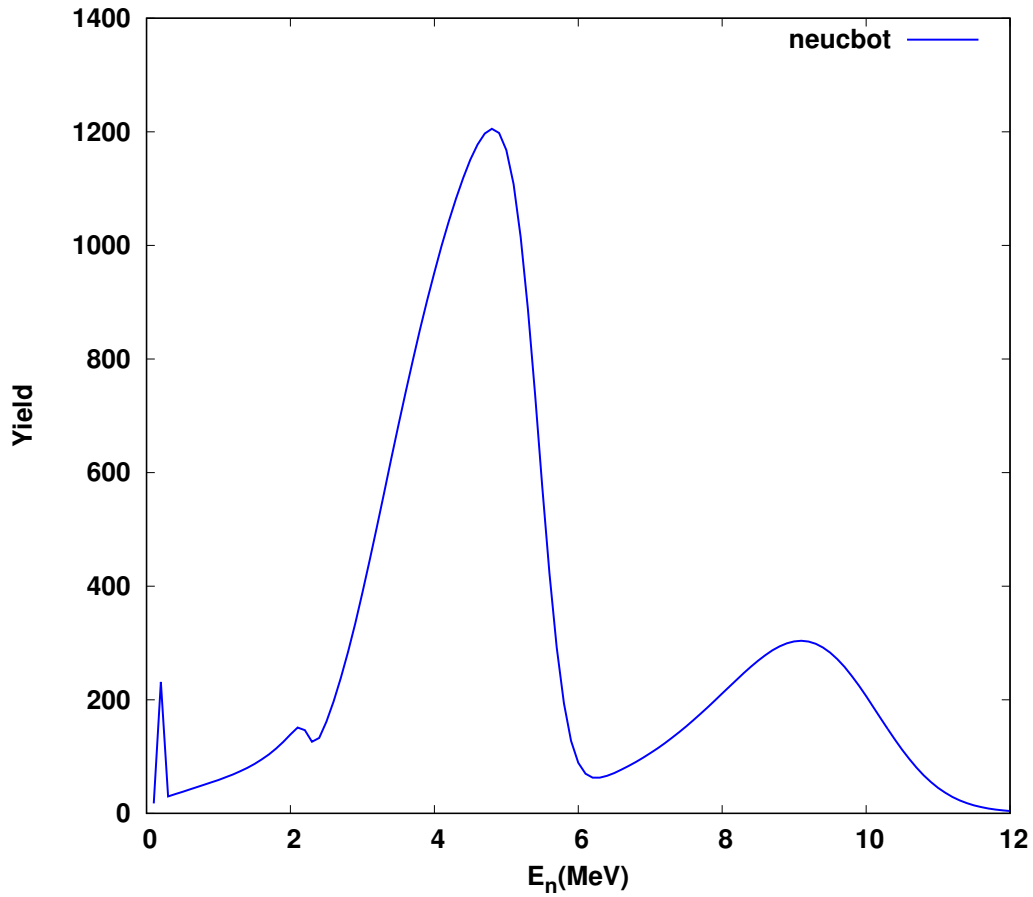


FIGURE 4.8: Neutron energy spectrum predicted by NeuCBOT

4.3.2 Theoretical formalism using EMPIRE-3.2 code

The neutron energy spectra for various combination of angles are calculated. Fig. 4.9 shows the neutron energy spectra at 90° for 5 MeV. Due to the reaction ${}^9\text{Be}(\alpha, n){}^{12}\text{C}$ which forms the compound nucleus ${}^{13}\text{C}$ results the formation of neutron with energies above 0.5 MeV.

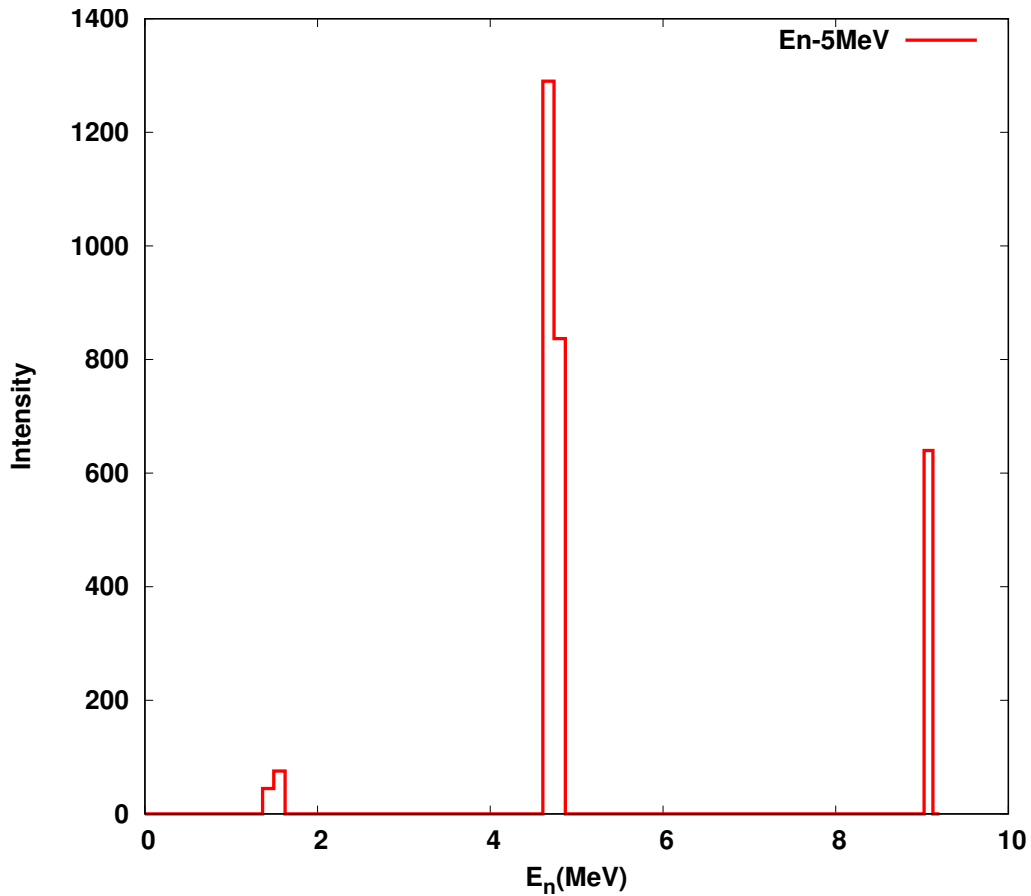


FIGURE 4.9: Neutron energy spectra at 90°

The peaks n_0 , n_1 , n_2 are the neutron energy distributions from the ${}^9\text{Be}(\alpha, n){}^{12}\text{C}$ reaction, leaving the ${}^{12}\text{C}$ in the ground (0 MeV), first (4.4) and second-excited states (7.65 MeV), respectively. They were calculated by setting the Q-values $Q_1 = 5.70$ MeV, $Q_2 = 1.27$ MeV, and $Q_3 = -1.95$ MeV, respectively. The spectra at other energies are also investigated. The calculation is based on an excitation curve for neutrons in the n_0 , n_1 , n_2 group. It is reasonable, to consider an α -particle passing through the target, slowing down and eventually stopping. As the α -particle enters the beryllium target, with energy 5.5 MeV, it produces neutrons in the n_0 group corresponding to

an energy $E(n_0)$ near 9.37 MeV.

Straggling and energy loss for alpha particles are also evaluated for Am-Be source. The value for incident particle using the SRIM code is computed for each energy, the corresponding longitudinal and lateral straggling is acquired, taking the square roots for each value gives the Δx , this results in the energy loss straggling corresponding to each energy. As seen in Fig. 4.10

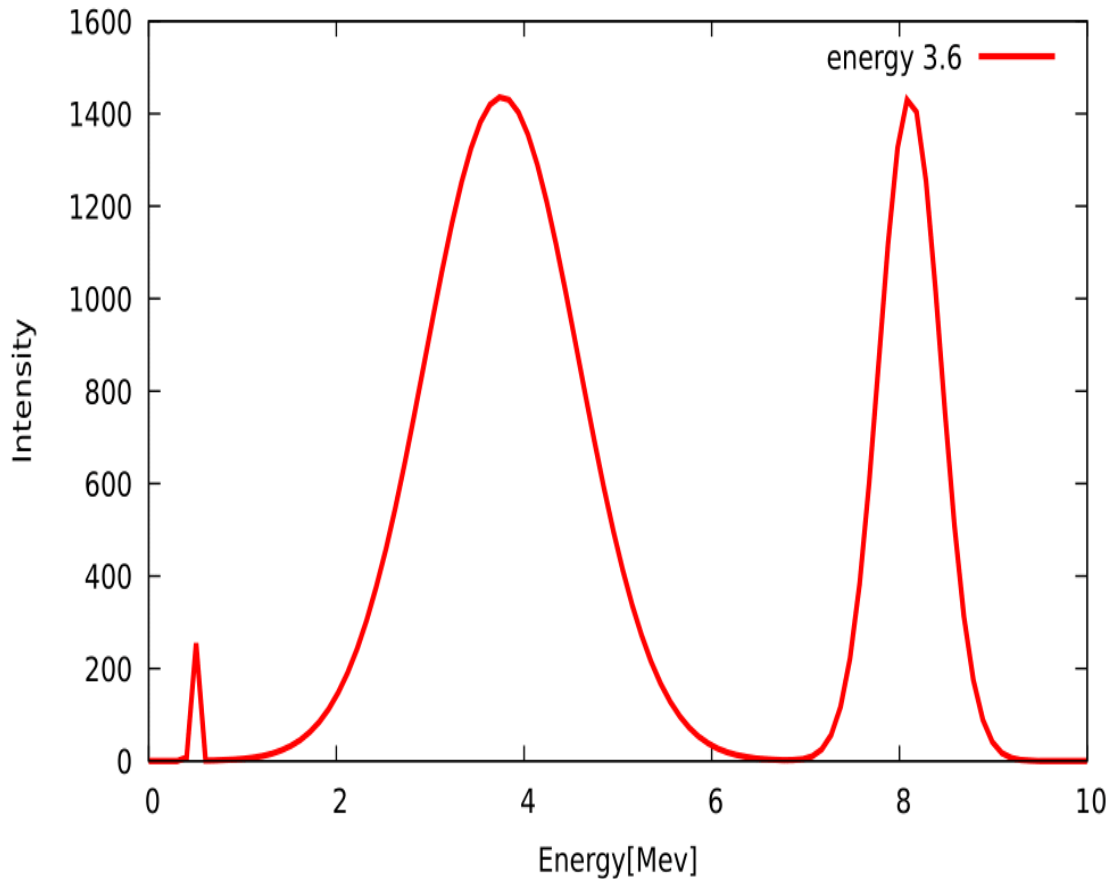


FIGURE 4.10: Observed Neutron spectra, including the straggling corresponds to energy 3.6 MeV

Integrating the neutron spectra over energy range (0-9.37 MeV), the total neutron yield of the reaction can be determined. The corresponding plot in histogram is shown in Fig. 4.11

The spread in energy represented mathematically by gaussian, the detailed expression was discussed above in equation. The range can be obtained by integrating the energy loss rate along the path. Hence the final spectrum. which is shown in Fig. 4.12

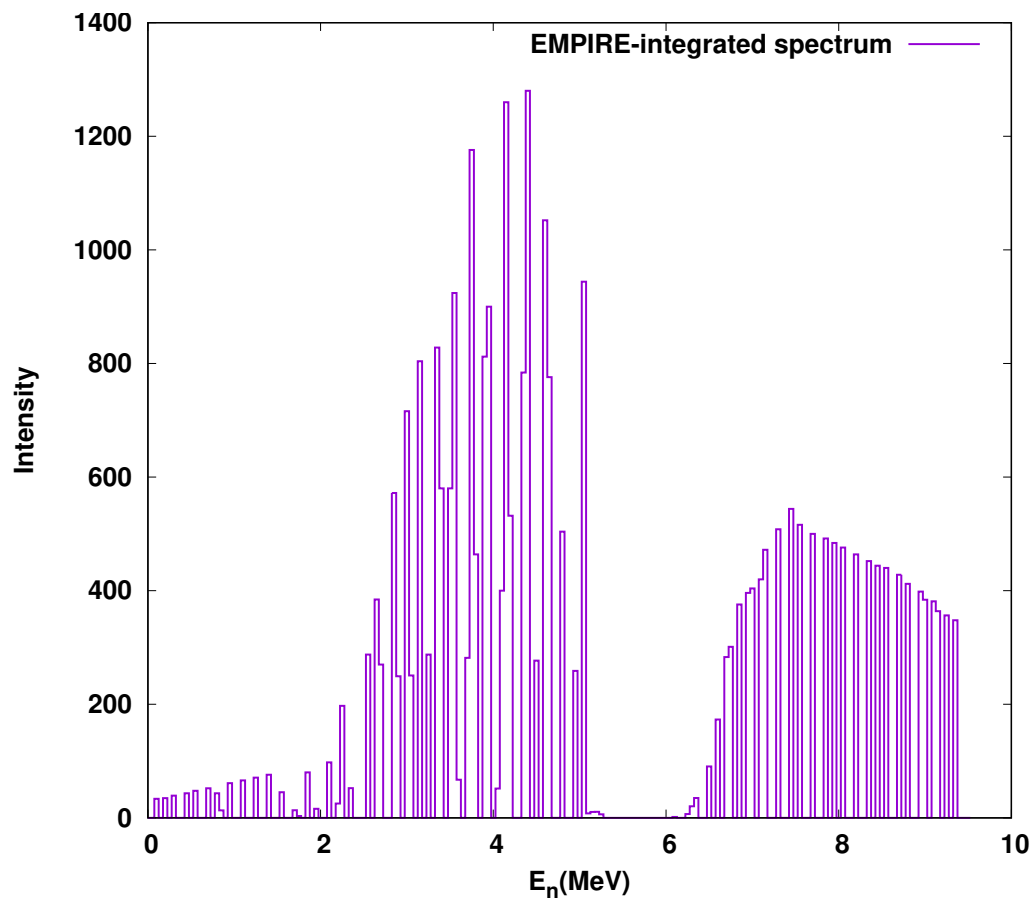


FIGURE 4.11: Integrated neutron energy spectrum

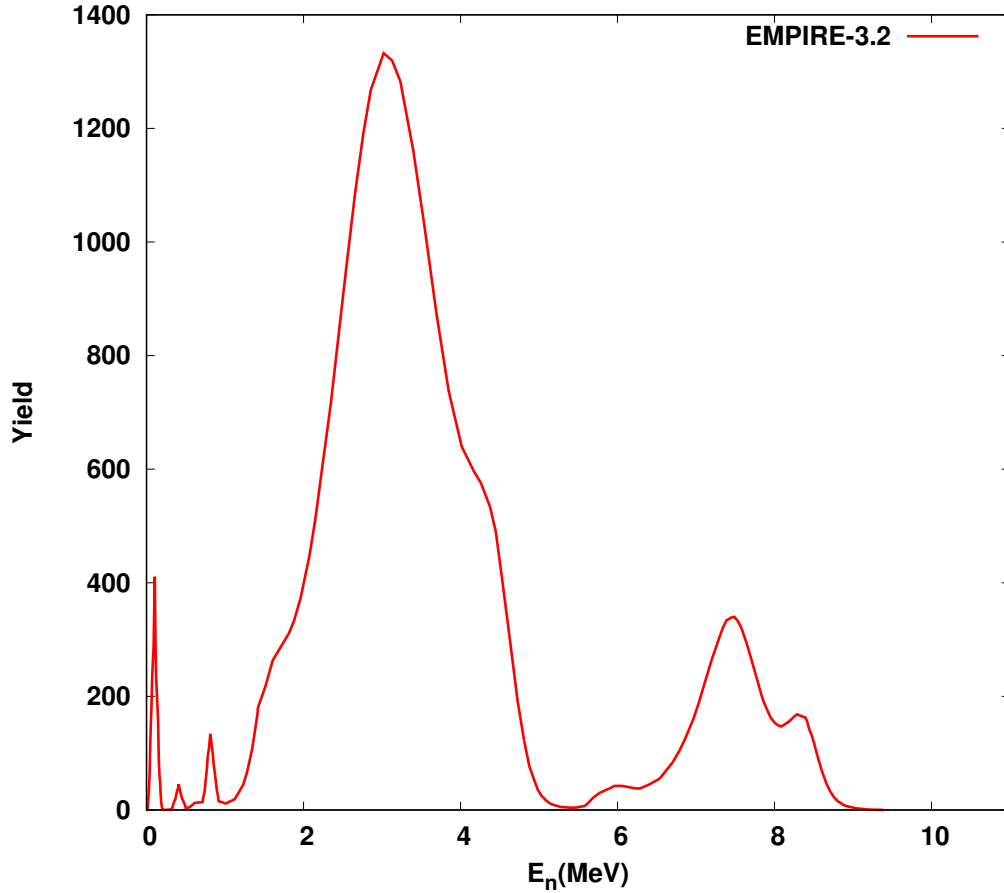


FIGURE 4.12: Neutron energy spectrum calculated using EMPIRE-3.2 with straggling

For various energies, energy straggling for alpha-particles of up to 10 MeV is determined. The straggling width is seen to decrease with particle energy increases. The observed neutron spectra can be interpreted as follows , As the α beam enters the beryllium target, with energy 5.54 MeV, it produces neutrons in the n_0 group corresponding to an energy E_n near 9.37 MeV. Further population of states around 13.5 MeV of ^{13}C causes neutron channels of energy 8.5 MeV. The energy loss due to straggling, scattering, with in the sample thickness, cause spreading and shifting of neutron energy resulting in n_0 colony with peaks around 9 MeV and 8 MeV respectively, after scattering, straggling and attenuation. Population of 4.439 MeV state of ^{12}C from ^{13}C produces

an energy range around 6.5MeV is also included in this colony. Similarly, the prominent peak observed at neutron energy 3.6 MeV is due to the level excitation of ^{12}C supported by neutron channels of ^{13}C giving energies around 1.9 MeV, 2.2 MeV and 4.8 MeV respectively contribute to the formation of n_1 colony. The resonances in ^9Be crosssection at lower alpha energies contribute to the various spikes formed from thermal to 1.5 MeV. This results the formation of n_2 colony.

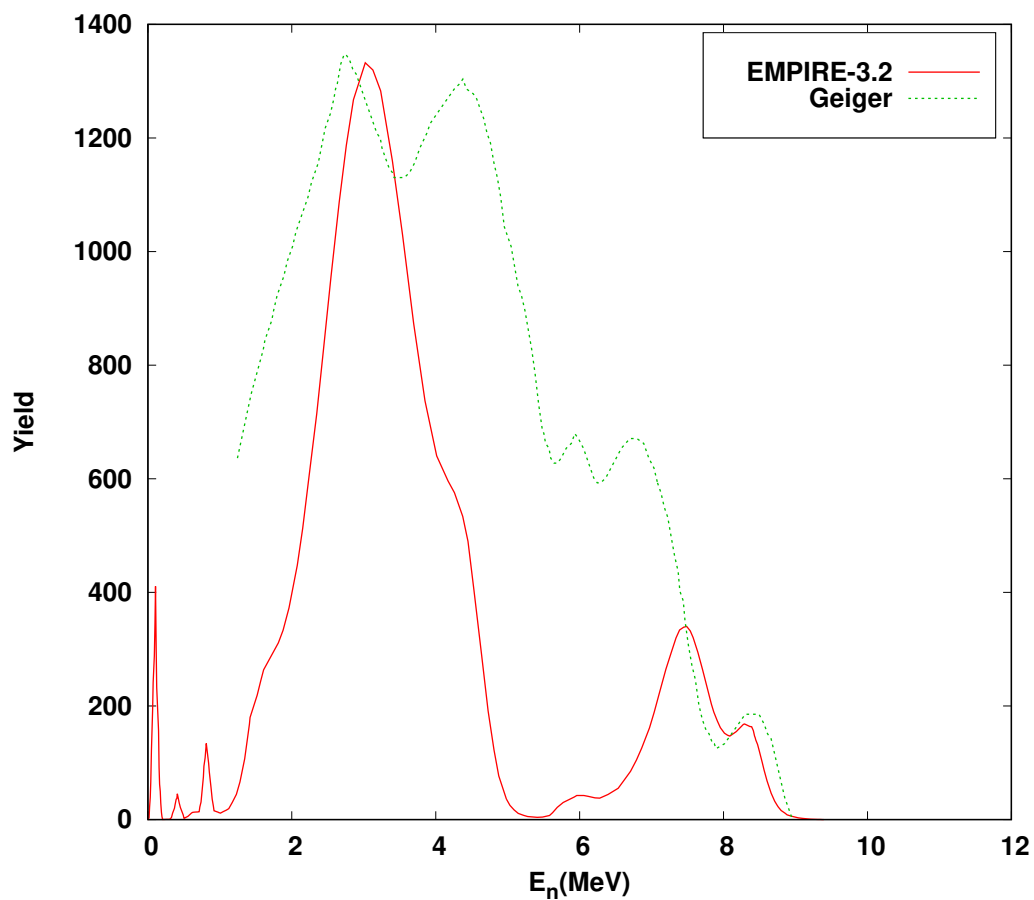


FIGURE 4.13: Resultant spectra from EMPIRE-3.2(red line),Geiger spectra(dotted green line)

Fig. 4.13 shows the resultant spectrum compared with the spectrum generated by Geiger[12]. In the case of Geiger the reported spectra is averaged

distribution without accounting straggling and internal scattering, initial resonance of n_2 colony is also lost here. The stopping power, energy straggling and alpha tunneling evaluation made a better precision for the present work over the previous publications.

4.4 Conclusion

The calculation is performed to generate neutron energy spectra using two different nuclear reaction modeling codes: NeuCBOT and EMPIRE-3.2. The angle integrated neutron energy spectra for thick targets of Magnesium, Silicon, Aluminium at four different α -particle energies 4.0, 4.5, 5.0 and 5.5 MeV are determined. In all these cases the values from the NeuCBOT are consistent with experimentally determined results. These findings concluded that in low energy neutron emission studies NeuCBOT code gives a better results as it can calculate energy loss in case of thick targets. To generate neutron energy spectra theoretically, a special case of Am-Be source is explored and it is noted that the spectra obtained both from NeuCBOT and EMPIRE-3.2 gave promising results. This suggests that these codes are performing well in simulating neutron energy spectra for the study.

Chapter 5

Measurement of neutron energy from Am-Be

5.1 Introduction

Based on the insights gained from the preceding chapter, the codes EMPIRE and NeuCBOT have provided good results, it's crucial to validate these predictions using experimental data. So an experiment is planned to conduct using Am-Be system to measure the neutron energy spectra taking it as a case study. The experimental results will serve as a benchmark to confirm the accuracy of the model predictions. It is specifically selected the Am-Be system for experimental measurement of neutron energy spectra as it is focusing on low-energy alpha particles. The main objective here is to validate the EMPIRE and NeuCBOT model codes by measuring the gamma-tagged neutron spectrum resulting from low-energy alpha interactions.

5.2 Facility Overview

The National Array of Neutron Detectors (NAND) experimental facility set up at IUAC, New Delhi was used to perform the experiment, which contains large array of neutron detectors. There are 100 liquid scintillators in the detector array, the structure is cylindrical size in which each cell having 5" x5" and type is BC501A (Saint Gobain) coupled to a 5" photomultiplier tube. All detectors are mounted at a fixed distance of 175 cm from the target position. The structure of these detectors are semi-spherical dome (geodesic). Here the target is placed inside a 100 cm diameter spherical scattering chamber with thin walls. Also the target chamber provides space for charged particle detectors, such as silicon detectors and large area position-sensitive multiwire proportional counters (MWPC) to detect neutron emitting sources (heavy ions and fission fragments) and other light charged particles in coincidence with neutrons. The whole array setup will enable the measurement of the neutrons' energy and angular distribution that are produced during nucleus-nucleus collision[59], the lab layout is shown in Fig. 5.1.

5.3 Materials and Methods

5.3.1 Am-Be source

The Am-Be radioactive source used in this study was supplied in a double-encapsulated stainless steel capsule of dimension 17.4 mm in diameter and 19.2 mm in height (shown in Fig. 5.2). The nominal activity of the source is 3.7 GBq (100 mCi) with approximate 2.1×10^5 neutron emission per sec. The source contain a homogeneous mixture of ^{241}Am and beryllium metal powder. ^{241}Am



FIGURE 5.1: NAND facility

decays by emission of α -particles of 5 different energies (~ 5.5 MeV weighted-mean energy). When these α particles are captured by ^9Be , fast neutrons and recoiling ^{12}C are produced via reaction $^9\text{Be}(\alpha,n) ^{12}\text{C}^*$. Depending upon the neutron decay channel of ^{13}C and the excited states of the recoiling ^{12}C nucleus, the neutron energy spectrum can have peak structures and continuous distribution up to a maximum energy of 11 MeV. If the recoiling ^{12}C nucleus is left in its first-excited state, the emitted neutron is accompanied by a prompt time-correlated 4.44 MeV de-excitation γ -ray with a branching ratio $\sim 80\%$ [60]. By detecting the prompt γ -rays in coincidence with neutrons in a TOF setup, the kinetic energy distribution of the tagged neutrons is determined.

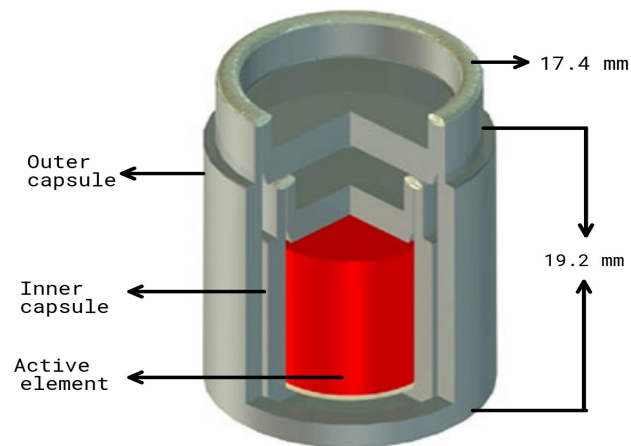


FIGURE 5.2: The encapsulated Am-Be source

5.3.2 BC501A neutron detector

BC501A liquid scintillator cell of NAND facility[61] was used in this measurement. A single detector (shown in Fig. 5.3) is made up of 5 in x 5 in cylindrical cell filled with organic liquid scintillator of type BC501A (M/s Saint Gobain)

and coupled to a 5 in diameter Hamamatsu Type R4144 μ -metal shielded photomultiplier tube (PMT). The PMT base consist of a home made voltage divider network and a preamplifier circuit. The operating voltage was set to -1800V and the energy calibration was determined using standard γ -ray sources. The performance characteristics of the detector has been already reported[61].

BC501A detector is one of the most commonly employed fast neutron detector for neutron TOF spectrometers. It is well known for its fast timing and pulse shape discrimination (PSD) capabilities[60]. In this work, the standard zero-cross (Z/C) timing technique is employed[62] to discriminate the neutrons from γ rays. This technique exploits the properties of the time dependence of the scintillation pulse on type of interacting radiation. The anode signal after passing through a shaping network generates a bipolar signal whose Z/C time interval with respect to the leading edge depends on the shape and rise time of the scintillation pulse. Measure of this time interval is used to differentiate the neutrons and γ -rays. The electronics circuit for this technique was incorporated into a custom built PSD module developed at IUAC[63].

5.3.3 BaF₂ Gamma detector

The γ detector used in this measurement is a BaF₂ detector from Saint Gobain Crystals. It is a tapered geometry scintillator of 30 mm (length) and 25.4/38.1 mm (diameter) coupled to a 2 in Hamamatsu Type R2059 fast PMT surrounded by μ -metal shield. An integrated passive voltage divider is used to apply the high voltage and to read out light output signal. The full assembly is housed in an aluminum enclosure. BaF₂ is a standard detector used for fast timing measurements with sub nanosecond time resolution. This detector was



FIGURE 5.3: 5 in (diameter) x 5 in (height) BC501A liquid scintillator cell mounted on a 5 in diameter PMT

used to trigger on the energy deposited by 4.44 MeV γ -rays and provide the fast timing reference for the TOF.

5.3.4 Measurement

The experiment was performed using one of the BC501A liquid scintillator mounted at NAND facility of IUAC. The Am-Be source was placed at the centre of 4 mm thick and 100 cm diameter scattering chamber with its cylindrical symmetry axis aligned to the vertical direction in the lab. The BaF₂ detector was kept close to the source at same height with its crystal front face approximately 3 cm from the source enclosure. A BC501A detector mounted on the array at same height with the source and at a radial distance of 175 cm from the centre of target chamber was selected for the measurement. A schematic diagram of the experimental setup is shown in the Fig. 5.4. The BC501A triggered on both 4.44 MeV γ -rays and fast neutrons from the source where as the BaF₂ triggered mostly on the energy deposited by 4.44 MeV γ -rays only.

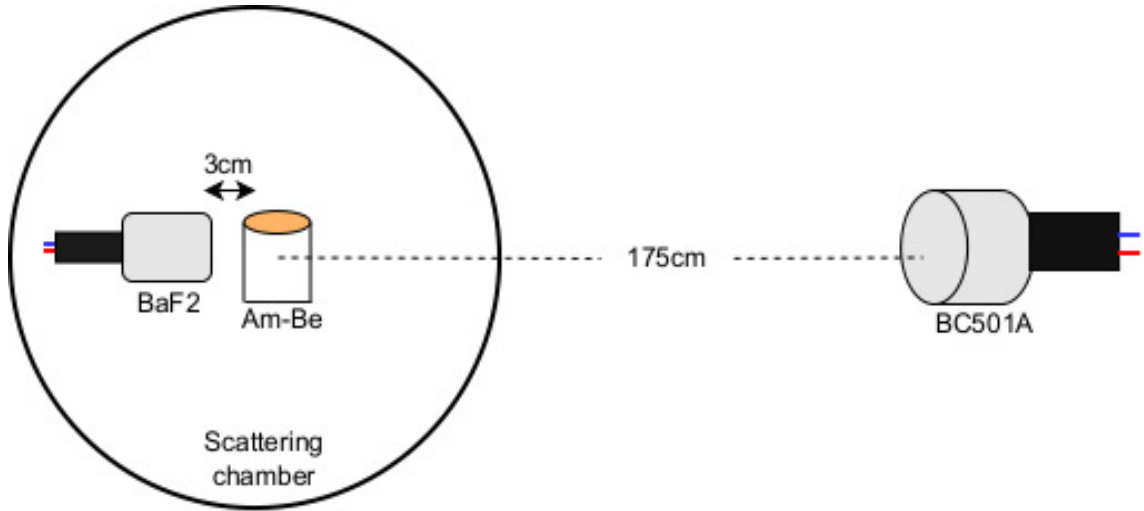


FIGURE 5.4: The schematic diagram of the experimental setup (not to scale)

5.3.5 Time of Flight method

The energy of outgoing neutrons is obtained from the time interval needed for a neutron to reach a neutron detector (time of flight). This method uses the detector's fast timing capability. The pulse from BaF₂ gamma detector produce start signal and the signals from BC501A neutron detector were provide the stop signal . The time difference between start and stop signals is defined as the relative flight time and is used to extract the energy of neutrons. In order to convert the TOF spectrum to the neutron energy spectrum, the following expression of the kinetic energy is used

$$E_n = \frac{1}{2}m_n \left(\frac{L}{TOF} \right)^2 \quad (5.1)$$

where E_n is the kinetic energy of neutron, m_n mass of neutron and L is the flight path.

5.4 Electronics setup and data acquisition system (DAQ)

A block diagram of electronics setup is shown in the Fig. 5.5 . The setup was configured to record the γ -ray energy deposited in BaF₂ detector, light output and the zero-cross timing of the BC501A detector signals for PSD and the ToF information by means of time difference between the signals of BaF₂ and BC501A detector. The anode and dynode signals from the BC501A detector were sent to a custom-built dual channel NIM based PSD module which contains electronics for processing the signals from BC501A detectors[63]. The PSD module generated a constant fraction discriminator (CFD) output which provided the 'stop' signal for the time to digital converter (TDC) of the ToF setup. Another analogue output corresponding to Z/C time with respect to leading edge of the signal was sent directly to analogue to digital converter (ADC). The dynode signal (light output) after pre-amplification(PA) was fed to a shaping amplifier (SA) circuit inside the PSD module. The semi-Gaussian shaped light output signal was fed to ADC. The timing signal from BaF₂ detector was put into a CFD followed by a gate and delay generator (GDG) to produce the 'start'signal for the TDC. The same signal was also used as the 'master trigger' for the data acquisition (DAQ) system. The BaF₂ dynode (light output) signal was fed to a pre-amplifier followed by a shaping amplifier whose output was fed to another channel of ADC. These signals were digitized, acquired on an event-by-event basis and stored on the disk-file using a VME based DAQ running on a LINUX PC. Data were also collected without imposing the gamma detector trigger condition in which the master trigger was generated from the CFD output of the PSD module to record the light output for all neutrons emitted from the Am-Be source. For offline data analysis, the

raw data were converted into ROOT [64] format. The TDC used in the ToF was calibrated with Ortec Model 462 time calibrator.

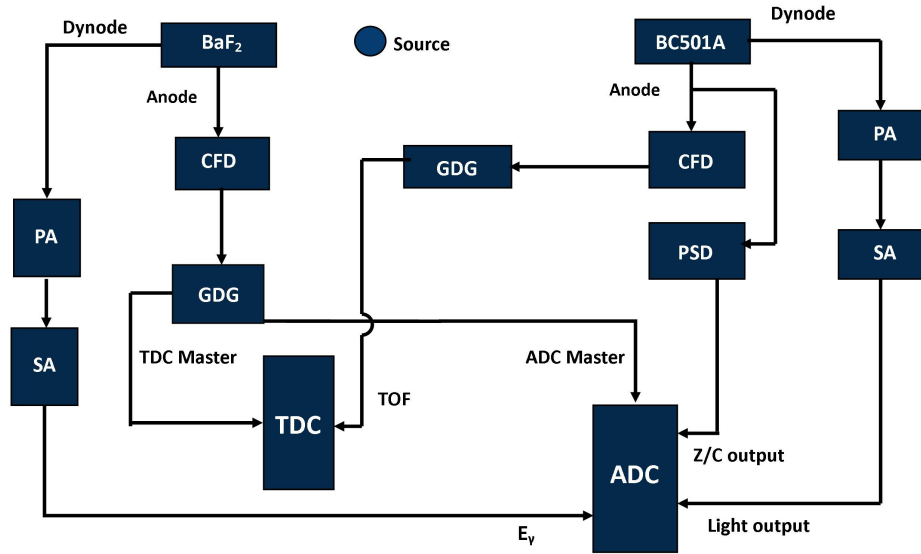


FIGURE 5.5: Block diagram of the electronics setup used for signal processing and data acquisition.

5.5 TOF energy spectrum

The zero-cross distribution obtained from the custom built PSD module was used to discriminate the neutron events from that of γ -rays detected by the BC501A detector. The BC501A detection threshold was kept at ~ 40 keVee which is equivalent to the light output from ~ 0.3 MeV neutron. Fig. 5.6 shows a typical Z/C time distribution obtained in this measurement. As seen in the figure, good neutron- γ discrimination is achieved by Z/C method. Two dimensional histogram of zero-cross time versus light output (light output signal

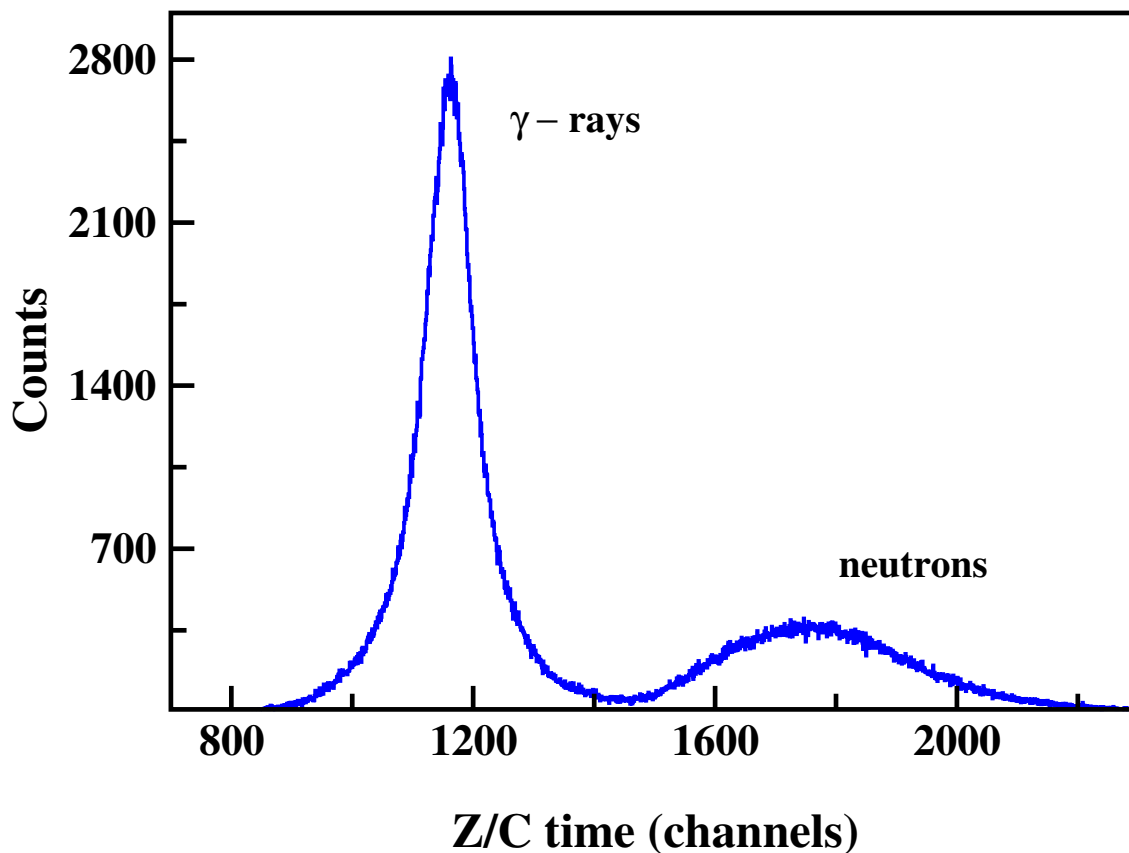


FIGURE 5.6: Zero-cross distribution showing distinct separation of neutrons and γ -rays interacting inside BC501A detector

is proportional to the energy deposited by the impinging radiation in the detector medium) provides a better separation of neutron and gamma events. A comparison of the zero-cross versus light output plots of the BC501A detector corresponding to the self triggered and BaF₂ triggered conditions are shown in Fig. 5.7. In the figure, the upper and lower bands of each panel correspond to neutrons and γ -rays respectively. For same number of collected triggers, untagged condition (upper panel) shows substantial neutron events having higher values of light output recorded in comparison to the tagged condition (lower panel). The significant difference in the neutron light output spectra qualitatively shows the effect of 4.44 MeV gamma-tagging which restricts the measured neutron energy spectrum below 7 MeV. The Compton edge (480

keV) for 662 keV gamma ray from ^{137}Cs corresponds to approximately 750 channels on the horizontal light output axis.

Nevertheless, a more definite separation of neutrons and γ -rays was obtained from a time correlated 2D plot of Z/C distribution. Fig. 5.8 shows a 2D histogram of the Z/C time from BC501A detector plotted as a function of ToF between BaF₂ and BC501A detector signals. Two distinct bands are seen which can be clearly identified as neutron and γ ray bands. The upper band (higher Z/C time) corresponding to neutron events are well separated from the γ -ray events (lower band). A clear separation between γ -ray and neutron events shows the excellent quality of PSD for light outputs even with detection threshold as low as ~ 40 keVee. A software gate around this neutron band was applied to generate only neutron events. For further analysis to convert ToF into energy histogram for gamma tagged events, an additional gating condition was imposed by applying software gate on 4.44 MeV gamma rays from the energy spectrum recorded by the BaF₂ detector. In order to verify the true ToF peak corresponding to gamma-rays, the time correlation measurement was done in the same setup by replacing the Am-Be source by a reasonably strong ^{60}Co γ -ray source. Considering the prompt γ -ray peak position in the ToF spectrum as reference time, the neutron ToF events were converted event-by-event into energy histogram using the expression of TOF. The neutron yield distribution was further corrected for detection efficiency of the BC501A scintillator. The neutron detection efficiency of a single 5 in. x 5 in. cell used in NAND array has been measured and compared with Monte-Carlo simulation[61]. Fig. 5.9 shows the simulation result for variation of neutron detection efficiency of a single cell as a function of neutron energies up to 10 MeV keeping the detection threshold at ~ 0.3 MeV.

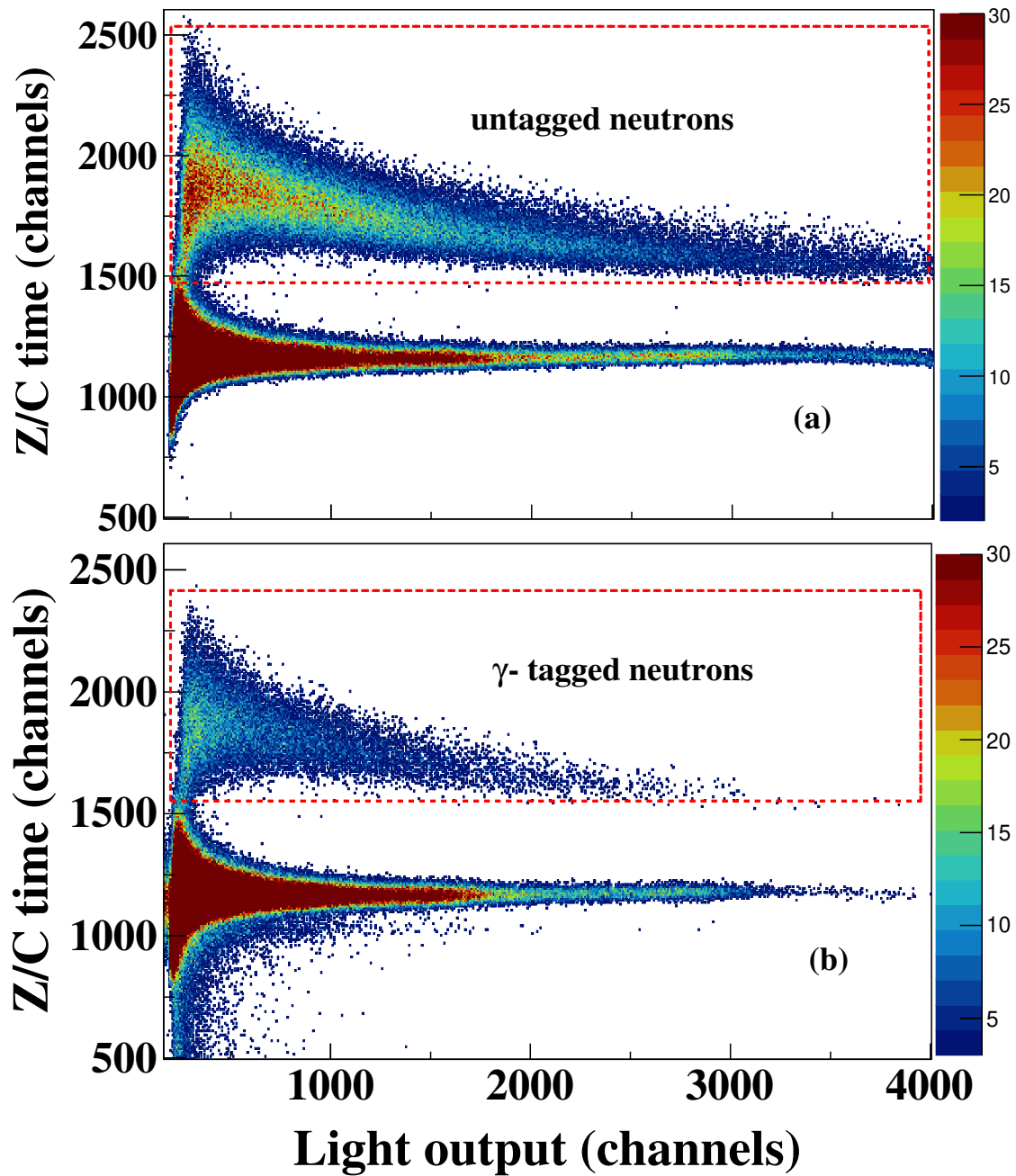


FIGURE 5.7: Two dimensional histograms of zero-cross time vs. light output for untagged and gamma-tagged conditions.

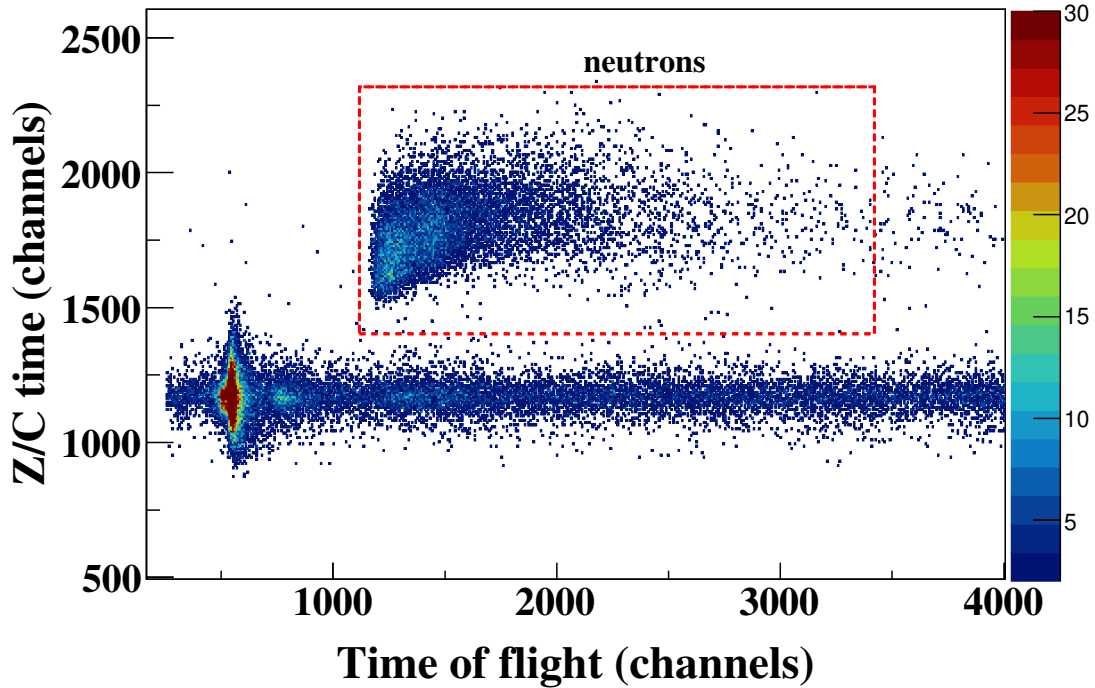


FIGURE 5.8: Two dimensional histogram of zero-cross time vs. time-of-flight.

The neutron yield obtained from ToF measurement was corrected for neutron detection efficiency factor for each energy bin. The efficiency corrected neutron yield distribution from Am-Be source is displayed in Fig. 5.10. For comparison, the standard ISO 8529-2 (ISO 8529-2, 2000) is shown recommended neutron energy distribution along with earlier measured data reported in [65]. The data shown here are normalized with respect to the maximum yield at ~ 3 MeV. The data shows the neutron yield distribution from ~ 0.3 MeV to ~ 6.5 MeV. The lowest energy corresponds to the hardware threshold set at ~ 0.3 MeV neutron. As evidenced by the trigger condition set by detection of γ -rays from 4.44 MeV de-excitation, data shows no yield beyond ~ 7 MeV.

As per the kinetics of the reaction, with 4.44 MeV spent for de-excitation of γ -rays, the available energies for time-correlated neutron is restricted to a maximum value ~ 7 MeV. The results for Am-Be spectrum shown good agreement

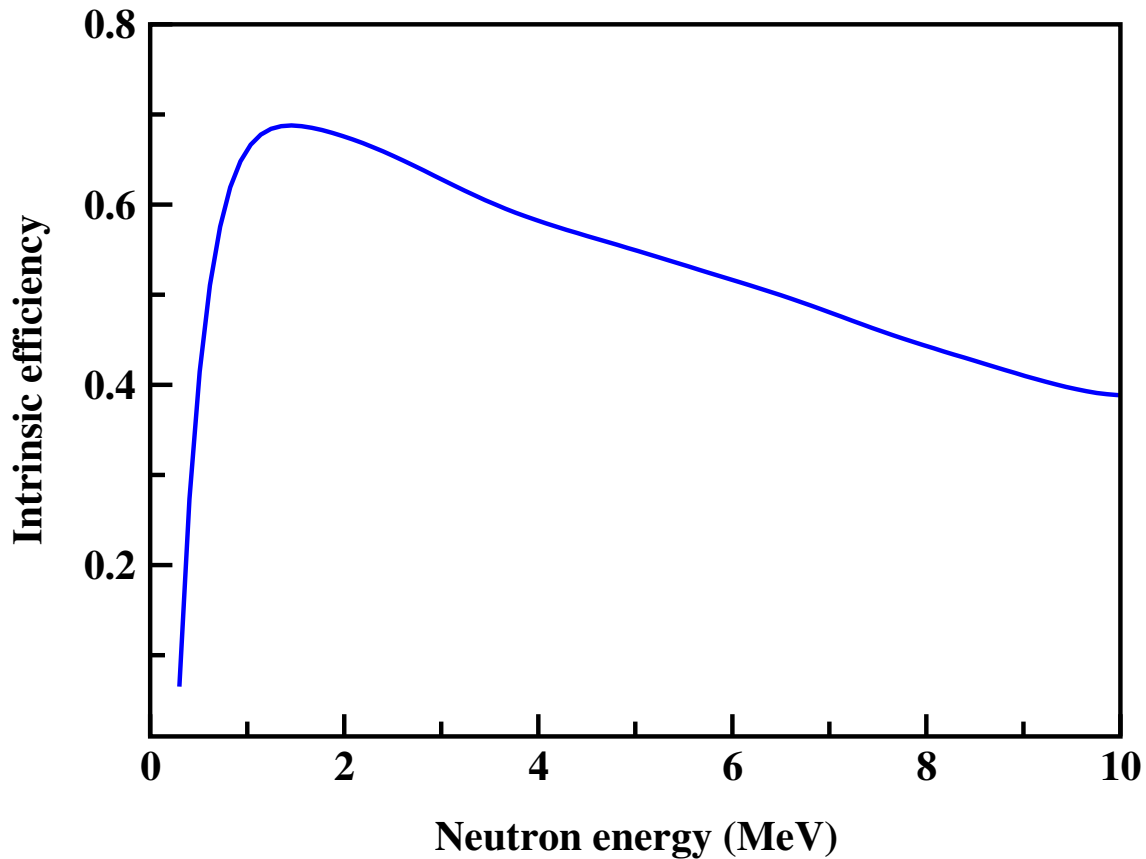


FIGURE 5.9: Simulated intrinsic efficiency of 5 in. x 5 in. single cell BC501A detector as a function of neutron energy.

with the reference spectrum for energy range from 0.3 MeV to 6.5 MeV. In the measurement reported in [65], similar tagged ToF method was employed with a 18.5 GBq Am-Be source and NE-213 neutron detector. Though in general there is good agreement between two data in overlapping energy range, significant discrepancies were observed within the energy interval from 0.3 to 3 MeV. However, the neutron yield distribution below 3 MeV from present measurement is in excellent agreement with the ISO reference data Ref (ISO-8529-2, 2000). As the measurement had a lower hardware threshold, the neutron yield is measured down to lowest energy 0.3 MeV. The contribution of any neutron

scattering in the low energy part of the spectrum can be neglected in the earlier study it is found that neutrons scattered from 4 mm thick scattering chamber wall contributes only small fraction of the total events (0.04)[61]. As neutron detection efficiency vary significantly in the measured low energy range (0.3to 2 MeV), the good agreement of the measured data with ISO reference data suggest the importance of detector efficiency correction in determining the yield distribution.

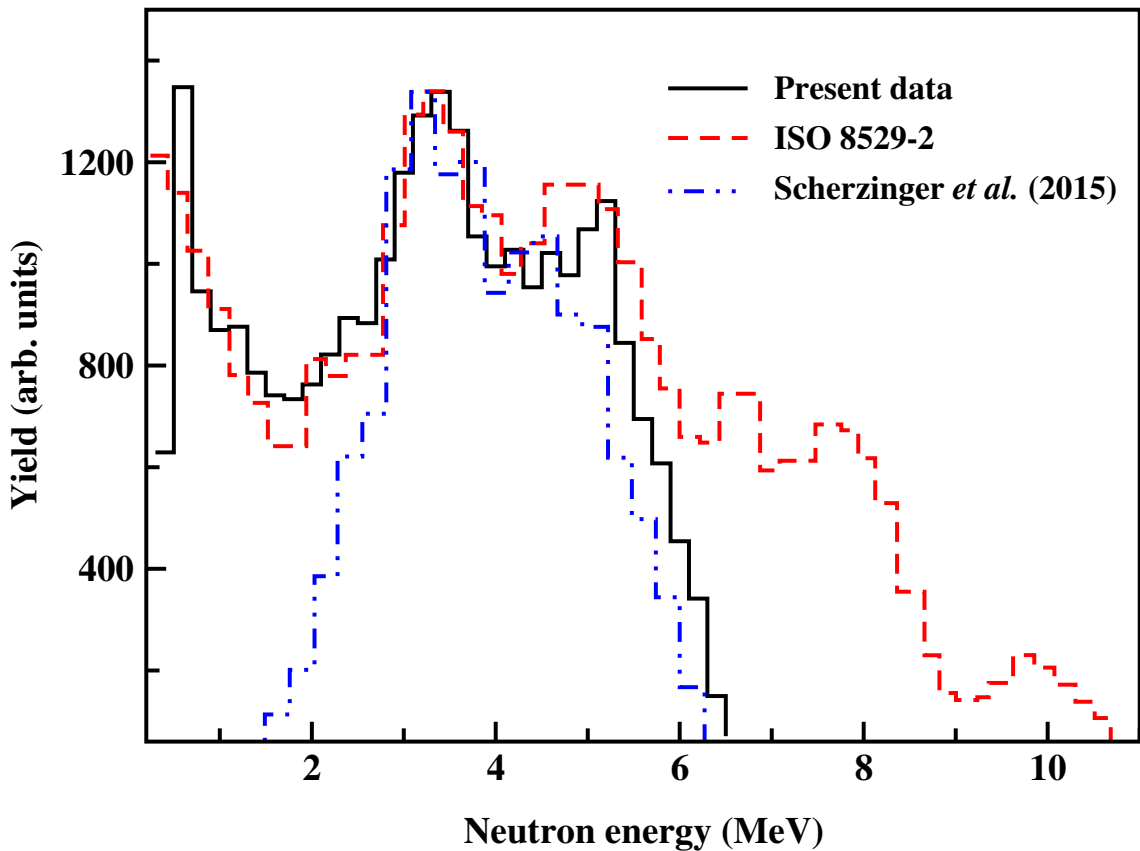


FIGURE 5.10: The Am-Be neutron energy spectrum from present measurement (solid line), compared with ISO 8529-2 reference spectrum[66] (red dashed line) and spectrum obtained by Scherzinger (2015) (blue dash-dotted line).

5.6 Comparison of experimental results with theoretical predictions

The neutron energy spectra measured vs EMPIRE-3.2 calculated are shown in Fig. 5.11. The 4.4 MeV tagged neutron spectra are visible in the energy range of 0.3 to ~ 6.5 MeV beyond which there is no strength. Agreement between measured data and simulated data is good between 2.5 MeV to 6 MeV. It is to be considered that in simulation, the energy loss of alpha particle is also taken into account.

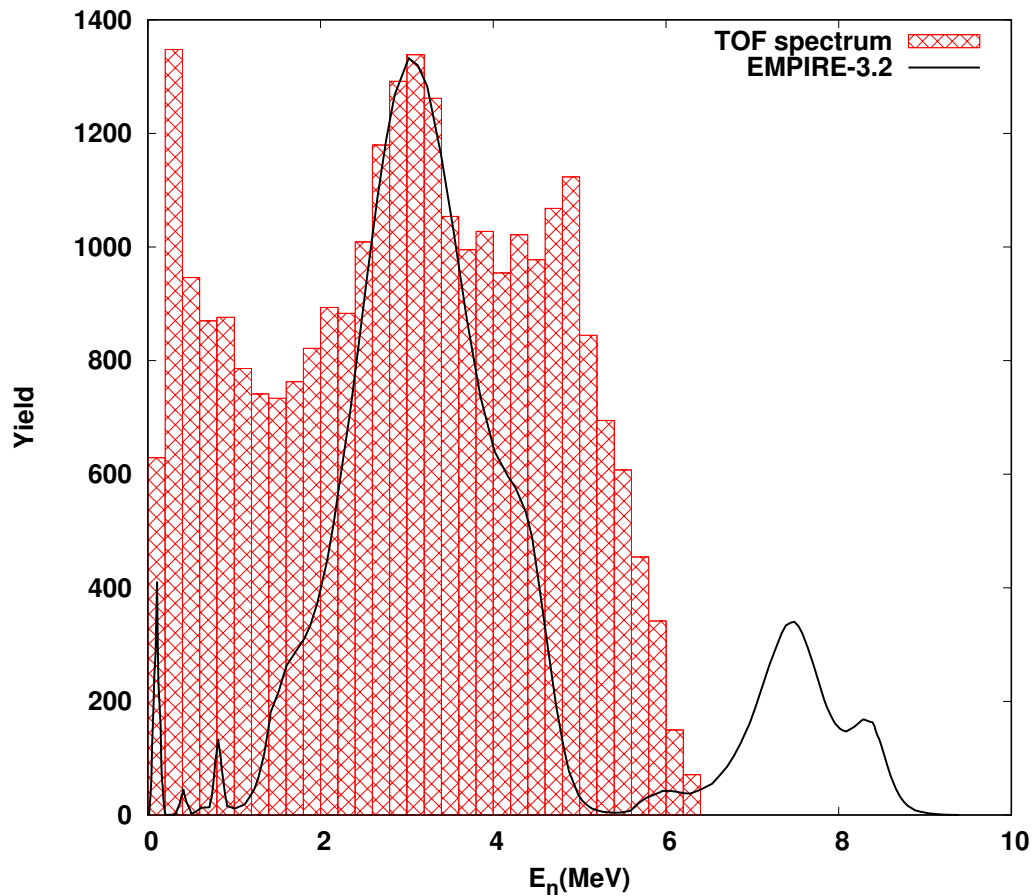


FIGURE 5.11: The neutron energy spectrum of Am-Be source measured compared with EMPIRE-3.2 calculated

Two prominent peaks energies corresponding to 2.8 MeV and 4.6 MeV are identified. The neutron colony for energy around 9 MeV corresponding to ground state of ^{12}C could not be measured as there is no gamma produced for tagging. Some of the weak lower energy colonies also could not be identified due to limited neutron flux available for the experiment. The gamma gated measurement made the present result more precise.

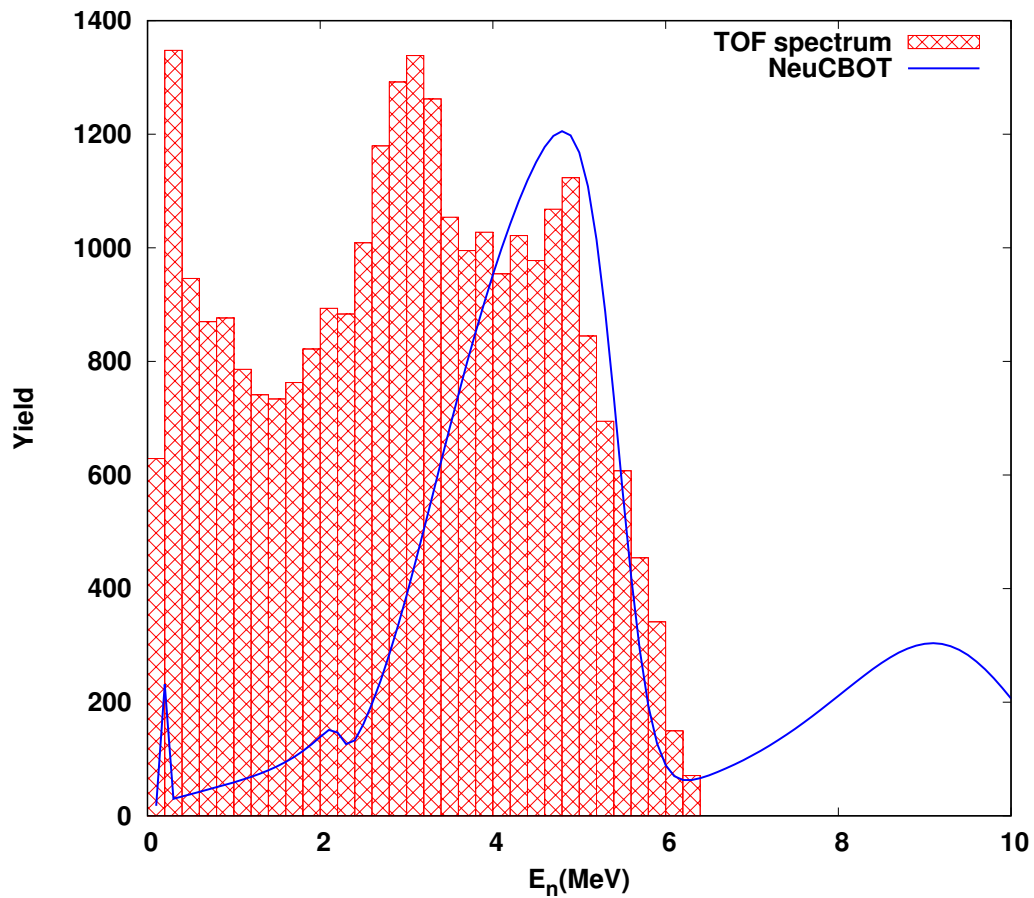


FIGURE 5.12: The neutron energy spectrum of Am-Be source compared with measured TOF and calculated NeuCBOT

The comparison of spectra of TOF and NeuCBOT is also shown in Fig. 5.12. The measured spectrum with NeuCBOT would certainly be of interest. There is a discrepancy observed for both spectra. The differences are largest in the

energy ranges, around 2 and 5 MeV. The way in which ^{241}Am -Be sources are made (mixture, cavity size) seems to have an influence on the neutron emission rate in these energy ranges.

5.7 Conclusion

In this chapter an experimental validation of model code was performed using Am-Be source, in order to validate the predictions and ensure accuracy of theoretical codes. The experimental data have been compared with the standard neutron reference spectrum (ISO 8529-2) as well as earlier measured data, EMPIRE-3.2 and NeuCBOT code. The measured and calculated energy distributions of neutrons produced in (α, n) reactions are represented in Fig. 5.11 and 5.12 using codes EMPIRE and NeuCBOT, agreement between measured data and EMPIRE-3.2 evaluated spectrum is found to be good with 2.5 MeV to 6 MeV, the two prominent peaks at 2.8 MeV and 4.6 MeV are estimated. The comparison with NeuCBOT with measured spectra is also made, it is found a discrepancy around 2 MeV to 5 MeV, this is due to the method in which Am-Be source are made, as the NeuCBOT code works with material composition.

Chapter 6

Thick target neutron yield-Intermediate energy

6.1 Introduction

So far this point, our focus has primarily been on compound reactions within the area of low-energy scenarios. However, as we move into higher energy regimes, we encounter a different phase of nuclear reactions, where mechanisms like pre-equilibrium emissions dominates. In this circumstance the EMPIRE-3.2 code assumes significance. Notably, EMPIRE-3.2 not only involves pre-equilibrium emission but also uses heavy ions as projectiles. As a result, we have chosen EMPIRE-3.2 as our preferred tool to investigate and understand the dynamics of pre-equilibrium neutron emissions in this context. Few measurements of thick target neutron yield using heavy ion reaction have been performed at 10 MeV/A or lower energies to get insights into the reaction mechanisms. Inorder to calculate the neutron yield data from ion induced reactions we use the code EMPIRE-3.2. EMPIRE-3.2 is the preferred choice

as it involves a broader range of nuclear reactions beyond alpha-induced reactions. It is found from the previous studies that at intermediate energy, the pre-equilibrium neutron emission is preferred [22].

In the present study, the emission of neutron yield has been estimated for systems: ^{12}C on ^{56}Fe , ^{27}Al , ^{nat}Ti . The corresponding pre-equilibrium (PEQ) neutron contributions has been estimated using the code EMPIRE-3.2. Here we have used the code PACE 4 for estimating the evaporation neutron yields from heavy ion reaction. We investigated the effect of pre-equilibrium, various level densities and optical potentials in this study. The calculations done with PCROSS-1.5 and PCROSS-0 input parameters to understand the effect of pre-equilibrium contribution in the yield. PCROSS is the input parameter which describes mean free path multiplier value in the Exciton model formalism. The calculations of the level densities was performed on the base of LEVDEN-0 option which is a default case for the level densities which is used for Enhanced Generalized Superfluid Model (EGSM), LEVDEN-1, 2, and 3 are used for Generalized Superfluid model (GSM), Gilbert-Cameron level densities and RIPL-3 microscopic HFB level densities. The following optical potentials proposed by Koning et al and Morillon et al[10] were considered. we are seeking for EMPIRE-3.2's pre-equilibrium contribution and whichever level density model and optical potential of EMPIRE-3.2 will produce the best theoretical result. The comparison of the estimated neutron yields from both the reaction model codes with the available experimental data is shown in the next subsections.

6.2 Study of intermediate energy neutron yield

6.2.1 ^{12}C on ^{27}Al

The neutron energy data of ^{12}C on ^{27}Al at different angles are reported by V. Suman[67], the available experimental datas are compared with EMPIRE-3.2 and PACE 4 at different available level density model is shown below.

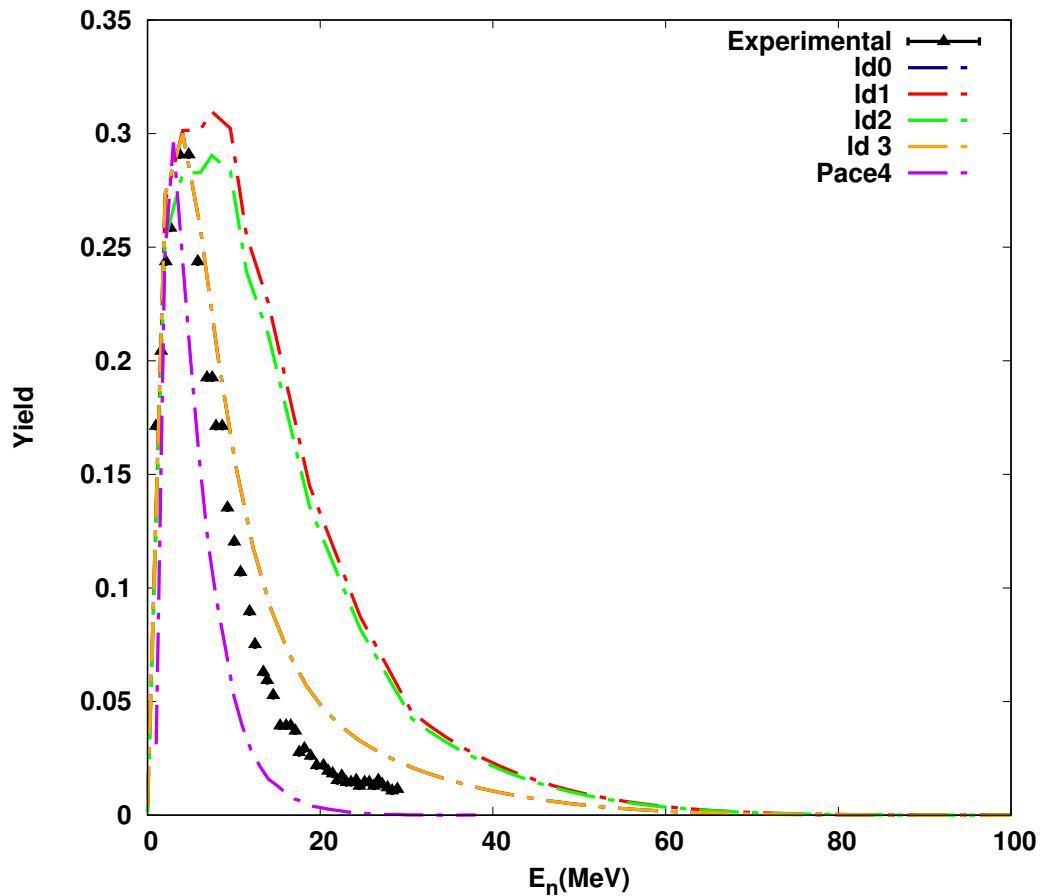


FIGURE 6.1: Comparison of Neutron yield data of ^{12}C on ^{27}Al at 0^0 reported by V. Suman et al[67],with theoretical data from EMPIRE-3.2 and PACE 4.

Fig. 6.1 shows the neutron energy spectrum of ^{12}C on ^{27}Al at 0^0 . The experimental data is found to be in good agreement with the theoretical result

made using ld model-3. Also the pre-equilibrium emission, is taken into account in theoretical calculations. It has been observed that the pre-equilibrium parameters of the code EMPIRE-3.2 satisfactorily reproduces the calculated data result, whereas PACE 4 predicts lower amount of high energy neutrons this is because PACE do not account pre-equilibrium emission. PACE 4 predictions are underestimated when compared to experimental data at the most forward angles and highest neutron energies.

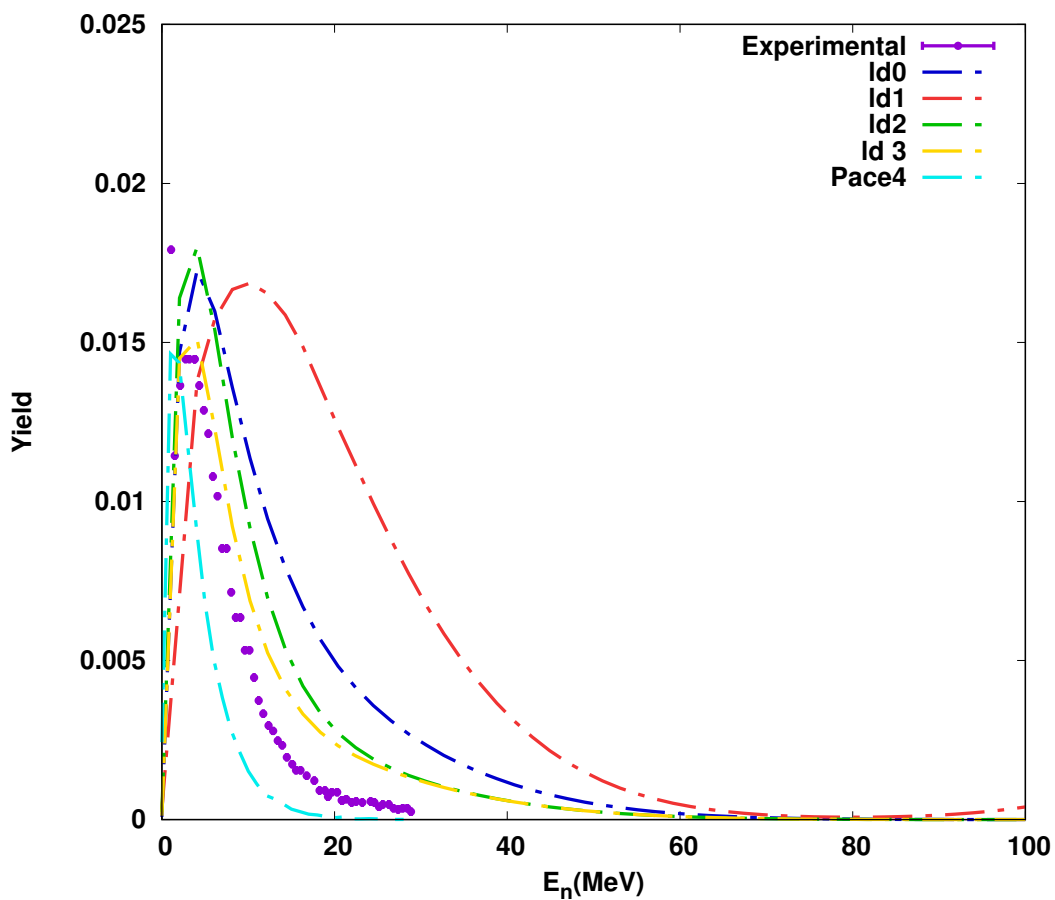


FIGURE 6.2: Comparison of Neutron yield data of ^{12}C on ^{27}Al at 30^0 reported by V. Suman et al[67],with theoretical data from EMPIRE-3.2 and PACE 4.

The neutron energy data of ^{12}C on ^{27}Al at 30^0 reported by V. Suman[67], is compared with EMPIRE-3.2 and PACE 4 at different available level density

model is shown in Fig. 6.2. The reported experimental data is found to be in good agreement with the theoretical result (shown in the yellow colour by dotted line) made using ld model-3. At this angle the PACE 4 calculation falls off faster than the EMPIRE-3.2 calculation, This is because the possibility of pre-equilibrium effects causing more neutron emission at higher energy.

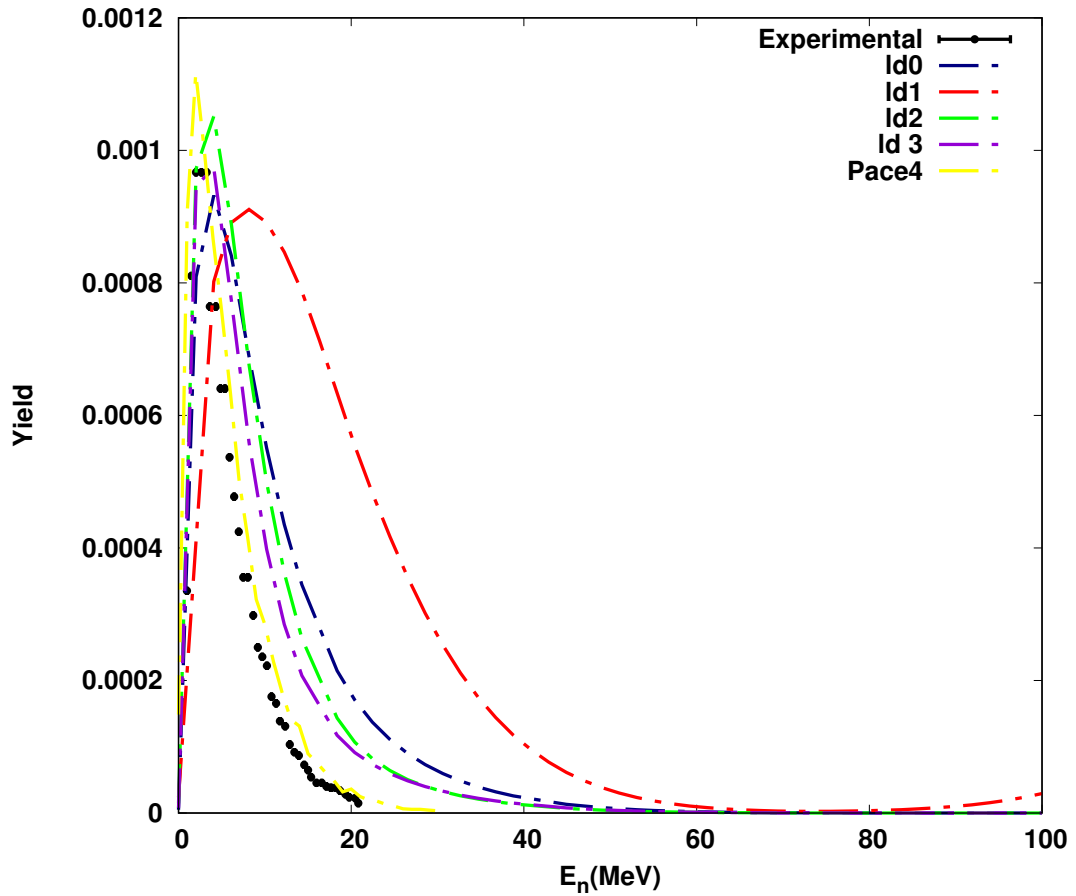


FIGURE 6.3: Comparison of Neutron yield data of ^{12}C on ^{27}Al at 60° reported by V. Suman et al[67] with theoretical data from EMPIRE-3.2 and PACE 4.

The experimental data of ^{12}C on ^{27}Al at 60° reported by V. Suman[67] is compared with EMPIRE-3.2 and PACE 4 at different available level density model is shown in Fig. 6.3. The reported experimental data is found to be in good agreement with the theoretical result made using ld model-3, theoretical

data follows the trend with experimental data, but slightly higher than the experimental data in the energy range of about 0-15MeV. At this intermediate angles EMPIRE-3.2 and PACE 4 calculations are fairly close with each other but over predicted experimental data.

The experimental data of ^{12}C on ^{27}Al at 90° reported by V. Suman[67], is compared with EMPIRE-3.2 and PACE 4 at different available level density model is shown in Fig. 6.4. The theoretical results obtained using ldmodel-3 are in good agreement with the present experimental data and which follows the trend of experimental results of this reaction, experimental data and PACE 4 estimates are quite similar for backward angle 90° .

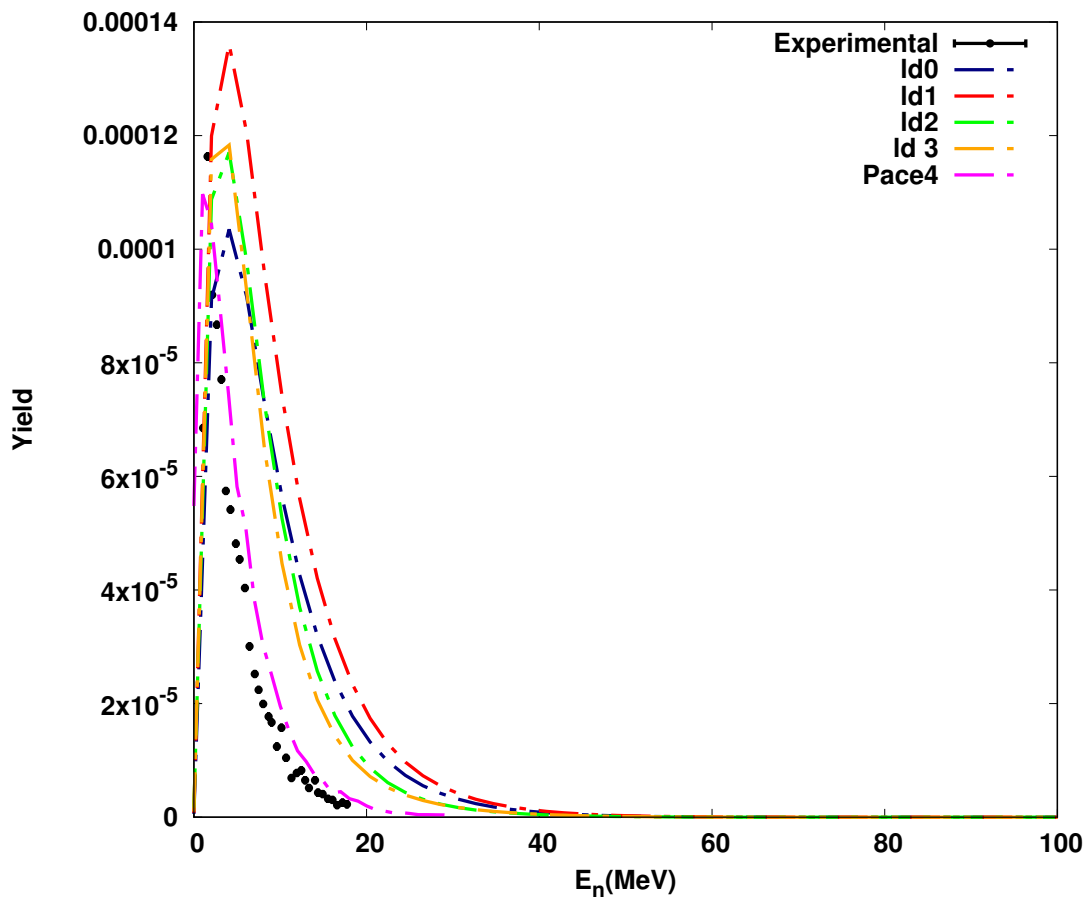


FIGURE 6.4: Comparison of Neutron yield data of ^{12}C on ^{27}Al at 90° reported by V. Suman et al[67],with theoretical data from EMPIRE-3.2 and PACE 4.

Similarly, we test the validation of code EMPIRE-3.2 with and without pre-equilibrium parameter (shown in Fig. 6.5). For that we done the calculation with PCROSS-1.5 and PCROSS-0 input parameter. The trend of result obtained from calculation with pre-equilibrium shows consistent with experimental data and without pre-equilibrium results good agreement with PACE 4 data. This shows PACE 4 didnt account pre-equilibrium contribution while EMPIRE gives an overall well fitted prediction.

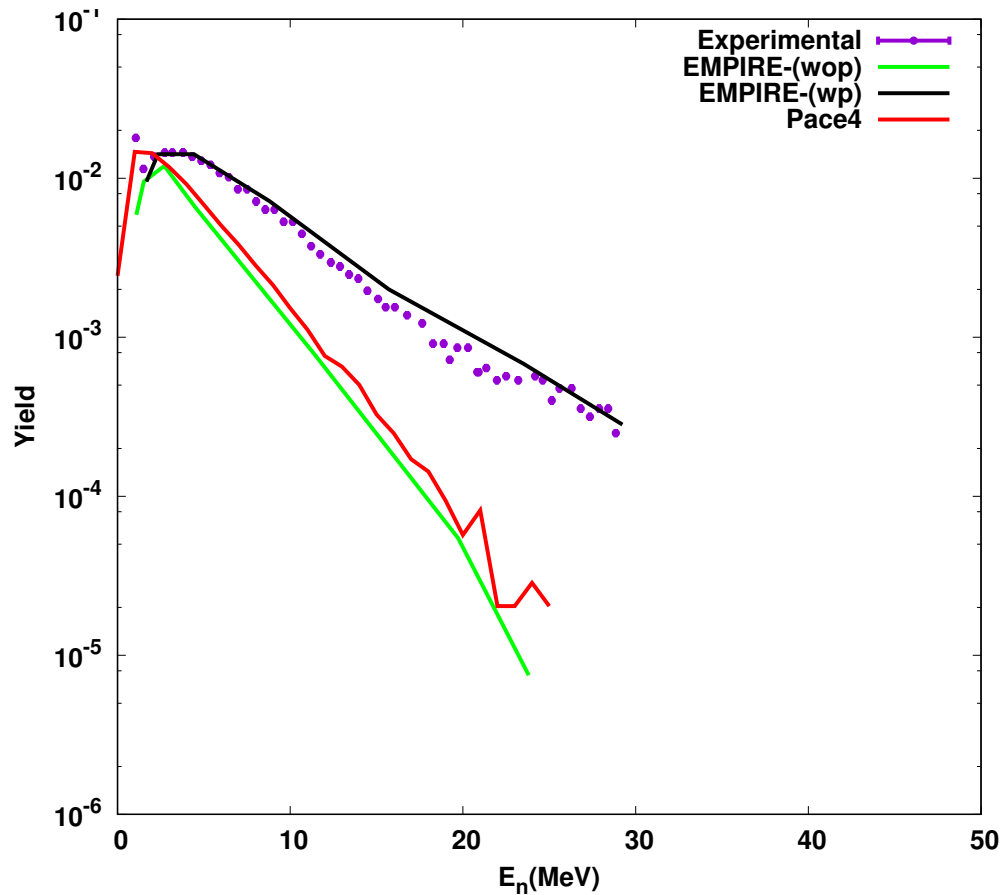


FIGURE 6.5: Comparison of Neutron yield data of ^{12}C on ^{27}Al reported by V. Suman et al[67], with theoretical data from EMPIRE-3.2 with pre-equilibrium(wp) and without pre-equilibrium(wop) and PACE 4.

From Figure 1-4 the neutron yield measured data reported by V.Suman et al[67] for the system ^{12}C on ^{27}Al is compared with EMPIRE-3.2 and PACE 4, here we found whichever parameters of EMPIRE-3.2 matches the experimental data well and summerises the contribution of pre-equilibrium.

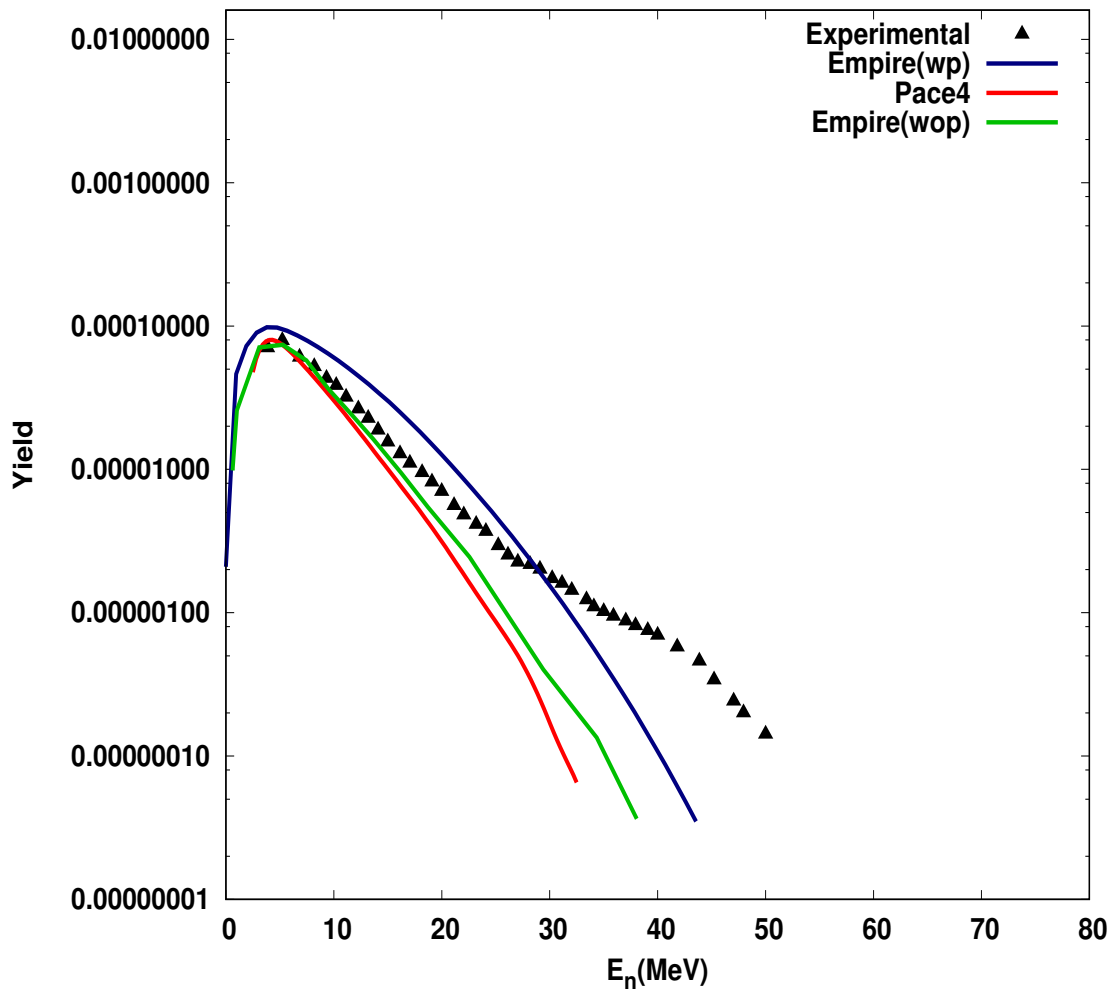


FIGURE 6.6: Comparison of neutron yield data reported by[24] with EMPIRE-3.2 and PACE 4 for ^{12}C on Ti at 144 MeV

Using the same set of input parameters for level density, PCROSS and optical model potential of EMPIRE-3.2, in the following sections we are producing the results for ^{12}C on ^{nat}Ti , ^{56}Fe systems along with the available experimental data, calculated HIC-1 code data and PACE 4 data for validation purpose.

6.2.2 ^{12}C on ^{nat}Ti

It is clear from the Fig. 6.6 that the trend of neutron yield made from the theoretical calculation EMPIRE-3.2 well matches with the experimental data given by Nandy et.al[24]. Here also we compared EMPIRE's with pre-equilibrium and without pre-equilibrium parameter.

6.2.3 ^{12}C on ^{56}Fe

Based on the above two studies with the systems ^{12}C on ^{27}Al and ^{12}C on ^{nat}Ti , a comparison of neutron yield from the system ^{12}C on ^{56}Fe with nuclear reaction model codes EMPIRE-3.2 and PACE 4 is considered, as for this study we use the same parameters to optimize the result for the system ^{12}C on ^{56}Fe , which is shown in Fig. 6.7 and Fig. 6.8 respectively. Since there is no available experimental data for ^{12}C on ^{56}Fe in the incident energy of 12MeV/nucleon we consider the available calculated data of ^{12}C on ^{56}Fe reported by H.W.Bertini [68].

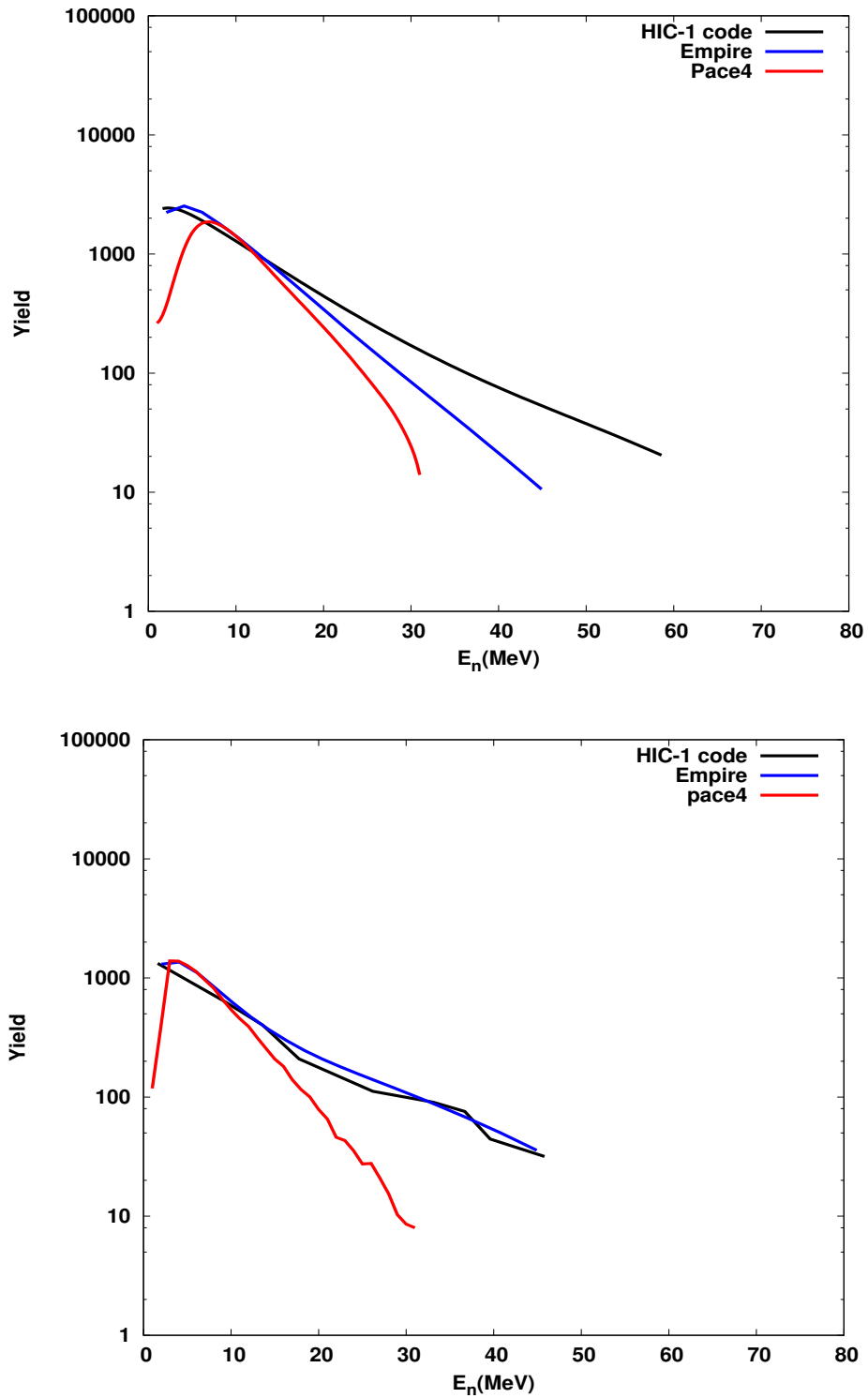


FIGURE 6.7: Comparison of Calculated neutron yield data from HIC-1 code data reported by H.W.Bertini[68] with those obtained from model calculations EMPIRE-3.2 and PACE 4 for ^{12}C on ^{56}Fe reaction at 0° and 30°

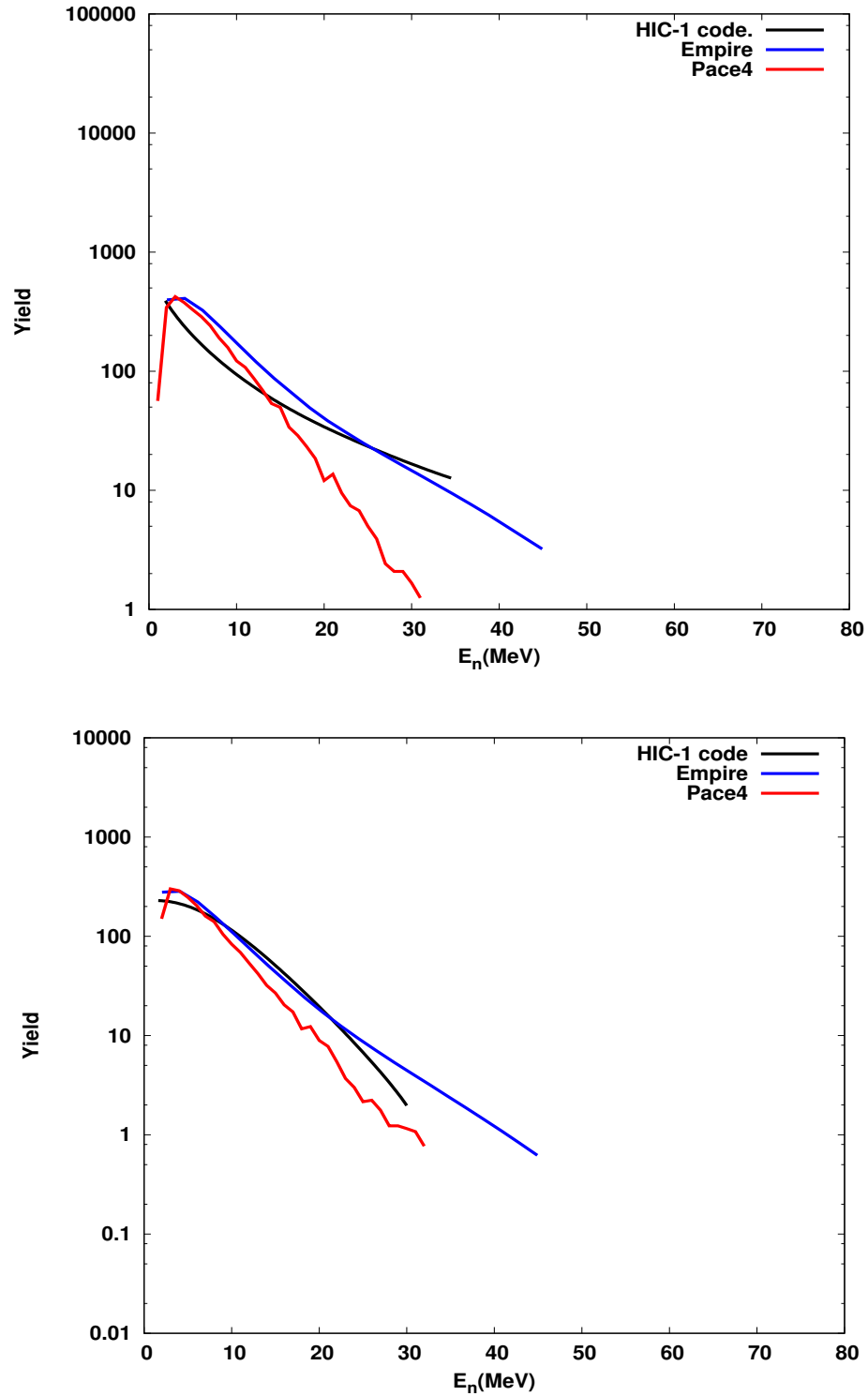


FIGURE 6.8: Comparison of Calculated neutron yield data from HIC-1 code data reported by H.W.Bertini[68] with those obtained from model calculations EMPIRE-3.2 and PACE 4 for ^{12}C on ^{56}Fe reaction at 60° and 90° .

6.3 Conclusion

It is interesting to examine that in all the three cases, it is observed that there is a fall in the PACE 4 calculations at high energies (above 5 MeV). At forward angles less than 50° there is a significant discrepancy between PACE 4 and EMPIRE-3.2. In this region, the PACE 4 calculation drastically underestimates the experimental result. This is to be expected because of pre-equilibrium emission. At backward angles higher than 50 degrees, PACE 4 calculation falls off faster than the EMPIRE-3.2 calculation, but the experimental and calculated data are in good agreement with EMPIRE-3.2 prediction. It is also observed that pre-equilibrium contributions increase with increase in incident energy of the neutron. Thus it is concluded that at intermediate beam energies significant amount of high energy neutrons are produced this neutrons in turn induces secondary reactions with core and structural materials. This will affect the criticality of the reactor. Such neutrons may be produced other structural materials like Nb, Ni, Cr etc.

Chapter 7

Summary and Conclusion

In summary, this extensive research work has been focused to the comprehensive evaluation of neutron yield from thick target materials, that spans a broad spectrum of nuclear reactions and scenarios. One of the central aspects of this study involved the detailed evaluation of neutron yield. This was achieved through the utilization of two prominent nuclear reaction model codes, EMPIRE and NeuCBOT. These codes served as powerful tools for predicting neutron production across a range of scenarios. Notably, several alpha bombardment experiments involving light target materials were also conducted and their neutron yields were calculated using the NeuCBOT code. A significant part of this research was the in-depth examination of model codes. The neutron spectra generated by EMPIRE and NeuCBOT were subject to detailed investigation. This analysis was conducted with a special emphasis on the Am-Be (Americium-Beryllium) system, which was selected as a relevant case study. The Am-Be system provided unique insights into the neutron spectra generation under specific conditions, offering a valuable benchmark for the performance of the model codes.

Furthermore, our investigations extended into the field of the intermediate energy range, a domain where EMPIRE-3.2 can be used. This comprehensive code not only calculated ion-induced reactions but also shed light on the contribution of pre-equilibrium emission. The study of neutron yield in this energy range expanded our understanding of nuclear reactions and their associated emissions.

7.1 Conclusion

The current work meets a demand for nuclear reaction model codes that can estimate neutron yields at low and intermediate projectile energies. In the present work a theoretical estimate of neutron yield from thick targets for low and intermediate energy projectile system for different energies has been carried out. The nuclear model codes were used as a tool to study the results. These nuclear models were used to predict the neutron emission results at various selected incident energies. The models are in accordance with the nuclear data available in experimental data library EXFOR. The theoretical code EMPIRE-3.2, NeuCBOT(TALYS+SRIM) and PACE 4 is used in the present work for the code validation.

The present work focuses on two distinct case studies, both involving neutron emission in thick targets and the validation of nuclear reaction model codes. In the first case study, the focus is on low-energy neutron emission from thick targets. This involves a comprehensive comparison of neutron yield predictions obtained from two nuclear reaction model codes, EMPIRE-3.2 and NeuCBOT, with experimental results. The experimental data is derived from α bombardment of several light elements, including Boron, Carbon, Oxygen, Fluorine, Magnesium, Aluminium and Silicon at four distinct

monoenergetic α -particle energies (4.0, 4.5, 5.0 and 5.5MeV). Furthermore, to generate neutron energy spectra theoretically, a special case of Am-Be source is explored, The neutron yield from Am-Be is evaluated as it is a case of (α,n) reaction. The spectra generated by NeuCBOT, calculates the neutron yield using TALYS, The mass stopping power are read from a library generated by SRIM. In EMPIRE-3.2 total neutron yield was achieved by integrating the neutron spectra over the range 0-9.37MeV. We computed the straggling and energy loss for alpha particle in Am-Be using SRIM code. It shows the peak corresponding to ground(0MeV), first(4.4MeV) and second-excited states(7.65MeV)respectively. To test the code validation the resultant spectrum from EMPIRE-3.2 code is compared with spectrum generated by Geiger. The code predicted a good spectrum with peaks of n_0 colony around 8MeV and 9MeV. Prominent peaks around 1.9MeV, 2.2MeV and 4.8MeV contribute n_1 colony and the spikes formed from thermal to 1.5MeV results the n_2 colony respectively. This work will be helpful in calibration facilities, in laboratories, shielding and the radiation protection protocols etc.

Furthermore, Inorder to validate these predictions and ensure their accuracy, an experimental validation of model code was also performed using Am-Be source. α -particles from ^{241}Am fuses with ^9Be at an incident α energy of 5.48MeV is measured using TOF method. experiment was performed using one of the BC501A neutron detector from NAND facility, IUAC, New Delhi. The neutron yield obtained from present TOF measurement shows the neutron yield distribution from 0.3 to $\sim 6.5\text{MeV}$. The experimental data have been compared with the standard neutron reference spectrum as well as earlier measured data. In the overlapping energy region of 0.3 - 6.5MeV, our data agrees well with the ISO 8529-2 reference neutron radiation spectrum. As compared to earlier measurements, we have extended the neutron yield measurements

down to 0.3MeV and applied neutron detection efficiency correction to the data. With respect to earlier measured data, we observed significant improvement within the energy interval from 0.3 to 3MeV. The technique provides a simple means for characterization of the neutron sources used in calibrating and optimizing the performance of BC501A based neutron ToF facility. The measured data is also compared with EMPIRE-3.2 and NeuCBOT code, agreement between measured data and EMPIRE-3.2 evaluated spectrum is found to be good between 2.5MeV to 6MeV, the two prominent peaks at 2.8MeV and 4.6MeV are estimated. The comparison with NeuCBOT with TOF spectra is also made. It is found a discrepancy around 2MeV to 5MeV, this is due to the method in which Am-Be source are made, this seems to have an influence on the neutron emission rate in these energy ranges, as the NeuCBOT code works with material composition.

So far we studied on compound reactions within the area of low-energy scenarios. However, as we move into higher energy regimes, we observed a different phase of nuclear reactions, where mechanisms like pre-equilibrium emissions dominates. Here we use the nuclear reaction model code EMPIRE-3.2 as it can account pre-equilibrium contribution. Inorder to study the pre-equilibrium emission, the neutron emission in intermediate energy range has been estimated for different target-projectile systems ^{12}C on ^{56}Fe , ^{27}Al , ^{nat}Ti . The chosen targets are important because these are prominent accelerator structural materials. This study results to understand the effect of PEQ contribution in intermediate energy range. Here we have used the code EMPIRE-3.2 and PACE 4 for estimating neutron yields. We investigated the effect of pre-equilibrium, various level densities and optical potentials in this study. The comparison of the estimated neutron yield from both the reaction model codes EMPIRE-3.2 and PACE 4 with available experimental data has been

made. In ^{12}C on ^{27}Al and ^{12}C on ^{nat}Ti , available experimental data were compared with EMPIRE-3.2 and PACE 4 code, the data is found to be in good agreement with theoretical results made using level density model-3 of code EMPIRE-3.2. It has been also observed that the PEQ parameters of the code EMPIRE-3.2 satisfactorily reproduces the result, whereas, the code PACE 4 calculations falls of faster than the EMPIRE-3.2 code because PACE 4 do not have the PEQ model included. For the system ^{12}C on ^{56}Fe available calculated data is compared with the codes with same optimized parameters of above systems. This comparison allows us to evaluate the reliability of our calculations by expecting experimental data to fall within the same region as our computational results.

Above findings concluded that in low energy neutron emission studies NeuCBOT code gives a better results as it can calculate energy loss in case of thick targets, while in intermediate data neutron emission EMPIRE-3.2 code gives better prediction and simulation as it can calculate for high energy ion projectiles. Also it is understood that at intermediate energy range approx 7 A MeV, the PEQ neutron emission is preferred and PEQ emission increases with increase in energy range. Theoretical codes based on various models, potentials, and phenomenological parameters made use of this model calculations to improve its working. These model calculation of neutron emission studies for different structural materials are important for evaluation of nuclear data which are having application in accelerator environment and nuclear energy programs.

Chapter 8

Recommendation

In the present work the nuclear reaction tool NeuCBOT and code EMPIRE-3.2 has reproduced different experimental systems. While there are scope for other reaction model codes like ALICE or HION by incorporating various formalisms. Alpha-neutron yield for compounds may not be readily available or well-documented in NeuCBOT hence a concerted effort is required to collect data on alpha neutron yields of compounds as well as developing theoretical models to predict these yields accurately. Also the future scope of alpha bombarded on heavy ions holds promising applications in advanced nuclear reactor designs, such as thorium based reactors or accelerator-driven systems, to improve efficiency, safety and waste management. Further the code EMPIRE-3.2 requires a modification for accurate calculations at high energies, the code is not optimized or designed to handle the computational demands associated with reactions above 500MeV. The model parameters and assumptions are often tuned and validated for specific energy regimes and extrapolating beyond these limits could lead to unreliable results, resolving the problem will make the code better suitable for the energy range above 500 MeV.

In the pre-equilibrium regime the investigation of neutron yields at higher energies above 10 A MeV is also a demanding area for future research. The studies on measurement of neutron yield from thick targets of various metals which are widely used in building accelerators and cavities when bombarded by ^{12}C will improve our understanding on Pre-equilibrium neutron emission, the new data are useful to the application of accelerator shielding design. Also there are finite probability of producing carbon in ternary fission of ^{235}U in reactors that promotes the study of secondary neutron generation. There are very few works reported in literature on neutron energy distribution from heavy ion reaction on thick target above 10MeV/amu energies. Thus new data on equilibrium and pre-equilibrium neutron emissions are very important for a better understanding of the nuclear reaction mechanism. Furthermore, there is an exciting opportunity for experimental work at institutions such as IUAC (Inter-University Accelerator Centre) to expand the scope of our research. By obtaining data in higher energy ranges, one can contribute valuable information to the NNDC (National Nuclear Data Center) nuclear reaction database, enriching this resource for public use and benefiting the broader scientific community.

Bibliography

- [1] H. Becquerel, “compt.rend.,” vol. 122, p. 450, 1896.
- [2] N. Bohr, “Neutron capture and nuclear constitution,,” *Nature*, vol. 137, pp. 344–348, 1936.
- [3] A. Lane and J. Lynn, “Analysis of experimental data on nucleon capture reactions,” *Nuclear Physics*, vol. 11, pp. 646–669, 1959.
- [4] P. Hodgson, “Heavy ion collision,” *proceedings of International Summer School, La Rabia*, p. 220, 1992.
- [5] M. Blann, “Precompound decay calculations for reactions induced by 10–100 mev/nucleon heavy ions,” *Phys. Rev. C*, vol. 31, pp. 1245–1254, Apr 1985.
- [6] H. Machner, “Pre-equilibrium emission in heavy ion reactions,” *Phys. Rev. C*, vol. 28, pp. 2173–2175, Nov 1983.
- [7] J. Pal, S. Saha, C. C. Dey, P. Banerjee, S. Bose, B. K. Sinha, M. B. Chatterjee, and S. K. Basu, “Pre-equilibrium and equilibrium emission of neutrons in $^{114}\text{Cd}(\alpha, xn)$ reactions,” *Phys. Rev. C*, vol. 71, p. 034605, Mar 2005.
- [8] A. Iwamoto, “Exciton-model approach to fast-particle emission in heavy-ion collisions,” *Phys. Rev. C*, vol. 35, pp. 984–993, Mar 1987.

- [9] G. Friedlander, J. W. Kennedy, E. S. Macias, and J. M. Miller, "Nuclear and radiochemistry, 3rd edition," *John Wiley and Sons*, 1 1981.
- [10] B. V. Raju and S. Jnanananda, "Fast neutron spectrum of Ra-Be source," *Nuclear Instruments and Methods*, vol. 31, no. 1, pp. 87–89, 1964.
- [11] J. Pal, S. Saha, C. Dey, B. Sinha, and M. Chatterjee, "Neutron energy spectrum of an Am-Be source by gamma gated ntof technique," *Radiation Physics and Chemistry*, vol. 51, no. 4, pp. 475–477, 1998.
- [12] K.W.Geiger and L.Vanderzwan, "The neutron spectrum of a Am-Be (α , n) source as simulated by accelerator produced α -particles," *International Journal of Applied Radiation and Imtopcs*, vol. 21, pp. 193–198, 1969.
- [13] H. Liskien and A. Paulsen, "Neutron yields of light elements under α -bombardment," *Atomkernenergie (ATKE)*, pp. 59–61, 1977.
- [14] H. Liskien and A. Paulsen, "Neutron production cross sections and energies for the reactions T(p,n)³He, D(d,n)³He, and T(d,n)⁴He," *Report CBNM/VG/21/78, Geel, Belgium*, pp. 1–2, 1978.
- [15] J. K. Bair and J. G. del Campo, "Neutron yields from alpha-particle bombardment," *J., Nucl. Sci. Eng.*, pp. 18–28, 7 1979.
- [16] R. Macklin *Nucl. Instr. Meth.*, pp. 335–339, 1957.
- [17] R. Macklin and J. Gibbons, "Absolute neutron yield from thick target ^{NAT}C(α ,n)," *J., Nucl. Sci. Eng.*, vol. 31, p. 343, 1968.
- [18] J. Bair, "Absolute neutron yields from alpha-particle interaction with tick targets of natural carbon," *J., Nucl. Sci. Eng.*, vol. 51, pp. 83–84, 1973.

- [19] D. West and A. Sherwood *Report Atomic Energy Research Establishment(AERE) Harwell*, pp. 1–5, 1978.
- [20] D. West and A. Sherwood, “Measurements of thick-target (α,n) yields from light elements,” *Ann. Nucl. Ener.*, vol. 9, pp. 551–577, 1982.
- [21] G. Jacobs, *Neutron energy spectra produced by alpha-bombardment of light elements in thick targets*. Phd thesis 1 (research TU/e / graduation TU/e), Applied Physics and Science Education, 1982. Proefschrift.
- [22] M. Nandy, T. Bandyopadhyay, and P. K. Sarkar, “Measurement and analysis of neutron spectra from a thick Ta target bombarded by 7.24MeV ^{16}O ions,” *Phys. Rev. C*, vol. 63, p. 034610, Feb 2001.
- [23] C. Sunil, M. Nandy, and P. K. Sarkar, “Measurement and analysis of energy and angular distributions of thick target neutron yields from 110MeV ^{19}F on ^{27}Al ,” *Phys. Rev. C*, vol. 78, p. 064607, Dec 2008.
- [24] M. Nandy, P. Sarkar, T. Sanami, T. Shibata, and M. Takada, “Neutron dose distribution from ^{12}C induced reactions on Ti and Ag using proton recoil scintillator,” *Radiation Measurements*, vol. 45, no. 10, pp. 1276–1280, 2010.
- [25] J. Acharya, S. Mukherjee, A. Chatterjee, N. L. Singh, K. Ramachandran, P. C. Rout, K. Mahata, V. Desai, E. T. Mirgule, S. V. Suryanarayana, B. K. Nayak, A. Saxena, and G. F. Steyn, “Neutron emission in ^{19}F -induced reactions,” *Phys. Rev. C*, vol. 97, p. 034607, Mar 2018.
- [26] E. Holub, D. Hilscher, G. Ingold, U. Jahnke, H. Orf, and H. Rossner, “Neutron emission in central heavy-ion collisions of $^{165}\text{Ho} + ^{20}\text{Ne}$ at 11,

- 14.6, and 20.1 MeV/nucleon,” *Phys. Rev. C*, vol. 28, pp. 252–270, Jul 1983.
- [27] D. Hilscher, H. Rossner, A. Gamp, U. Jahnke, B. Cheynis, B. Chambon, D. Drain, C. Pastor, A. Giorni, C. Morand, A. Dauchy, P. Stassi, and G. Petitt, “Energy and linear-momentum dissipation in the fusion reaction of $^{165}\text{Ho} + ^{20}\text{Ne}$ at 30 MeV/nucleon,” *Phys. Rev. C*, vol. 36, pp. 208–219, Jul 1987.
- [28] H. Singh, K. S. Golda, S. Pal, Ranjeet, R. Sandal, B. R. Behera, G. Singh, A. Jhingan, R. P. Singh, P. Sugathan, M. B. Chatterjee, S. K. Datta, A. Kumar, G. Viesti, and I. M. Govil, “Role of nuclear dissipation and entrance channel mass asymmetry in pre-scission neutron multiplicity enhancement in fusion-fission reactions,” *Phys. Rev. C*, vol. 78, p. 024609, Aug 2008.
- [29] V. Singh, B. R. Behera, M. Kaur, P. Sugathan, K. S. Golda, A. Jhingan, J. Sadhukhan, D. Siwal, S. Goyal, S. Santra, A. Kumar, R. K. Bhowmik, M. B. Chatterjee, A. Saxena, S. Pal, and S. Kailas, “Search for an effect of shell closure on nuclear dissipation via a neutron-multiplicity measurement,” *Phys. Rev. C*, vol. 86, p. 014609, Jul 2012.
- [30] N. K. Rai, A. Gandhi, A. Kumar, N. Saneesh, M. Kumar, G. Kaur, A. Parihari, D. Arora, K. S. Golda, A. Jhingan, P. Sugathan, T. K. Ghosh, J. Sadhukhan, B. K. Nayak, N. K. Deb, S. Biswas, and A. Chakraborty, “Measurement of neutron multiplicity to investigate the role of entrance channel parameters on the nuclear dissipation,” *Phys. Rev. C*, vol. 100, p. 014614, Jul 2019.

-
- [31] S. Westerdale and P. D. Meyers, “Radiogenic neutron yield calculations for low-background experiments,” *Nucl. Instrum. Meth. in Phys.*, vol. 875, p. 57–64, 04 2017.
- [32] E. Mendoza, D. Cano-Ott, P. Romojaro, V. Alcayne, P. G. Abia, V. Pseudo, L. Romero, and R. Santorelli, “Neutron production induced by α -decay with geant4,” *Nuclear Instruments and Methods in Physics Research Section A: Accelerators, Spectrometers, Detectors and Associated Equipment*, vol. 960, p. 163659, 2020.
- [33] W. B. Wilson, R. T. Perry, W. S. Charlton, T. A. Parish, and E. F. Shores, “SOURCES: a code for calculating (α ,n), spontaneous fission, and delayed neutron sources and spectra,” *Radiation Protection Dosimetry*, vol. 115, pp. 117–121, 12 2005.
- [34] A. C. Fernandes, A. Kling, and G. N. Vlaskin, “Comparison of thick-target (α , n) yield calculation codes,” vol. 153, p. 07021, 2017.
- [35] V. F. Weisskopf and D. H. Ewing, “On the yield of nuclear reactions with heavy elements,” *Phys. Rev.*, vol. 57, pp. 472–485, Mar 1940.
- [36] W. Hauser and H. Feshbach, “The inelastic scattering of neutrons,” *Phys. Rev.*, vol. 87, pp. 366–373, Jul 1952.
- [37] G. Breit and E. Wigner, “Capture of slow neutrons,” *Phys. Rev.*, vol. 49, pp. 519–531, Apr 1936.
- [38] J. J. Griffin, “Statistical model of intermediate structure,” *Phys. Rev. Lett.*, vol. 17, pp. 478–481, Aug 1966.

- [39] C. Kalbach-Cline, “Residual two-body matrix elements for pre-equilibrium calculations,” *Nuclear Physics A*, vol. 210, no. 3, pp. 590–604, 1973.
- [40] C. Kalbach and F. M. Mann, “Phenomenology of continuum angular distributions. i. systematics and parametrization,” *Phys. Rev. C*, vol. 23, pp. 112–123, Jan 1981.
- [41] H. A. Bethe, “Nuclear physics b. nuclear dynamics, theoretical,” *Rev. Mod. Phys.*, vol. 9, pp. 69–244, Apr 1937.
- [42] M. Herman, “Empire-3.2 malta modular system for nuclear reaction calculations and nuclear data evaluation,” *Nucl. Phys*, 2013.
- [43] A. Gilbert and A. G. W. Cameron, “A composite nuclear-level density formula with shell corrections,” *Canadian Journal of Physics*, vol. 43, pp. 1446–1496, 1965.
- [44] W. Dilg, W. Schantl, H. Vonach, and M. Uhl, “Level density parameters for the back-shifted fermi gas model in the mass range $40 < A < 250$,” *Nuclear Physics A*, vol. 217, no. 2, pp. 269–298, 1973.
- [45] A. V. Ignatyuk, K. Istekov, and G. N. Smirenkin *Sov. J. Nucl. Phys*, vol. 4, p. 450, 1979.
- [46] A. V. Ignatyuk, J. L. Weil, S. Raman, and S. Kahane, “Density of discrete levels in ^{116}Sn ,” *Phys. Rev. C*, vol. 47, pp. 1504–1513, Apr 1993.
- [47] A. D’Arrigo, G. Giardina, M. Herman, A. Ignatyuk, and A. Taccone, “Semi-empirical determination of the shell correction temperature and spin dependence by means of nuclear fission,” *Journal of Physics G: Nuclear and Particle Physics*, vol. 20, no. 2, p. 365, 1994.

-
- [48] S. Goriely, F. Tondeur, and J. Pearson, “A Hartree–Fock nuclear mass table,” *Atomic Data and Nuclear Data Tables*, vol. 77, no. 2, pp. 311–381, 2001.
- [49] S. Goriely, S. Hilaire, and A. J. Koning, “Improved microscopic nuclear level densities within the Hartree-Fock-Bogoliubov plus combinatorial method,” *Phys. Rev. C*, vol. 78, p. 064307, Dec 2008.
- [50] S. Goriely, M. Samyn, and J. M. Pearson, “Further explorations of Skyrme-Hartree-Fock-Bogoliubov mass formulas. VII. Simultaneous fits to masses and fission barriers,” *Phys. Rev. C*, vol. 75, p. 064312, Jun 2007.
- [51] A. Koning, S. Hilaire, and S. Goriely, “Talys-1.6 a nuclear reaction program,” *User Manual, NRG, The Netherlands*, 2013.
- [52] S. Westerdale, Meyers, and P. Daniel, “Radiogenic neutron yield calculations for low-background experiments,” *Nuclear Instruments and Methods in Physics Research Section A: Accelerators, Spectrometers, Detectors and Associated Equipment*, vol. 875, pp. 57–64, 2017.
- [53] M. Herman, R. Capote, and B. V. Carlson, “Empire: Nuclear reaction model code system for data evaluation,” *Nuclear Data Sheets*, vol. 108, pp. 2655–2715, 2007.
- [54] J. Tuli, “Evaluated nuclear structure data file,” *Nuclear Instruments and Methods in Physics Research Section A: Accelerators, Spectrometers, Detectors and Associated Equipment*, vol. 369, no. 2, pp. 506–510, 1996.
- [55] J. F. Ziegler and J. P. Biersack, *The Stopping and Range of Ions in Matter*, pp. 93–129. Boston, MA: Springer US, 1985.

- [56] P. De Bièvre and P. Taylor, “Table of the isotopic compositions of the elements,” *International Journal of Mass Spectrometry and Ion Processes*, vol. 123, no. 2, pp. 149–166, 1993.
- [57] D. Kumar, M. Maiti, and S. Lahiri, “Experimental probe for the production of ^{97}Ru from the $^7\text{Li} + ^{93}\text{Nb}$ reaction: A study of precompound emissions,” *Phys. Rev. C*, vol. 94, p. 044603, Oct 2016.
- [58] R. Bass, “Nucleus-nucleus potential deduced from experimental fusion cross sections,” *Phys. Rev. Lett.*, vol. 39, pp. 265–268, Aug 1977.
- [59] P. Sugathan, A. Jhingan, K. S. Golda, T. Varughese, S. Venkataramanan, N. Saneesh, V. V. Satyanarayana, S. K. Suman, J. Antony, R. Shanti, K. Singh, S. K. Saini, A. Gupta, A. Kothari, P. Barua, R. Kumar, J. Zacharias, R. P. Singh, B. R. Behera, S. K. Mandal, I. M. Govil, and R. K. Bhowmik, “Neutron detector array at iuac: Design features and instrumentation developments,” *PRAMANA- Journal of Physics*, vol. 83, pp. 807–815, 2014.
- [60] M. Moszynski, G. Bizard, G. Costa, D. Durand, Y. E. Masri, G. Guillaume, F. Hanappe, B. Heusch, A. Huck, J. Peter, C. . Ring, and B. Tamain, “Study of n- γ discrimination by digital charge comparison method for a large volume liquid scintillator,” *Nucl. Instr. and Meth. in Physics Research A*, vol. 317, pp. 262–272, 1992.
- [61] N. Saneesh, K. Golda, A. Jhingan, S. Venkataramanan, T. Varughese, M. Kumar, M. Thakur, R. Mahajan, B. Behera, P. Sugathan, A. Chatterjee, and M. Chatterjee, “Performance results of national array of neutron detectors (nand) facility at iuac,” *Nuclear Instruments and Methods in*

- Physics Research Section A: Accelerators, Spectrometers, Detectors and Associated Equipment*, vol. 986, p. 164754, 2021.
- [62] M. Roush, M. Wilson, and W. Hornyak, “Pulse shape discrimination,” *Nuclear Instruments and Methods*, vol. 31, no. 1, pp. 112–124, 1964.
- [63] S. Venkataramanan, A. Gupta, K. S. Golda, H. Singh, R. Kumar, R. P. Singh, and R. K. Bhowmik, “A compact pulse shape discriminator module for large neutron detector arrays,” *Nuclear Instruments and Methods in Physics Research Section A: Accelerators, Spectrometers, Detectors and Associated Equipment*, vol. 596, no. 2, pp. 248 – 252, 2008.
- [64] R. Brun and F. Rademakers, “Root — an object oriented data analysis framework,” *Nuclear Instruments and Methods in Physics Research Section A: Accelerators, Spectrometers, Detectors and Associated Equipment*, vol. 389, no. 1, pp. 81–86, 1997.
- [65] J. Scherzinger, R. Al Jebali, J. Annand, K. Fissum, R. Hall-Wilton, S. Koufigar, N. Mauritzson, F. Messi, H. Perrey, and E. Rofors, “A comparison of untagged gamma-ray and tagged-neutron yields from ^{241}Am -Be and ^{238}Pu -Be sources,” *Nuclear Instruments and Methods in Physics Research Section A: Accelerators, Spectrometers, Detectors and Associated Equipment*, vol. 127, pp. 98–102, 2017.
- [66] “Reference neutron radiations. characteristics and methods of production,” *International Organization for Standardization.ISO-Standard 8529*, 2001.
- [67] V. Suman, C. Sunil, S. Nair, S. Paul, K. Biju, G. Sahoo, and P. Sarkar, “Thick target double differential neutron energy distribution from $^{12}\text{C}+^{27}\text{Al}$ at 115MeV,” *Nuclear Instruments and Methods in Physics Research*

Section A: Accelerators, Spectrometers, Detectors and Associated Equipment, vol. 800, pp. 29–33, 2015.

- [68] H. W. Bertini, R. T. Santoro, and O. W. Hermann, “Calculated nucleon spectra at several angles from 192-, 500-, 700-, and 900-MeV ^{12}C on ^{56}Fe ,” *Phys. Rev. C*, vol. 14, pp. 590–595, Aug 1976.